# Design aspects of a ventilated façade with integrated photovoltaics

## Evaluation of a box façade as a refurbishment solution for office buildings in Sweden

Evangelia Foulaki and Ioannis Antonios Moutsatsos

Master thesis in Energy-efficient and Environmental Buildings
Faculty of Engineering | Lund University

# Lund University

Lund University, with eight faculties and a number of research centres and specialized institutes, is the largest establishment for research and higher education in Scandinavia. The main part of the University is situated in the small city of Lund which has about 112 000 inhabitants. A number of departments for research and education are, however, located in Malmö. Lund University was founded in 1666 and has today a total staff of 6 000 employees and 47 000 students attending 280 degree programmes and 2 300 subject courses offered by 63 departments.

# Master Programme in Energy-efficient and Environmental Building Design

This international programme provides knowledge, skills and competencies within the area of energy-efficient and environmental building design in cold climates. The goal is to train highly skilled professionals, who will significantly contribute to and influence the design, building or renovation of energy-efficient buildings, taking into conconsideration the architecture and environment, the inhabitants' behaviour and needs, their health and comfort as well as the overall economy.

The degree project is the final part of the master programme leading to a Master of Science (120 credits) in Energy-efficient and Environmental Buildings.

Keywords: double skin façade, photovoltaics, refurbishment, energy efficiency, thermal comfort

# Abstract

Swedish office buildings of the 60's present at least 27% higher heating demand than from the current standards foreseen. This underlines their need for energy renovation. Meanwhile, office buildings are occupied during daytime, thus internal and solar gains are in phase. Consequently, such buildings could experience overheating problems. A seasonal adaptable envelope, such as a ventilated double skin façade, can be a potential improvement to both, heating and cooling issues of office spaces. At the same time, EU regulations imply that by 2020 all buildings should produce the energy they consume, on an annual basis. This energy should come from renewable sources. Solar electricity systems linked to buildings are often integrated in building envelopes. However, the electricity conversion efficiency of these systems decreases with increasing temperature.

In the first part of this thesis the aim is to examine the critical design parameters of a ventilated façade with integrated photovoltaics, and analyze its impact on the thermal performance of a typical cell office with a 60's envelope, located in Southern Sweden. Investigations are focused on the energy use and the thermal comfort quality of the room and they are performed for two window-to-wall ratios and four orientations. In the second part of the work, the focus is given on evaluating the effect of the cavity's ventilation on the PV's efficiency and annual energy production.

The study concluded that an upgrade to a ventilated double skin façade can yield a decrease of 30% to 60% on the energy use of a typical cell office, achieving the current requirements. The lowest energy use is attained through a low emittance external glazing combined with a reflective shading. The integration of solar cells does not lead to an overall improved performance compared to a case without photovoltaics. The cavity ventilation resulted in a maximum increase of 6.5 % on the solar cells' efficiency, but the increase of the annual electricity output is at maximum 2% and was considered negligible.

# Acknowledgements

We would like to thank our supervisor Susanne Gosztonyi for her support and her detailed feedback on our work. Moreover we would like to acknowledge our colleagues Mihail Todorov and Amir Avdic for the valuable discussions and support during the whole thesis. Moreover we would like to acknowledge Dr. Harris Poirazis, who took up his personal time in order to discuss with us about this work and offered his expertise and ideas several times throughout this thesis. Finally we would especially like to thank Dr. Bengt Hellström who took up an enormous amount of time in helping us with IDA – ICE and thermal modelling. We were lucky to meet him towards the end of our work. Without his help this thesis would have not been completed.

Table of Contents

# Nomenclature

## Mathematical notation

### *Double Skin Façade part*

Latin characters

| | | |
|---|---|---|
| ȧ | cavity opening | m |
| $A_{eq,in}$ | area of the inlet opening | $m^2$ |
| $A_{eq,out}$ | area of the outlet opening | $m^2$ |
| $A_{facade}$ | facade area | $m^2$ |
| $A_{open}$ | area of opening | $m^2$ |
| $A_s$ | area of the cavity | $m^2$ |
| $A_{temp}$ | heated floor area | $m^2$ |
| $C_c$ | coefficient of contraction | - |
| $C_d$ | discharge coefficient | - |
| $C_v$ | coefficient of velocity | - |
| $c_p$ | heat capacity | J/kg·K |
| $d$ | depth | M |
| $ELA_{bottom}$ | equivalent leakage area of inlet | $m^2$ |
| $ELA_{top}$ | equivalent leakage area of outlet | $m^2$ |
| ġ | acceleration of the gravity | $m/s^2$ |
| $g$ | total solar transmittance | - |
| $g_{eff}$ | g-value, effective | - |
| $g_{low\ iron}$ | total solar transmittance of low iron glass | - |
| $g_{PVR}$ | total solar transmittance of PV module | - |
| $H$ | height | m |
| $h_c$ | heat convection coefficient | $W/m^2K$ |
| $h_{cv}$ | heat convection coefficient for ventilated cavity | $W/m^2K$ |
| $H_o$ | characteristic height | m |
| $L$ | facade width | m |
| $Q$ | heating power | W |
| $Q_G$ | useful solar gains | $W/m^2$ |
| $q_v$ | heat removal | W |
| $r$ | solar reflectance | - |
| $r_b$ | solar reflectance of back surface | - |
| $r_f$ | solar reflectance of front surface | - |
| *R-value* | thermal resistance | m·K/W |
| $T_{av}$ | average temperature | °C |
| $T_b$ | back temperature | °C |
| $T_{bc}$ | balance temperature | °C |
| $T_{cav}$ | temperature in the cavity | °C |
| $T_{cav,in}$ | air temperature at inlet | °C |

| | | |
|---|---|---|
| $T_{air,\ room}$ | room air temperature | °C |
| $T_{cav,\ m}$ | mean cavity temperature | °C |
| $T_{cav,\ out}$ | air temperature at outlet | °C |
| $T_f$ | front temperature | °C |
| $T_{op}$ | operative temperature | °C |
| $T_{out}$ | temperature outdoors | °C |
| $T_{sol}$ | direct solar transmittance | - |
| $T_{sp}$ | Heating setpoint temperature | °C |
| $T_{vis}$ | visible transmittance | - |
| $U'$ | overall heat loss coefficient | W/K |
| $U_g$ | center of glass thermal transmittance | $W/m^2K$ |
| $U_{ov}$ | thermal transmittance, overall | $W/m^2K$ |
| *U-value* | thermal transmittance | $W/m^2K$ |
| $v$ | mean air velocity | $m/s^2$ |
| $z_{in}$ | pressure loss factor at the inlet | - |
| $z_{out}$ | pressure loss factor at the outlet | - |

Greek characters

| | | |
|---|---|---|
| $\alpha$ | solar absorptance | - |
| $\alpha_1$ - $\alpha_3$ | solar absorptance of layers 1-3 | |
| $\Delta P$ | driving pressure difference | Pa |
| $\Delta Pz$ | pressure loss in openings | Pa |
| $\Delta P_B$ | Bernoulli pressure loss | Pa |
| $\Delta P_{HP}$ | Hagen Poiseuille pressure loss | Pa |
| $\varepsilon$ | emittance | - |
| $\varepsilon_b$ | emittance of back surface | - |
| $\varepsilon_f$ | emittance of front surface | - |
| $\theta$ | angle between window and vertical axis | ° |
| $\lambda$ | thermal conductivity | W/mK |
| $\mu$ | dynamic viscosity | kg/m·s |
| $\rho$ | density | $kg/m^3$ |
| $\rho_0$ | density at 10°C | $kg/m^3$ |
| $\tau$ | solar transmittance | - |
| $\tau_1$ - $\tau_3$ | solar transmittance of layers 1-3 | - |
| $\tau_{external\ shade}$ | Solar transmittance of external shade | - |

***Photovoltaics part***

Latin characters

| | | |
|---|---|---|
| $a$, $b$ | empirical coefficients for modules | - |
| $A_{module}$ | area of the module | $m^2$ |
| $d_{module}$ | thickness of PV module | m |
| $dT$ | temperature difference between $T_{cell}$ and $T_{back}$ at reference conditions | °C |
| $E_0$ | reference irradiation | $W/m^2$ |
| $E_{incident}$ | incident solar radiation | $W/m^2$ |
| $F_{Temp,\ corr}$ | temperature correction factor | - |
| $r_{module}$ | overall solar reflectance of PV module | |
| $P_{mp\ module}$ | hourly DC power from PV module | W |
| $R_{EVA}$ | thermal resistance of EVA | m·K/W |
| $R_{glass}$ | thermal resistance of glass | m·K/W |
| $R_{module}$ | overall thermal resistance of PV module | m·K/W |
| $T_{back}$ | temperature of the back of the module | °C |
| $T_{cell}$ | temperature, cell | °C |
| $T_{ref}$ | temperature, reference | °C |
| $v_{win}$ | speed of wind | m/s |

Greek characters

| | | |
|---|---|---|
| $\alpha_{cell}$ | absorptance of the cell | - |
| $\alpha_{module}$ | overall solar absorptance of PV module | - |
| $\gamma$ | maximum power temperature coefficient | - |
| $\eta$ | efficiency | - |
| $\eta_{module}$ | efficiency of PV module | |
| $\lambda_{module}$ | thermal conductivity of PV module | $m^2K/W$ |
| $\tau_{module}$ | overall solar transmittance of PV module | - |

## Acronyms / Abbreviations

| | |
|---|---|
| A, MA, R | Absorptive, medium absorptive, reflective |
| ASHRAE | American Society of Heating, Refrigerating and Air-conditioning engineers |
| BBR | Bovergets Byggregler, Swedish building regulations |
| BC | Base case |
| BELOK | Beställargruppen Lokaler |
| BIPV | Building integrated photovoltaics |
| DSF | Double skin façade |
| ELA | Equivalent leakage area |
| EVA | Ethylene vinyl Acetate |
| FEBY | Forum för Energieffektiva byggnader |
| ISO | International organization for Standardization |

| | |
|---|---|
| low-E | Low Emittance |
| NOCT | Nominal operating cell temperature |
| PVR | Photovoltaic ratio |
| S, N, E, W | South, North, East, West |
| STC | Standard test conditions |
| TGU | Triple glazed unit |
| WWR | Window to wall ratio |

# 1 Introduction

## 1.1 Background

### 1.1.1 Energy savings and energy production

According to the International Energy Agency [1], the building sector consumes 40% of the primary energy worldwide, which is higher than the energy use for transportation or industry. Therefore, the building sector offers high potential for energy savings, which according to [1] could reach up to 27% and 30% for residential and commercial buildings respectively.

In Sweden, as in the majority of European countries, the building regulations set strict criteria concerning the energy performance of buildings. At the same time the need for refurbishment of the existing building stock, constructed under older regulations, is highlighted. According to ECOFYS [2], 53% of Swedish non-residential buildings represent offices and 50% of them were constructed between the decades of 1960 – 1990. Among these, the office buildings of the 1960's have the highest annual heating energy demand [3], which is 27% higher than the maximum allowable energy use for offices in Sweden, according to the current requirements. Consequently there are significant energy saving potential for these buildings that could be met by several renovation measures.

Meanwhile, the demand for energy production based on renewable sources becomes crucial. Conventional energy sources, such as fossil fuels, are limited and finite, as well as harmful to the environment, contributing to global warming and air pollution. Renewable and environmental friendly energy sources, such as solar or wind power, could replace to a certain extent the traditional ones. Photovoltaic (PV) systems can be integrated on buildings, on roofs or on façades, by replacing conventional envelope materials, while producing and covering a part of the building's electricity demand.

Nowadays, solar energy conversion systems such as photovoltaics are included in many new buildings which aim on onsite energy conversion and in many cases direct use of the generated electricity for the building's need. Regarding the existing building stock, refurbishment methods target on both energy savings and production. A type of building which could highly benefit by PV integration is offices, as they are occupied during the day and thus consume larger amount of energy when solar radiation is present.

### 1.1.2 Office buildings in Sweden

#### *1.1.2.1 Current energy requirements*

The requirements regarding the energy performance of buildings in Sweden are set by the Swedish National Board of housing, building and planning and are published in the different versions of Boverket's Building Regulations (BBR) [4]. In addition, the voluntary Swedish forum for energy efficient buildings (Forum för Energieffektiva byggnader -FEBY) [5] sets the criteria for Passive House certification. Both standards have requirements for office premises and their latest versions are BBR 22 [6] and FEBY 12 [7] respectively. The energy use requirements are latitude dependent. The FEBY 12 criteria follow the climate zones of the older building regulations, namely BBR 19 [7] , as shown in Figure 1.1. According to the current BBR, however, Sweden is divided into four climatic zones, and Malmö, which is the study area of this thesis, belongs to the forth.


*Figure 1.1: Climate zones in Sweden according to BBR 19, as implemented in the FEBY 12 standard.*

For both standards, the requirements are set in terms of specific energy use, which is the energy required for heating, comfort cooling, tap hot water and property electricity [6]. The latter is the electricity required for building services including permanently installed lighting of common spaces and utility rooms as well as fans, pumps and the like for heating and cooling equipment. Table 1.1 presents the energy use criteria according to BBR 22 and FEBY 12. It should be noted that the FEBY standard assumes that no installed cooling system is required. The requirements for Southern Sweden and specifically Malmö are noted in bold.

*Table 1.1: Energy use criteria according to FEBY 12 and BBR 22 for climate zones I-IV.*

| | **Specific Energy Use / (kWh/(m$^2$·year))** | | | |
|---|---|---|---|---|
| Climate Zone | I | II | III | IV |
| FEBY 12 | 53 | 49 | **45** | - |
| BBR 22 | 105 | 90 | 70 | **65** |

#### *1.1.2.2 Swedish office building of the 1960's*

According to a report by Dr. Åke Blomsterberg [3] the highest total energy consumption for office buildings in Sweden is observed for the ones built in the 1960's. The report analyzes the energy performance of residential and office buildings in Sweden, built between 1950 and 2000. Figure 1.2 shows the annual energy use for heating and cooling of the ten cases of office buildings constructed in the 60's, as presented in the report. Two of the buildings included are in the region of Skåne. The red line shows the requirements of the current BBR according to the buildings' location.

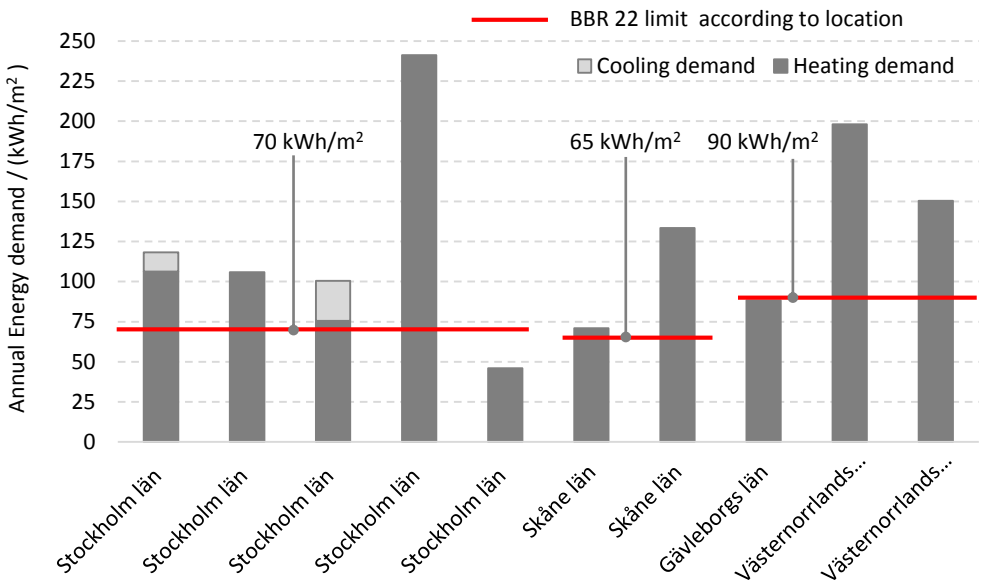


*Figure 1.2: Heating and cooling energy use of 10 office buildings from the 60's at different locations.*

It can be seen that most of the cases do not fulfill the current energy requirements. Nevertheless it becomes obvious that energy reduction measures could be taken in order for the existing stock to meet the current standards. It should be also noted that according to [3], the lack of cooling demand does not necessarily mean that no overheating problems exist but that the presented buildings did not include any cooling system.

Typically, office buildings are occupied during daytime when the outdoor temperature is high. Depending on the amount of the internal heat gains, the envelope characteristics and the ventilation strategy, they may face overheating problems, which can be a cause of extra energy demand or bad quality of thermal comfort. Such problems can be exaggerated in cases of highly insulated buildings, which tend to trap internally generated heat and/or solar gains throughout the year. A climate adaptive envelope which responds to the building's seasonal energy needs, could be a beneficial refurbishment option for buildings with both heating and cooling demand.

### 1.1.3 Ventilated double skin facades

#### *1.1.3.1 General introduction*

According to [8], "A double skin façade (DSF) is a system consisting of two glass skins placed in such a way that air flows in the intermediate cavity. The ventilation of the cavity can be natural, fan supported or mechanical. Apart from the type of the ventilation inside the cavity, the origin and destination of the air can differ depending mostly on climatic conditions, the use, the location, the occupational hours of the building and the HVAC strategy. The glass skins can be single or double glazing units with a distance from 0.2m up to 2m. Often, for protection and heat extraction reasons during the cooling period, solar shading devices are placed inside the cavity."

Also, according to [9], a double skin façade is an adaptable façade system, which aims to exploit solar gains when the demand for heating is dominant. During this period the cavity between the inner and outer skin is closed and performs as a thermal buffer zone. The inner skin has usually an insulating role while the outer one aims to reduce weather exposure of the inner layers and protect any shading devices positioned in the cavity. On the other hand, the cavity becomes

ventilated as well as shaded, in order to remove accumulated heat, when there is need for cooling.

The air inside the cavity can be additionally used in the building. The cavity can be connected with the HVAC systems or it can be directly in contact with the peripheral zones to provide natural ventilation through openings on the inner skin.

The main classification categories that can be found in literature [8] are given below and summarized at Figure 1.3:

- Multi-storey facades: The façade covers the whole building and the cavity is not divided in parts.
- Corridor facades: The façade covers the whole building but is divided horizontally at every floor
- Box window facades: These facades are divided horizontally and vertically (make a box enclosure)
- Shaft box facades: A vertical shaft is created to extract air from box or corridor facades connected with it.

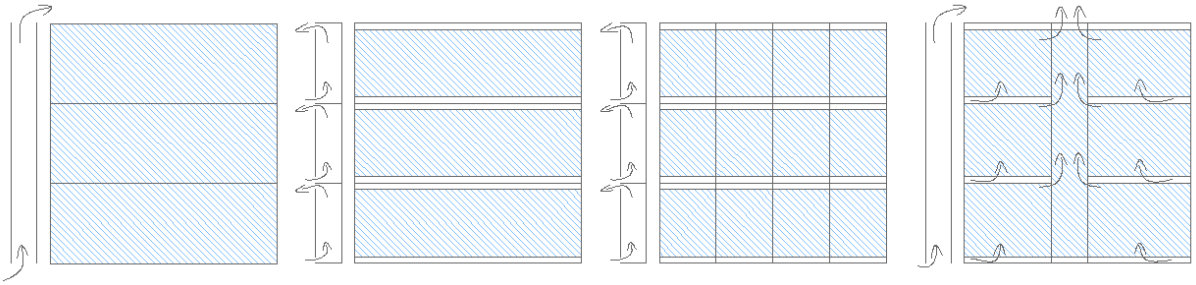

*Figure 1.3 Double skin facade types. From left to right: multistory, corridor, box window and shaft box façade.*

Many studies have analyzed the performance of a DSF as a system and evaluated its impact on the energy use of buildings where it is integrated. Giancola et al [10] examined an open joint ventilated façade in the Mediterranean climate and demonstrated that during warm seasons, when temperature and solar radiation are high, the ventilation through the cavity of a double skin façade removes a large amount of heat loads. On the other hand, during colder seasons with high solar radiation the DSF improves the thermal insulation of the envelope. For the same climate C. Aparicio-Fernandez et al. [11] concluded on 74% reduction of the annual heating demand, when the double skin is applied on a south orientation. A. Andelkovic et al [12] highlighted the importance of shading devices in the cavity and the properties of the outer skin on the inner pane temperatures of the window, during summer. They also showed that cavity temperature is higher than the outdoor temperature during winter, reducing the heat losses from the indoor space to the outdoor.

Research carried out on double skin facades has proven that there are crucial parameters to be taken into account when such a façade system is designed. Shameri et al [13] mentioned that the magnitude of energy reduction is dependent on the type of shading device, the glazing of the outer skin and the opening area of the cavity. Therefore, the design of the façade is critical for the highest energy reduction to be accomplished. Similarly, Barbosa et al. [14] emphasized the significance of the cavity geometry, the properties and type of shading, the properties of the outer skin's glazing, the inner skin's Window to Wall ratio (WWR) and the building's orientation for achieving optimum energy performance and thermal comfort quality.

Double skin facades are typically designed for modern glazed offices. However, the concept could be adopted as a refurbishment method for highly or partly glazed as well. The complexity of construction works would be simplified, as the inner skin would be preserved. Moreover, the useful inner floor area is not decreased either.

#### *1.1.3.2 Critical parameters of double skin facades*

***Cavity geometry***

The height and depth of the cavity as well as the size of the ventilation openings are the main geometry characteristics of a double façade. The depth of the cavity can vary from 0.2 m – 2m. Narrow cavities are considered to be better for heat extraction [14]. They enhance the stack effect and present higher air speeds, which give higher convection coefficients and larger heat removal. On the contrary the air speed decreases at deeper cavities resulting in more heat gain towards the adjacent zone. Larger openings give larger airflows and lower cavity temperatures [14]. High cavities can achieve stronger stack effect, due to increased thermal buoyancy force, resulting in larger airflow rates [14]. Air temperatures at tall cavities can be significantly high at the higher levels. In this case the adjacent zones can face severe overheating problems especially, in an event of poor air extraction [9].

***Glass***

Glass is one of the key components of double glass facades and its properties have a significant impact on the thermal behavior of the cavity. Outer skins with reflective or absorptive panes limit solar gains and result in lower airflow rates, as solar radiation is blocked before reaching the cavity consequently limiting the buoyancy force [14]. External skins with high solar transmittance allow penetration of solar gains during winter and enhance the ventilation of the cavity when combined with proper shading.

A glazing can transmit, absorb and reflect certain amounts of the total incident solar radiation. If $a$, $\tau$ and $r$ are the absorptance, transmittance and reflectance of a glazing respectively, the relationship between them is described as:

$$a + \tau + r = 1 \qquad \textit{( Equation 1.1)}$$

The portion of incident solar radiation transmitted through a glazed structure to the interior is called total solar transmittance or g-value. The g-value is defined as the sum of the directly transmitted solar radiation (due to the transmittance $\tau$ of the glazing) and the so called secondary or indirect transmittance, which is the portion of the absorbed solar radiation transferred to the interior space via the mechanisms of convection and longwave radiation. The secondary transmittance is highly affected by the ability of a pane to emit longwave radiation [9]. High secondary transmittance can be responsible for high temperature at the inner layer surface which can in turn be a reason for thermal discomfort.

The g-value is calculated for normal incident solar radiation (i.e. perpendicular to the window) and for specific environmental conditions that are specified in [15]. It should be noted that the g-value is a metric useful for comparing different glazing systems but it does not represent real time performance. Solar radiation is seldom ever normal on a façade system, while the transmittance ($\tau$) and reflectance ($r$) of a glazing are properties dependent on the angle of incidence of solar radiation, which consequently affects the direct transmittance. Moreover the environmental conditions vary continuously and thus, affect the secondary transmittance.

Heat gains through a glazing system can be useful for lowering the heating demand of a building, although they can be a potential cause of overheating. There are several ways to control the amount of solar gains through a glazing system. Solar control glazing can block solar radiation either by absorption or reflection. In addition, there are coatings, as the so called selective coatings, which provide high daylight transmittance while blocking invisible solar radiation (near infrared).

***Shading devices***

Solar protection devices integrated in the cavity play a double role for the performance of a ventilated façade. Heat penetration in the adjacent zone can be efficiently controlled by solar shadings that reflect or absorb solar radiation. Absorbing shading devices can lead to an increase of the air temperature in the cavity and result in higher ventilation rates, due to larger temperature differences between the cavity and the outdoor space. On the other hand, high shading temperatures can lead to non-comfortable inner pane temperatures due to longwave radiation exchange between the shading and inner skin.

Based on their position, shading devices could be categorized as follows:

- External shading: this is the most efficient way for reducing solar gains, since radiation is blocked before reaching the glazing system. Absorbed heat can be efficiently removed by convection as the shading is exposed to the outdoor air. However, weather exposure can cause maintenance problems.
- Internal Shading: this is the most inefficient way of solar control as solar radiation is already in the room when reaching the shading device. However internal shades are easily controlled by the users and have low maintenance need.
- Interstitial shading: this option performs better than internal shading but not as good an external one. Interstitial shading can be a potential reason for extremely high temperatures in the glazing cavity, which could in turn cause structural issues in the glazing unit. Nevertheless, the shading devices are protected from weather exposure, but still can have high maintenance costs.

Internal and interstitially positioned shading devices increase the secondary transmittance of a window system. Therefore, they can be a reason for thermal discomfort due to high radiant temperatures. This, of course, depends on the solar and thermal properties of the shading. Reflective devices combined with clear panes reject higher amount of solar radiation than absorptive devices.

Two of the most common shading devices used in double skin facades are venetian blinds and roller screens. Venetian blinds are angle dependent and can allow some view out while screens cover the window completely.

### 1.1.4 Solar systems

#### *1.1.4.1 General introduction*

The conversion of solar radiation into electricity is based on the photovoltaic effect. In this phenomenon the electrons of specific semi conducting materials are released from their atom bonds and are able to flow as current through an electricity circuit [16]. One of the most common semi conducting materials used for the production of solar cells is silicon.

Silicon based solar cells are classified into three main categories namely polycrystalline, monocrystalline and thin film. The main differences between them relate to the cell production process and their electricity conversion efficiency. Polycrystalline and monocrystalline cells are made from silicon ingots while thin films use amorphous silicon [17].

The amount of generated current depends on the intensity of incoming (absorbed) solar radiation and the electricity conversion efficiency of the semiconductor, i.e. the portion of the absorbed energy transformed into electricity. The efficiency of a solar cell decreases at high cell temperatures. Table 1.2 gives typical electricity conversion efficiencies for different types of solar cells [17] and Figure 1.4 shows the efficiency of a PV module as a function of temperature [18].

*Table 1.2: Electricity conversion efficiency for different cell types.*

| Cell Type | Electricity conversion efficiency (η) |
|---|---|
| monocrystalline | 16%-17% |
| polycrystalline | 14%-15% |
| thin film | 5%-7% |

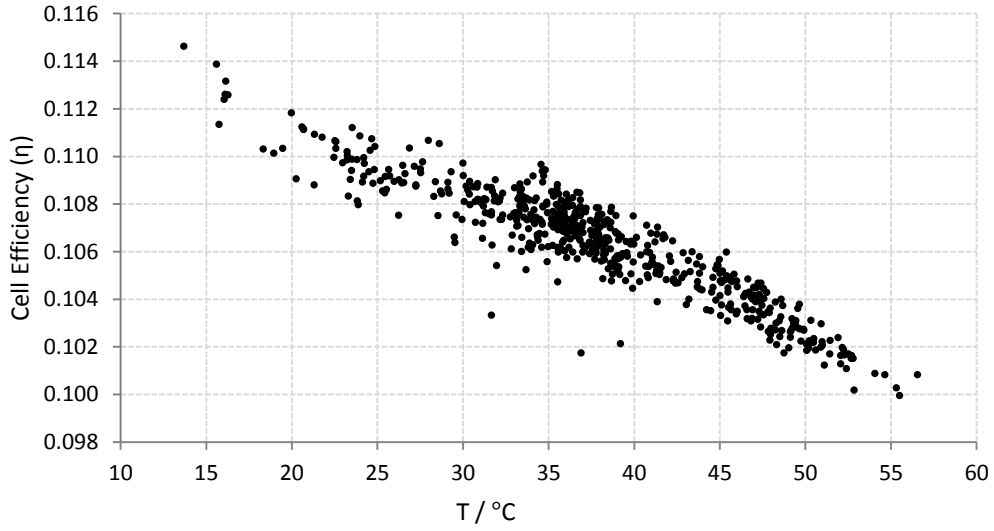


*Figure 1.4: Efficiency of a PV module as a function of temperature.*

Solar cells are connected in series in order to form PV modules. A standard module typically features 36 serially connected solar cells [16]. The electricity conversion efficiencies usually given by manufacturers are for standard test conditions (STC) or nominal cell operating temperature (NOCT) [19].

### *1.1.4.2 Building integrated photovoltaics*

The term Building Integrated Photovoltaics (BIPV) refers to a type of modules, designed for integration on the building envelope. Consequently BIPVs are considered a multifunctional element which provides electricity while replacing building envelope components.

Several ways of classifying BIPV products can be found in the existing literature. The products are classified according to the materials used for their construction (ex. PV foils), their design to imitate a building component (ex. roof tiles) or their application on specific building parts (ex. Façade systems or solar shading) [19].

One distinct type of BIPVs is solar cell glazing, usually also referred as semitransparent PV modules. The cells in semitransparent PV modules are mounted between two layers of glazing and an encapsulated sheet of Ethylene Vinyl Acetate (EVA). The spacing between the cells (usually 3mm -50mm) controls the amount of transmitted radiation and the module can act as a glazing and shading element at the same time. Typical dimensions of the solar cells integrated in solar cell glazing are 125mm · 125mm or 156mm · 156mm [19]. Jelle and Breivik [19] present several commercially available solar glazing products with different types of integrated cells and conversion efficiencies.

The solar properties of such systems are crucial, in terms of building energy performance. Solar glazing systems tend to decrease the cooling demand, while increasing the heating and lighting energy use. Chae et al [20] mentioned the significance of these parameters on optimizing the energy performance of a building where BIPVs are incorporated. They also indicated that the selection of the optimum solar properties depends highly on the location of the building. Olivieri et al [21] tested different semi-transparent PV cases with different solar properties and found that when they are integrated in medium and large WWRs, the energy savings have a magnitude of 18% to 59% compared to solar control glass. Therefore, BIPVs as a shading element could be beneficial for the energy use of the building. However, their solar properties should be appropriately selected, in order to achieve the required energy reduction.

Several methods and approaches can be found in the existing literature on the thermal modelling of semitransparent PV glazing. A main issue that usually arises is related to the calculation of the heat gain through a PV glazing, which is a highly significant factor for thermal simulations. Typically the g-value is calculated in window simulation software by applying the thermal and optical properties of the individual layers, which compose the PV element. However, there is quite an uncertainty on the chosen optical and thermal properties that correspond to the solar cells. Some authors and researchers use spectral optical properties to model the solar cells, obtained either by their own measurements [22] or by manufacturers for specific modules [23]. Others [24], [25] use weighted optical properties, without distinction in the spectrum part (visible or not), based on manufacturer's data.

It should be noted that the g-value of a PV window varies, depending on whether there is a load connected to the system or not. In the first case, a portion of the absorbed solar radiation is transformed into electricity and thus less heat is transmitted to the inside. In the latter, all of the absorbed radiation is transformed in heat and therefore the g – value of the PV window is higher. However, Chen et.al [26] measured the g-value of different semitransparent PV windows with and without load and found a relative decrease of the g-value between 3% - 6%. However, the actual values decrease was between 0.01 – 0.03, which was considered to be in the range of measurement uncertainty.

Meanwhile, many studies have investigated methods for cooling PV systems to maximize their efficiency, while some of them have been performed specifically for BIPV structures. Eldin et al [27] showed that inclined and naturally ventilated PVs, where buoyancy is the driving force of the airflow, could bring an increase of 8% at the efficiency of BIPVs. Similarly, Guohui et al [28] investigated different PV ventilated arrangements and different inclinations, concluding that ventilation is more beneficial for inclined PV arrangements than flat ones. Mirzaei et al [29] examined different cavity depths for ventilated façades with BIPVs and highlighted the significance of the air gap on improving the efficiency of the integrated PVs. Consequently, natural ventilation could be a way to cool the PV systems and improve their efficiency.

### 1.1.5 Thermal comfort

#### *1.1.5.1 General introduction*

According to [30], thermal comfort is "That condition of mind which expresses satisfaction with the thermal environment". The main parameters affecting the quality of thermal comfort are the air temperature of the room, the mean radiant and the operative temperature.

Thermal comfort assessments should take into account:

- The radiant energy exchange between the occupant and the surrounding surfaces, indicated by the mean radiant temperature. The radiant energy exchange is affected by the view angle between the occupant and the surfaces, which affects the thermal sensation. This is illustrated in Figure 1.5.
- The temperature of the air in the room.
- Operative temperatures, which are usually used in comfort assessments as they effectively combine air and radiant temperature. The operative temperature is defined as the uniform temperature of a radiantly black enclosure in which an occupant would exchange the same amount of heat by radiation and convection as in the actual non-uniform environment [31].

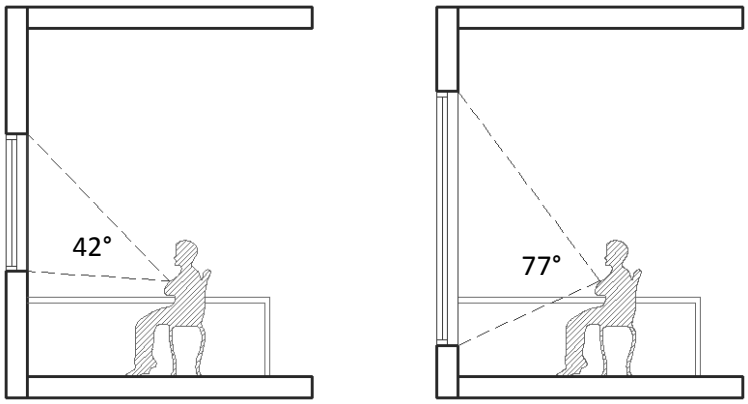


*Figure 1.5: View angle between window and occupant for a small (left) and a large (right) window.*

.

#### *1.1.5.2 Thermal comfort and glazing systems*

Occupants sitting close to either warm or cold surfaces, such as windows or walls, are likely to be affected more by the radiant temperature of the surfaces than by the air temperature of the room. Cold discomfort could be especially attributed to glazed surfaces which experience high heat losses and therefore have low surface temperatures. Low inner layer temperatures can be also a cause of local draughts due to air touching the cold window surface. High differences of the surface temperatures of a room can cause radiant asymmetries or non-uniform thermal radiation.

As mentioned in section 1.1.3.2, the type of shading protection is a potential reason for thermal discomfort. This depends on the shading's properties and especially its absorption of solar radiation. High absorption could result in high radiant temperatures. These effects are more critical in large window to wall ratios (WWR) due to larger view angles between the window and the occupant. Moreover, the secondary transmittance of a glazing system is of utmost importance for achieving comfortable inner layer temperatures as very high secondary

transmittance can lead to increased temperatures of the window system. The emittance of the inner surface is also crucial for the thermal comfort quality.

#### *1.1.5.3 Thermal comfort requirements for offices*

The current building regulations do not specify regulatory criteria for the thermal environment in office buildings. However, the FEBY standard suggests that the achieved operative temperatures fulfill one of the BELOK (Beställargruppen Lokaler) classes 24°C, 25°C, 26°C [7]. The value of the selected class should not be exceeded for more than the 10% of the operational hours between April and September.

With respect to the radiant temperatures, there are no standardized requirements set by the building standards in Sweden. Nevertheless the thermal comfort quality is improved when the radiant temperatures are closer to the required air temperatures.

## 1.2 Objectives

The main goals of this thesis are:

- To analyze the design parameters of a façade system comprised of a ventilated double skin facade with integrated photovoltaics.
- To evaluate the impact of such a system on the energy use and thermal comfort quality of a refurbished cell office with a 60's envelope construction in the climatic context of Southern Sweden.
- To evaluate the impact of the cavity ventilation on the performance of the integrated photovoltaics for the above climatic conditions.

Figure 1.6 shows the façade concept examined.

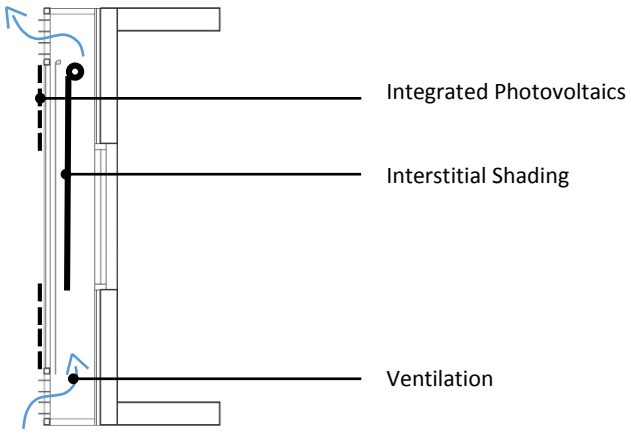


*Figure 1.6: Conceptual graph of the ventilated double skin façade with integrated PVs.*

The façade system performs as a thermal buffer zone during the heating dominated periods. On the other hand, during the cooling season, the cavity is ventilated for removing the unnecessary heat. A shading screen is integrated in the cavity. The external skin can be a solar cell glazing structure where the integrated cells perform as additional fixed shading while producing electricity. The ventilated cavity aims to improve the performance of the integrated cells via natural ventilation, during the periods with high outdoor temperatures.

On overall, the main research questions to be answered are:

- Can a ventilated double skin facade be an adequate refurbishment measure for improving the energy use and the thermal comfort quality of a typical cell office of the 60's to the current standards?
- Are integrated PVs beneficial as a fixed shading element to the thermal performance of the studied room?
- Can the natural ventilation of the cavity be beneficial for the performance of the integrated PVs?

## 1.3 Methodology

This study is divided in two parts. The first analyzes the different parameters of the ventilated façade with integrated PVs in terms of the energy use and thermal comfort performance of a single cell office. The second step analyzes the influence of naturally driven ventilation on the PV performance.

### 1.3.1 Structure of the thesis

Figure 1.7 shows a schematic structure of the thesis, along with the tools used.

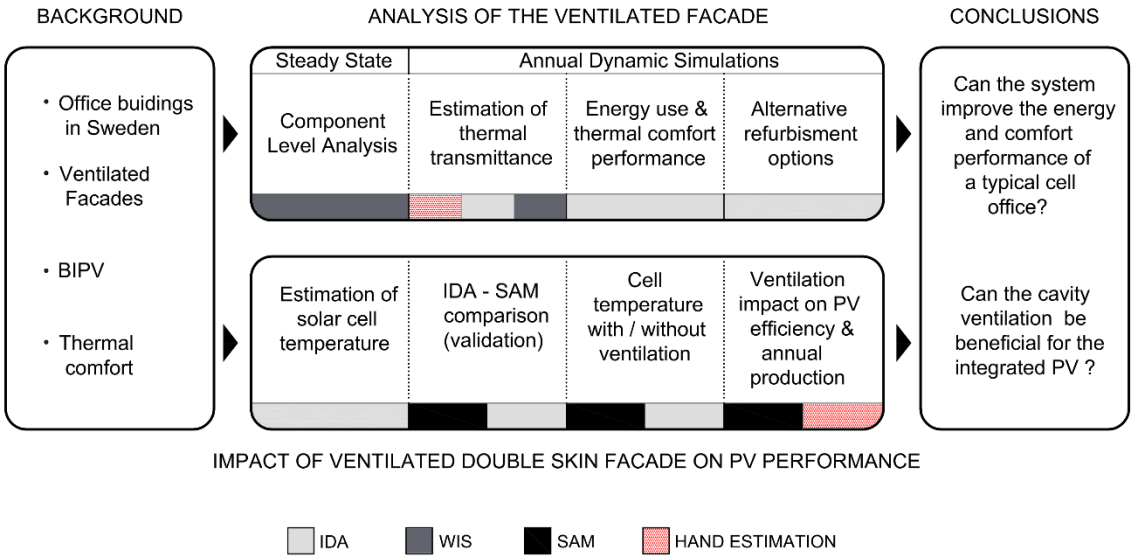


*Figure 1.7: Schematic structure of the thesis.*

#### *1.3.1.1 Analysis of the ventilated facade*

At first, the ventilated facade was analyzed as a component, on steady state simulations for winter and summer boundary conditions. The physical behavior of the system and the critical design parameters affecting its performance were identified.

The second step aimed to define the thermal transmittance of the system when this is applied as external skin of the chosen room. In addition, the simulation tool, used in the energy simulations, was evaluated. This step included annual dynamic simulations and excel based calculations of the annual heating demand of the room.

The third step included annual energy simulations of different double skin facade cases. The analysis was performed on the basis of the system's physical behavior, as well as in terms of heating and cooling energy demand and thermal comfort. The parameters examined were the window to wall ratio (WWR) on the inner skin, the type of external glazing, the inner wall cladding, the type of shading, the amount of photovoltaic ratio on the outer skin (PVR) and the geometrical characteristics of the cavity. The studies were performed for four orientations (south, east, west, and north).

At the forth step, the performance of the best ventilated configurations was examined in comparison to an alternative base case with a better initial window and one alternative refurbishment method chosen for each examined WWR.

#### *1.3.1.2 Impact of natural ventilation on PV performance*

A methodology was developed in order to estimate the temperature of the integrated PV cells on an hourly basis. In order to evaluate the method, the results were compared with hourly temperatures calculated with a PV simulation software, for a BIPV structure at the same climatic conditions. After the method was evaluated, the annual electricity output was calculated, for a ventilated and a non - ventilated cavity. The impact of ventilation on the PVs' efficiency and its relationship with the cell temperature were examined.

### 1.3.2 Simulation tools

Three different simulation tools were used throughout this study. Two of them (Window Information System -WIS and IDA-ICE Indoor Climate and Energy – IDA-ICE) have integrated models for evaluating the performance of ventilated facade systems. The third software (System Advisor Model – SAM) performs analyses of solar energy systems. In addition, several own developed methods for estimations and calculations were used along with Excel based calculations. A brief description of the simulation tools is given below.

#### *1.3.2.1 Window Information System - WIS*

WIS [32] is a simulation software for evaluating the solar and thermal performance of different window systems. Input consists of thermal, solar and optical properties of panes and shading layers as well as thermal properties of frame and spacers within glazed cavities. Boundary conditions for indoor and outdoor air and radiant temperatures, internal and external convection coefficients and external direct irradiation on the façade have to be set.

Output consists of overall and center of glass thermal transmittance of a window system, overall solar transmittance (g – value), primary and secondary solar transmittance as well as visible transmittance. Natural ventilation due to buoyancy can be simulated as well as forced ventilation based on the equations described in [33] and [15]. The program cannot perform dynamic simulations.

#### *1.3.2.2 IDA-ICE indoor Climate and Energy – IDA-ICE 4.6.2*

IDA-ICE [34] was used for annual energy and thermal comfort simulations of different ventilated cases. The software is a dynamic simulation program, offering the opportunity for a detailed analysis of thermal comfort and energy use of a building. The software handles simultaneously building design factors as shape, envelope, glazing and shading, HVAC systems, lighting and control systems for shading devices, window openings etc. It provides

detailed results on the energy use and on the parameters affecting the thermal behavior of the studied cases.

The integrated double façade model in IDA-ICE is based on specified leakage areas at the top and bottom of a window system. The leakages represent the systems openings and the airflow through them is based on air pressure differences between the façade cavity and the external environment. It should be noted that the program accounts only for thermally driven airflow through the cavity and any wind effects are not considered. The temperature in the cavity and at the different layers is based on heat balance equations, while the program has a detailed window model partly based on [34].

#### *1.3.2.3 System Advisor Model – SAM*

System Advisor Model (SAM) [35] is a software developed from the National Renewable Energy Laboratory (NREL) and can be used for the calculation of performance parameters and costs of different solar energy systems including solar thermal and photovoltaics. The program offers four different calculation models for the performance of photovoltaic systems. Three of these are based on parameters given for specific modules and therefore require detailed input. The forth one is more general and is based on typical conversion efficiencies and empirical coefficients accounting for the temperature dependency of the PV cells efficiency. This method is the least accurate but can be used for preliminary analyses when a specific type of module has not yet been chosen [36]. This method was preferred as the aim of this study was to evaluate the relative impact of different parameters on the annual electricity output rather than calculate a detailed PV performance.

## 1.4 Scope and limitations

### 1.4.1 Scope

Due to a limited amount of time, only a ventilated box façade was analyzed. Consequently, the results of this study are valid for such a façade type and not for multi-storey cavities. The performance of the chosen room was analyzed only in terms of energy for heating and cooling as well as for thermal comfort quality. Daylight aspects were not considered. The energy use for lighting, however, was checked from time to time in order not to neglect any significant increase of it due to the different choices taken through the parametric studies. Possible moisture and/or condensation issues were not examined as well as no specific structural details of the examined system were designed. A cost or environmental performance analysis was not conducted in this thesis.

### 1.4.2 Software limitations

Due to specific software issues in IDA – ICE, it was not possible to simulate a façade with a low emittance coating on the inside surface without simultaneously changing the emittance of the integrated shading device. This means that all simulations including a low emittance (low – E) coating on the façade were performed for one type of shading device (reflective) which comes from the manufacturer with a low - E surface. All other examined shadings were combined with low – Iron glass.

The PVs integrated on the outer skin of the ventilated facade where modeled as an exterior shading screen in IDA-ICE. The shading takes as input only a transmittance factor (transparency) and not all specific solar properties such as absorptance and reflectance.

### 1.4.3 Limitations on photovoltaic simulations

There was lack of data concerning the spectral distribution of the solar properties of the integrated photovoltaics. Contact with the industry did not provide such information, so general values found in existing literature were used instead. This fact limits the study to only one type of module where the semitransparency is obtained from the gaps between the cells. The temperature stratification of the air in the cavity (i.e. that air at the top is warmer than in the middle or the bottom) was not taken into account for the calculation of the solar cell temperature. Instead the average cavity air temperature was considered in the heat balance equations and consequently the solar cell temperature.

## 1.5 Contributions

The steady state simulations and the calculations of the overall thermal transmittance of the ventilated façade were performed by Ioannis. All annual dynamic simulations, the estimation of solar cell temperatures and the annual electricity output were performed by both Evangelia and Ioannis. All the methods and simulation approaches presented in this thesis were decided after discussion of both Evangelia and Ioannis. All results and conclusions were discussed and analyzed equally by both team members.

# 2 Analysis of the ventilated façade

This chapter gives information on the different simulations performed in order to analyze the performance of the ventilated box façade in terms of energy use and thermal comfort. In section 2.1, a brief description of the climate file used in this study is given. A description of the geometry and construction characteristics of the chosen room as well as the parameters held constant in the simulations are given in sections 2.2 and 2.3 respectively. The different parameters examined in this study are presented in detail in section 2.4. The performance of the ventilated façade was analyzed on a component level through steady state simulations performed in WIS and in annual dynamic simulations performed in IDA-ICE. Detailed information regarding the setup of these simulations (steady state and annual) are given in sections 2.5 and 2.6 respectively.

## 2.1 Climate

The location of the study is Malmö. A weather file from the ASHRAE IWEC 1.1 [37] database for Copenhagen was used in the simulations, due to lack of specific climatic data for Malmö. Figure 2.1 shows the daily outdoor temperature for Copenhagen during the whole year. Figure 2.2 gives the monthly cumulative solar radiation (sum of direct, diffused and ground reflected solar radiation) incident on a vertical surface for south, east, west and north orientations.


*Figure 2.1: Hourly outdoor dry bulb temperature through the year for Copenhagen.*

The above graph indicates a cold climate as the outdoor dry bulb temperature is lower than 10°C for a long period of the year. The amount of time with outdoor temperatures below 0°C is high. For a considerable part of the year the outdoor dry bulb temperature remains between 10°C – 20°C. The period with high temperatures (> 20 °C) is low.

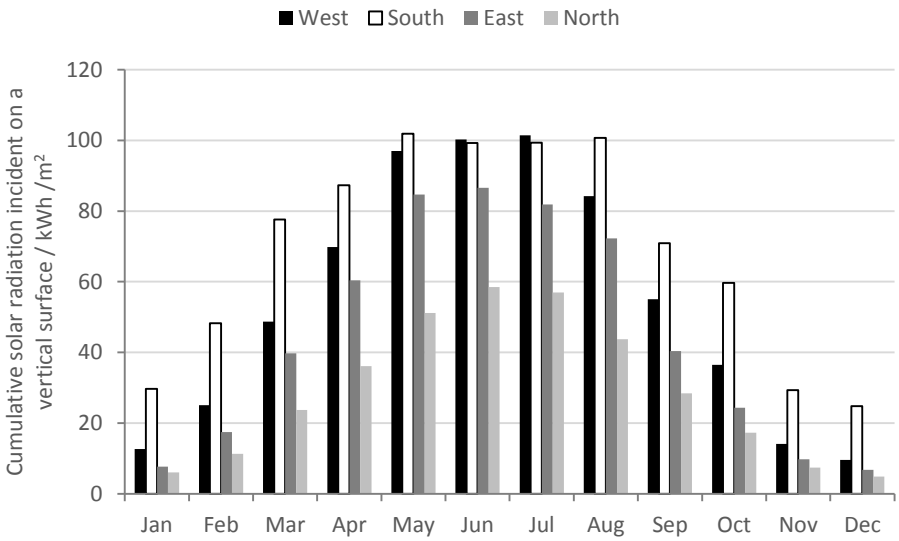


*Figure 2.2 Accumulative monthly incident solar radiation on a vertical surface for different orientations.*

East and west orientations receive similar amount of energy during January, November and December. During May, June and July the cumulative values are similar for south and west orientations. In general, the south oriented facades receive considerably higher solar radiation than the rest of the orientations, especially during the colder months (October - December and January – February, the radiation is more than 50% higher than the rest of the orientations). North façades receive the lowest amount of irradiation. Interesting to note that for November, December and January, north and east facades receive almost the same amount of energy.

## 2.2 Base case description

The room of the study was a typical single cell office. The dimensions of the room were based on [9]. Figure 2.3 shows a plan view and a section of the studied room. As can be seen (red dashed line) the room had only one surface exposed to the outdoor conditions.

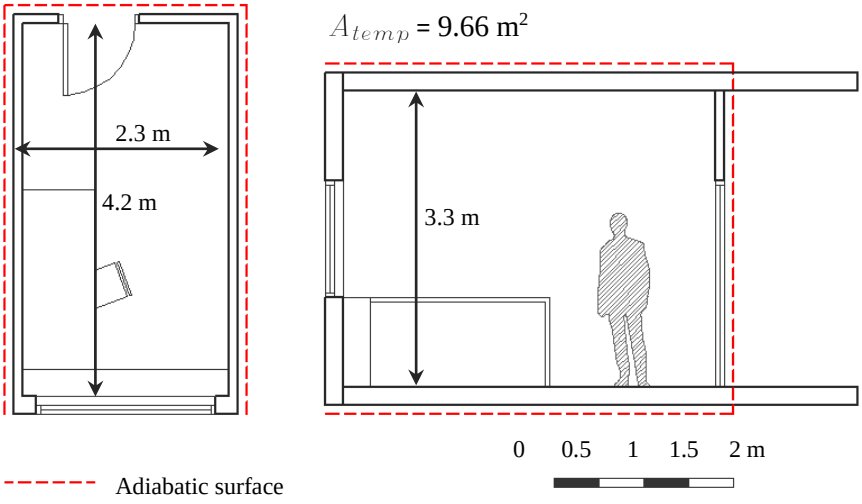


*Figure 2.3: Plan (left) and section (right) of base case room. The red dashed line notes the surfaces that are not exposed to the outdoor conditions.*

### 2.2.1 External wall

The external wall construction was based on the report "Stomkonstruktioner I moderna kontorhus" [38]. The report describes different office buildings built in the 60's and gives construction details of the external wall for some of the presented cases. The wall construction shown in Table 2.1 was chosen for the base case, as it was the construction type with the clearest information on the dimensions of the different layers.

*Table 2.1: Base case exterior wall construction.*

| Layer | Thermal conductivity λ / (W/(mK)) | Thickness d / m | R-value / ($(m^2K)/W$) |
|---|---|---|---|
| | | | $R_{se}$ = 0.04 |
| Lightweight concrete | 0.38 | 0.065 | 0.171 |
| EPS | 0.04 | 0.05 | 1.25 |
| Air gap | 0.2 | 0.02 | 0.1 |
| Clear float cladding | 1.05 | 0.004 | 0.004 |
| | | | $R_{si}$ = 0.13 |
| | | Total R-value | 1.695 |
| | | U-value/ ($W/(m^2K)$) | 0.589 |

### 2.2.2 Window and shading

A double glazed window was assumed for the base case as shown in Table 2.2. The U-value of the chosen window corresponds to the requirements of the Swedish Building Code of 1967 [39]. The terms $g_{eff}$ and $U_{eff}$ describe the total solar transmittance and the thermal transmittance of the window respectively when the shading device is applied.

*Table 2.2: Base case window construction with solar and thermal properties.*

| Outer pane | Gap | Inner pane | Shading | g | Tsol | Ug ($W/(m^2K)$) | $g_{eff}$ | $Tsol_{eff}$ | $Ug_{eff}$/ ($W/(m^2K)$) |
|---|---|---|---|---|---|---|---|---|---|
| 6mm clear | 13mm | 6mm clear | reflective screen | 0.71 | 0.604 | 2.81 | 0.249 | 0.038 | 1.24 |

An internal reflective shading screen was assumed as solar protection for the base case room. Since the shading was chosen to be placed in the room, it was assumed that a reflective screen would reject as much solar radiation as possible. Detailed solar and thermal properties for the shading device assumed for the base are given in section 2.4.3 in Table 2.7 under the term reflective shading. The shading was used when the room air temperature exceeded 24.5°C.

The frame U-value was set to 3 $W/m^2K$ including the external and internal film coefficients. Two different window to wall ratios (WWR) were assumed, namely 30% and 70%. The frame corresponds to 32 % of the window area on the case of 30% WWR and 24% in the case of 70% WWR. Figure 2.4 shows the assumed dimensions and the position of the windows on the façade and notes the overall thermal transmittance including wall, window and frame for the two WWR. A detailed calculation of the overall thermal transmittance is given in Appendix E. It should be noted that the actual dimensions presented in the graph result in 34% and 69% WWR but the ratios are referred to in the thesis as the approximated values of 30% and 70%. However, all calculations in terms of overall U-values etc. were performed on the basis of the presented dimensions.

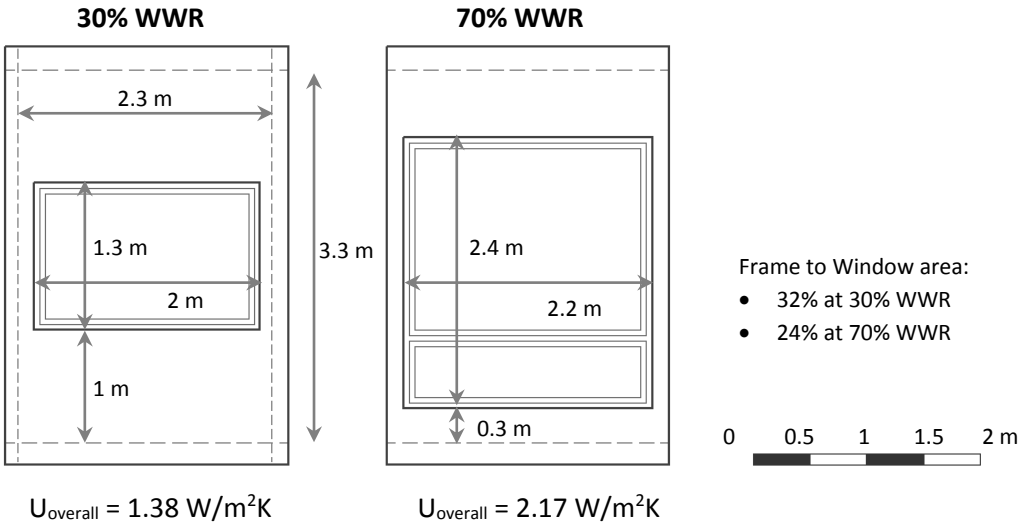


*Figure 2.4: Window position on the façade with dimensions for 30% and 70% WWR.*

### 2.2.3 Internal floors and partition walls

The interior floors were assumed to be made of dense concrete. Table 2.3 shows the floor construction along with its main thermal properties.

*Table 2.3: Floor construction of base case.*

| Material | Thickness / m | $C_p$ / (J/(kg K)) | ρ /( kg/m$^3$) | λ / (W/(mK)) |
|---|---|---|---|---|
| linoleum | 0.002 | 1260 | 1200 | 0.156 |
| Dense concrete | 0.18 | 840 | 2100 | 1.4 |

Table 2.4 shows the construction assumed for the internal partition walls.

*Table 2.4: Internal partition construction of the base case.*

| Material | Thickness / m | $C_p$ / (J/(kg K)) | ρ /( kg/m$^3$) | λ / (W/(mK)) |
|---|---|---|---|---|
| Plasterboard | 0.015 | 1000 | 900 | 0.25 |
| Light insulation | 0.18 | 750 | 20 | 0.036 |
| Plasterboard | 0.015 | 1000 | 900 | 0.25 |

## 2.3 Constant parameters

This section gives a brief description of the parameters held constant in the IDA-ICE simulations.

### 2.3.1 Occupancy

The studied typical cell office was occupied by one person. The activity level was set to 1 MET, which corresponds to approximately 100 W of heat loss from the occupant [40]. The room was assumed to be fully occupied during weekdays between 08:00 and 12:00 a.m. and between13:00 and 18:00 p.m. During July 50% of the occupancy was assumed.

### 2.3.2 Heating and cooling

An “ideal heater” and “ideal cooler” were assumed as the devices for heating and cooling the room in IDA-ICE. The maximum power for the heater was 0.955 kW and for the cooler 2 kW. The heating setpoint was set to 22°C during occupied hours and at 18°C during non-occupied times. The cooling setpoint was set to 25°C during occupancy time while no setback temperature was assumed during the unoccupied hours.

### 2.3.3 Lighting and equipment

The room was assumed equipped with one computer of 125 W and one telephone device of 10W according to [41]. The equipment were assumed to operate at full power (100%) during the occupied hours and at 15% of the nominal power during non-occupied hours according to [41].

Internal heat gains from lighting were set to 10W/m$^2$ according to [41]. Efficient lighting devices were assumed with a luminous efficacy of 47 lm/W. The lights were assumed to operate between 08:00 – 12:00 and 13:00 – 18:00. The light output was controlled according to the available daylight. When the work plane illuminance was below 200 lux the lights were set on nominal power. When the work plane illuminance exceeded 500 lux the lights were turned off. With daylight levels between these limits (200 lux – 500 lux) the lights were dimmed in order to deliver a work plane illuminance of 500lux.

### 2.3.4 Ventilation and infiltration

The ventilation airflow supplied to the room was set to 1.1 l/s per m$^2$ of heated floor area during the occupied hours. This value corresponds to 10 l/s per person, which is a typical ventilation rate for office premises according to [41]. During non-occupied hours the fan was assumed to operate at 35% of its maximum speed (i.e. when delivering 1.1 l/s per m$^2$ of heated floor area) in order to provide a minimum airflow of 0.35 l/s per m$^2$ of heated floor area.

The supply air temperature varied between 19°C and 17°C depending on the outdoor temperature based on [9].

Figure 2.5 shows the relation between supply air temperature and outdoor dry bulb temperature.

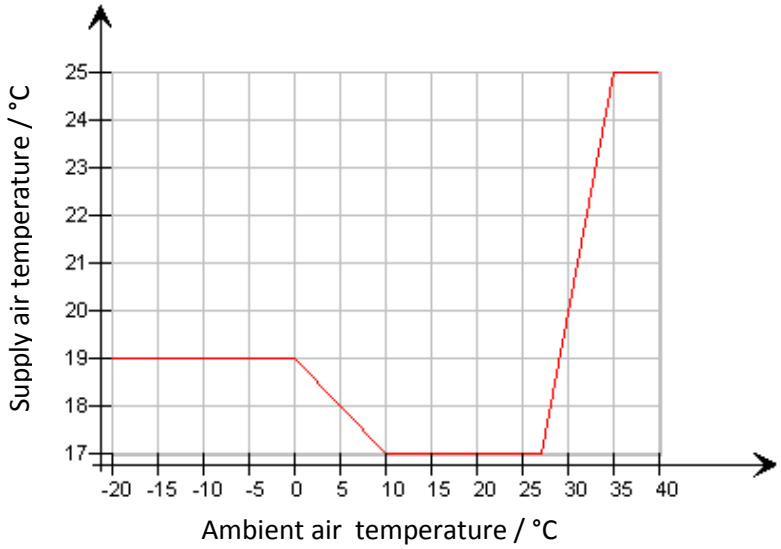


*Figure 2.5: Ventilation supply air temperature as a function of outdoor air temperature.*

The infiltration rate was set to 1.6 l/s per m$^2$ of external wall area at 50Pa, based on the BBR 19 requirements [42].

Table 2.5 summarizes the parameters held constant in IDA – ICE.

*Table 2.5: The main input settings in IDA-ICE.*

| | |
|---|---|
| Heating setpoint/setback | 22°C / 18°C |
| Cooling setpoint/setback | 25°C / none |
| Number of occupants | 1 |
| Occupancy schedule | Weekdays:100%<br>July: 50%<br>Period:08:00 – 12:00 and 13:00 – 18:00 |
| Internal gains from equipment | 1 computer:125 W, 1 telephone:10 W |
| Equipment schedule | During occupied hours: 100%<br>During unoccupied hours: 15% |
| Internal gains from lighting | 10W/$m^2$ |
| Lighting Schedule | Weekdays: 08:00 – 12:00 and 13:00 – 18:00 |
| Lighting Control | Proportional dimming from 100% at 200 lux to 0% at 500 lux |
| Ventilation rate | 10 l/sec per person at occupied time<br>0.35 l/sec per $m^2$ of heated area at non-occupied hours |
| Infiltration | 1.6 l/s per $m^2$ of external wall area at 50Pa |

## 2.4 Variables

This section describes all the parameters examined in the thesis in order to analyze the performance of the ventilated façade on a component level (studies in WIS) and in annual energy and thermal comfort simulations (IDA-ICE simulations).

At first, the performance of the ventilated façade was analyzed in combination with the double clear window of the base case as described in section 2.2. This part involves both steady state and dynamic annual simulations. The variables related to these studies are described in sections 2.4.1 – 2.4.6.

Thereafter the performance of the façade was examined for an alternative initial window and with the option of improving the performance of the room with a highly insulated triple glazed unit (TGU). This part involves only dynamic annual simulations in IDA – ICE. The parameters related to these studies are described in sections 2.4.7 and 2.4.8.

Figure 2.6 shows a section of the façade where all the varied parameters are noted.

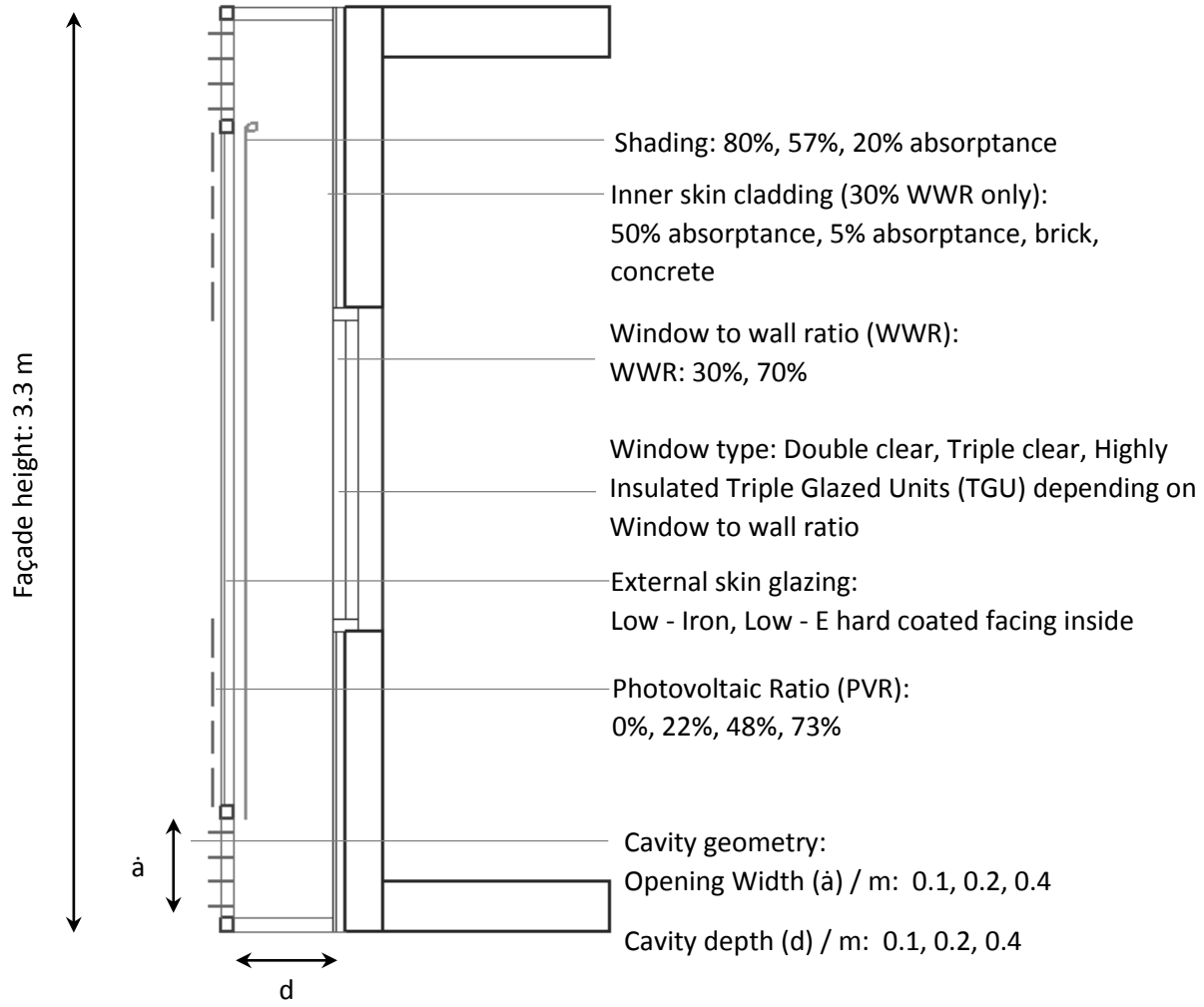


*Figure 2.6: Parameters examined for the analysis of the ventilated façade.*

### 2.4.1 Window to wall ratio

Two window to wall ratios (WWR) were examined namely 30% and 70% WWR. The frame to window ratio corresponds to 32% for the 30% WWR and to 24% for the 70% WWR. The dimensions assumed for the windows were presented in Figure 2.4 and result in 34% and 69% WWR. However, the ratios are referred to in the thesis as the approximated values of 30% and 70%. Detailed properties of the window are given in section 2.2.2 for the base case and in sections 2.4.7 and 2.4.8 for the alternative refurbishment options.

### 2.4.2 External skin glazing

Two types of glazing were chosen to be studied for the external skin. The first is a low-iron glass, which will maximize solar gains in the room and the cavity depending on the WWR. The second is an insulating glazing with a low emittance hard coating facing the cavity. The main aim of this choice was to provide insulation by reducing radiation losses from the whole façade (window, wall and frame) without affecting the initial window.

Table 2.6 summarizes the main thermal and solar properties of the glazings used as external skins. The resulting solar and thermal transmittances when these skins are combined with the window of the base case are also shown. The presented thermal transmittances are only relevant

for the improvement of the U-value of the glazed parts of the base case and not the whole façade including wall and frame.

*Table 2.6: Outer skin glazings examined. External skin properties for each glazing as well as in combination with the base case double clear window.*

| | | External skin properties | | | | | Overall properties in combination with base case window (double clear) | | |
|---|---|---|---|---|---|---|---|---|---|
| | | Solar | | | Thermal | | Solar | | Ug ($W/(m^2K)$) |
| Name | Type | $\tau$ | $r_f$ | $r_b$ | $\varepsilon_f$ | $\varepsilon_b$ | g | $T_{sol}$ | |
| Optiwhite | 6mm low-Iron glass | 0.88 | 0.08 | 0.08 | 0.84 | 0.84 | 0.69 | 0.54 | 1.81 |
| K – glass | 6mm low-E hard coated | 0.68 | 0.11 | 0.09 | 0.84 | 0.16 | 0.54 | 0.41 | 1.34 |

### 2.4.3 Shading devices

Three types of shading devices were examined. For the base case, the shading was assumed to be positioned in the room, while for all ventilated facades the shading was positioned in the ventilated cavity. The shadings were chosen to have similar solar transmission ($\tau$), but different solar absorption ($\alpha$). Higher absorption is expected to increase the ventilation rate in the cavity and consequently affect the energy use for cooling and the quality of thermal comfort.

Table 2.7 summarizes the main thermal and solar properties of the shading devices examined, as well as the resulting effective solar transmittance values ($g_{eff}$) when the window of the base case (double clear) is combined with the low-Iron and the low–E external skins. The presented effective solar transmittances do not include ventilation effects that would reduce the g-value of the system. It can be noted that the solar absorption increases significantly from the first shading to the third.

*Table 2.7: Shading devices of the study and their properties.*

| Shading type | Shading properties | | | | |
|---|---|---|---|---|---|
| | Solar | | | Thermal | |
| | $\tau$ | $r_f$ | $r_b$ | $\varepsilon_f$ | $\varepsilon_b$ |
| 20% Absorptance | 0.058 | 0.74 | 0.68 | 0.16 | 0.83 |
| 57% Absorptance | 0.04 | 0.39 | 0.39 | 0.85 | 0.85 |
| 85% Absorptance | 0.0558 | 0.086 | 0.248 | 0.87 | 0.87 |

Table 2.8 summarizes the solar and thermal properties of the ventilated options resulting from the combination of the above shadings with the low-Iron and low-E external skins, presented in section 2.4.3. The initial window (double clear) properties are also included.

*Table 2.8: Solar and thermal properties of the examined external skins in combination with a double clear initial window and different shadings.*

| | g | Tsol | Ug (W/(m2K)) | $g_{eff}$ | $Tsol_{eff}$ | $Ug_{eff}$ (W/(m2K)) |
|---|---|---|---|---|---|---|
| double clear + Reflective shading | 0.71 | 0.604 | 2.81 | 0.249 | 0.038 | 1.24 |
| low-Iron + Reflective shading + double clear | 0.69 | 0.54 | 1.81 | 0.139 | 0.036 | 0.994 |
| low-Iron + Medium Absorptive shading + double clear | | | | 0.17 | 0.023 | 1.335 |
| low-Iron + Absorptive shading + double clear | | | | 0.21 | 0.031 | 1.347 |
| low-E + Reflective shading + double clear | 0.54 | 0.41 | 1.34 | 0.121 | 0.027 | 0.928 |
| low-E + Medium Absorptive shading + double clear | | | | 0.179 | 0.017 | 1 |
| low-E + Absorptive shading + double clear | | | | 0.218 | 0.023 | 1.012 |

For all examined cases, the shading device was controlled by the air temperature of the room. The setpoint was assumed to be $T_{air,room}$= 24.5°C. This setpoint was chosen in order for the shading to be used when the room was almost in need for cooling as the cooling setpoint was set to $T_{air,room}$ = 25 °C (see section 2.3.2).

### 2.4.4 Geometry

#### *2.4.4.1 Cavity depth and opening height*

The main geometry characteristics of a ventilated façade are the height and width of the cavity as well as cavity depth and the size of the openings. As this study examined only ventilated box facades, positioned outside of the base case room the focus was only on the cavity depth and opening. The façade height was constant at 3.3 m and the façade width was set at 2.3 m. The openings of the façade were assumed to have equal length with the façade's width (2.3 m), and therefore only the opening height was varied, with respect to the openings' dimensions.

For all simulations performed in IDA-ICE, three cavity depths and openings were examined namely 0.1m, 0.2m and 0.4m. The ratio between the opening height and cavity depth was set to 1, i.e. equal cavity depth and opening height.

For the steady state simulations on a component level, a cavity depth and opening of 0.05 m was additionally examined. Two ratios between the opening height and cavity depth were studied namely 0.5 and to 1, which means openings equal to half of the façade depth and openings equal to the façade depth.

The openings of a box façade are typically positioned on the lower and upper part of the front face (Figure 2.6). However, both IDA-ICE and WIS assume the openings at the top and bottom horizontal planes of the façade as is illustrated in Figure 2.7. This means that the maximum

opening width (or height) can be equal to the cavity depth, i.e. the maximum ratio between the opening height and cavity depth is 1.

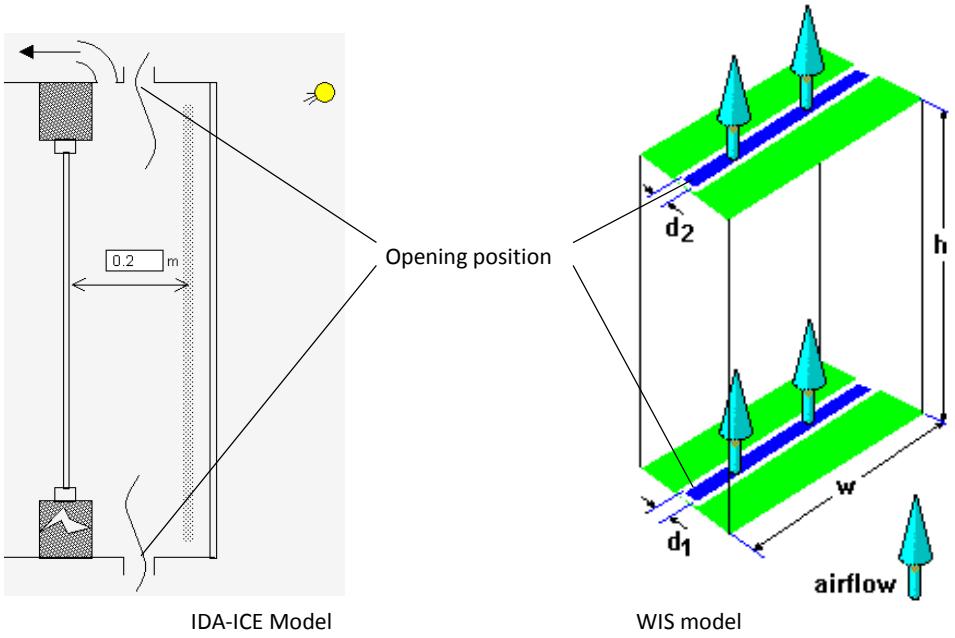


*Figure 2.7: Position of the openings in the Double Facade model of IDA – ICE and in WIS.*

### *2.4.4.2 Discharge Coefficient*

The airflow is discharged when entering or exiting the cavity due to pressure differences and friction losses. In order to calculate the airflow entering and leaving the cavity a discharge coefficient ($C_d$) has to be considered.

Typically, the discharge coefficient is calculated as the product of the contraction coefficient ($C_c$), which represents the decrease of the area of the air jet when it enters the cavity (usually found between 0.6-0.65) [43], and the velocity coefficient ($C_v$), which corresponds to the reduction of the air flow velocity due to friction losses (normally between 0.95-0.99) [43].

In all IDA-ICE simulations, the openings were defined as leakages positioned at the top and bottom horizontal planes of the façade. The area of the openings is defined in terms of Equivalent Leakage Area (ELA) which equals:

$$ELA = A_{open} \cdot C_d = L \cdot \dot{a} \cdot C_d \quad [9] \qquad \textit{( Equation 2. 1)}$$

Where: $A_{open}$ is the area of the opening, $L$ is the length of the cavity, $\dot{a}$ is the height of the opening (which is equal to the cavity depth) and $C_d$ is the discharge coefficient, which was assumed equal to 0.65 for the upper opening and 0.55 for the lower opening based on [9]. Table 2.9 shows the equivalent leakage area (ELA) corresponding to each cavity opening.

*Table 2.9: Depth and equivalent leakage area at the top and bottom of the cavity.*

| **Depth / m** | **$ELA_{top}$ / $m^2$** | **$ELA_{bottom}$ / $m^2$** |
|---|---|---|
| 0.1 | 0.15 | 0.127 |
| 0.2 | 0.299 | 0.253 |
| 0.4 | 0.598 | 0.506 |

The openings were controlled by dampers, which opened and allowed for airflow to enter when the air temperature of the room exceeded 24.5 °C. For lower air temperatures the cavity

remained closed in order to perform as a thermal buffer zone. In this case a minimum leakage area of 0.01m$^2$ was always assumed as the cavity is never completely sealed.

The discharge coefficient in WIS is assumed to be equal to 0.6. Consequently, this value was assumed for the studies performed on a component level. A detailed calculation of the airflow across the openings and through the cavity in WIS, can be found in Appendix D.

### 2.4.5 Inner wall cladding

In order to study the influence of the inner wall cladding on the performance of the ventilated façade, four different types of materials with different solar properties and thermal capacities were considered. The materials were studied only for the room with 30% WWR as the larger wall area would demonstrate more clearly any effects of the inner wall cladding on the thermal performance of the façade, than the 70% WWR. A brief description of the examined material is given below:

- Base case cladding
  The cladding of the base case has a significant solar absorptance (50%) and a low thermal capacity as it is a very thin layer (see also section 2.2.1).
- Reflective cladding
  This cladding option has similar thermal capacity as the base case but a solar absorptance of 5%. This choice may be unrealistic but it would demonstrate the importance of the solar absorption properties for the cavity temperature rise.
- Concrete Cladding
  Concrete is a material with high thermal capacity. It can absorb heat during sunny mornings and release it during night when the outside air temperature is lower. The released heat will keep the cavity warmer and thus reduce heat losses at a time of the day with low outdoor temperatures.
- Brick Cladding
  Brick has similar behavior with concrete but also has lower thermal conductivity.

Concrete and especially brick are materials typically used in Sweden as external wall claddings.

Table 2.10 summarizes the properties of the examined inner skins, for the 30% WWR, which corresponds to a surface of 5m$^2$. The properties were based on [44]. The resulting thermal transmittance of the external wall with the different materials is also presented.

*Table 2.10: Thermal and solar properties of the examined Inner skin claddings.*

| Exterior cladding | Absorptance (α) | d / m | λ / (W/(mK)) | Wall U -value (W/m$^2$K) | Cp / (J/(kg K)) | ρ / (kg/m$^3$) | Thermal mass / (J/K) |
|---|---|---|---|---|---|---|---|
| Base Case | 0.5 | 0.004 | 1.05 | 0.59 | 750 | 2500 | 37500 |
| Reflective | 0.05 | 0.004 | 1.05 | 0.59 | 750 | 2500 | 37500 |
| Brick | 0.7 | 0.09 | 0.42 | 0.525 | 1400 | 936 | 589680 |
| Concrete | 0.6 | 0.06 | 1.7 | 0.58 | 900 | 2300 | 621000 |

### 2.4.6 Photovoltaic ratio

Three different Photovoltaic ratios (PVR), namely 22%, 48% and 73%, were modelled. All simulations that included PV integration were performed in IDA-ICE. The cell dimensions were assumed equal to 0.156m · 0.156m [19]. The cells were assumed to be integrated at the upper and lower part of the external skin in order to always allow for an open viewing area. Figure 2.8 presents the different PVR studied as well as the position of the cells on the façade. The PVR amount is calculated as a percentage of cell coverage on each of the areas available for PV integration.

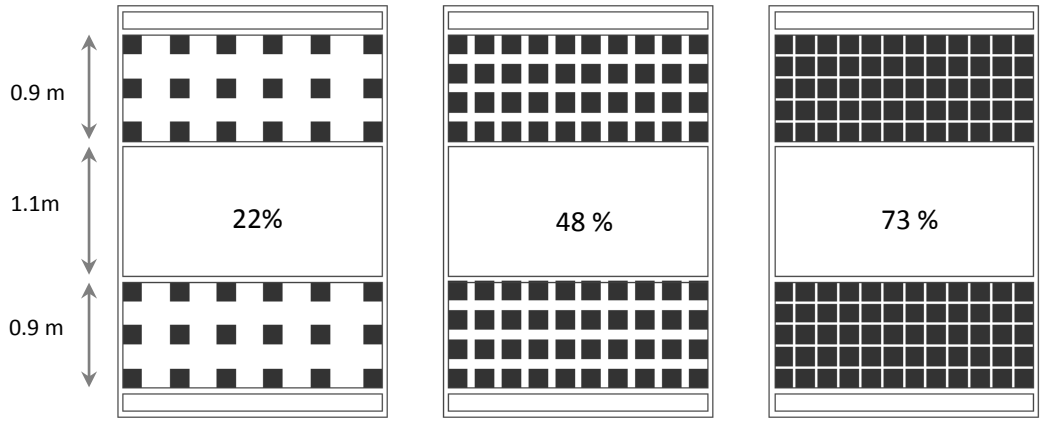


*Figure 2.8: PV coverage ratio cases.*

The solar cells were assumed integrated on the façade with the low–Iron external skin as this type of glazing is typically used in photovoltaic modules in order to maximize the transmission of solar radiation. A description of the main assumptions for calculating the total solar transmittance of the outer skin at the parts with the integrated solar cells and the modelling of the integrated cells in IDA-ICE is given in the following sections.

#### *2.4.6.1 Total solar transmittance of the photovoltaic glazing*

Figure 2.9 illustrates the structural setup assumed for the parts of the facade with integrated solar cells and the main assumptions for the irradiation passage through the semitransparent PV glazing.

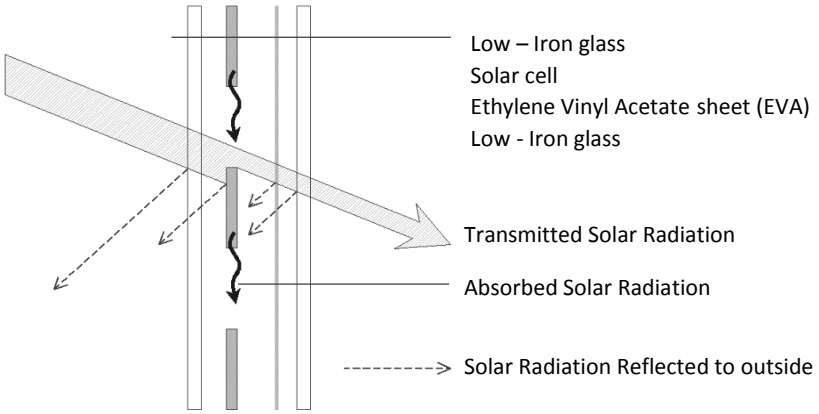


*Figure 2.9: Structural setup of the module and irradiation passage through the PV.*

The total solar transmittance (g-value) of the parts with integrated solar cells was calculated based on the thermal and solar properties of each layer, presented by [25]. The properties are presented in Table 2.11

*Table 2.11: Properties of the layers of a semitransparent PV module.*

| Layer | r | τ | α | d/mm | λ / (W/(m·K)) | R /((m²K)/W) |
|---|---|---|---|---|---|---|
| Low-Iron glass | 0.082 | 0.81 | 0.108 | 6 | 1 | 0.006 |
| Silicon cell | 0.03 | - | 0.97 | 0.3 | 168 | $1.8 \cdot 10^{-6}$ |
| Ethylene Vinyl Acetate (EVA) | 0.04 | 0.9 | 0.06 | 1.8 | 0.116 | 0.015 |
| Low-Iron glass | 0.082 | 0.81 | 0.108 | 6 | 1 | 0.006 |
| Summation | - | - | - | 14.1 | - | 0.027 |

The main part of incident solar radiation on the module will be transmitted through the external low - Iron glass, a part will be reflected while, a small amount will be absorbed in the first layer. The transmitted portion will thereafter be absorbed in, reflected back or transmitted through the second layer of silicon cell and the Ethylene vinyl acetate sheet (EVA). The higher the PVR on the module, the higher the absorption of solar radiation and the lower the transmission. The part of solar radiation passing through the second layer of the module (silicon cell and EVA) will be mainly transmitted through the inner low iron glass, a small part will be reflected back and the remaining portion of radiation will be absorbed by the glass.

It should be noted that when solar radiation is reflected from one layer back to another, there should be again transmission, absorption and reflection at the layers. However, for this study any inter-reflection of solar radiation was not accounted for, as its portion was considered relatively small compared to the amount of directly transmitted or absorbed energy.

In order to calculate the g-value of the external skin at the parts with PV integration, an overall solar transmittance, reflectance and absorptance representative of the whole structure was calculated.

The overall transmittance of the module equals:

$$\tau_{module} = \tau_1 \cdot \tau_2 \cdot \tau_3 \cdot (1 - PVR) \quad \textit{( Equation 2. 2)}$$

Where: $\tau_{module}$ is the total transmittance of the module, $\tau_1$and $\tau_3$are the solar transmittances of the outer and inner glazing respectively, $\tau_2$ is the solar transmittance of the EVA layer and $PVR$ is the Photovoltaic ratio on the module.

The overall absorptance in the module equals:

$$a_{module} = a_1 + a_2 \cdot \tau_1 \cdot (1 - PVR) + \alpha_{cell} \cdot \tau_1 \cdot PVR + \alpha_3 \cdot \tau_1 \cdot \tau_2 \cdot (1 - PVR)$$

*( Equation 2. 3 )*

Where: $a_{module}$ is the total absorptance of the module, $a_1, \alpha_3, a_2$ and $\alpha_{cell}$ are the absorptance of the external and internal glazing, the EVA and PV cell layers respectively.

The overall reflectance of the module equals:

$$r_{module} = 1 - (\tau_{module} + a_{module}) \quad \textit{( Equation 2. 4)}$$

Table 2.12 summarizes the equivalent solar properties calculated for each PVR.

*Table 2.12: Equivalent solar properties for each PVR.*

| PVR | τ | r | α |
|---|---|---|---|
| 22% | 0.55 | 0.16 | 0.28 |
| 50% | 0.36 | 0.14 | 0.50 |
| 75% | 0.18 | 0.12 | 0.70 |

Each module was modelled in IDA-ICE as an equivalent glazing using the solar properties defined above. The same properties were assumed for the solar and the visible part of the spectrum, as there were no available data for the spectral distribution of the reflectance and transmittance.

The front and back emittances of the module were set to 0.84 which is the emittance of low iron glass. The thickness of the equivalent glazing systems was set equal to the total thickness of the different layers and an equivalent thermal conductivity describing the module as a whole was calculated based on the summation of the resistances of each layer as follows:

$$R_{module} = 2 \cdot R_{glass} + R_{cell} + R_{EVA} \quad \textit{( Equation 2. 5 )}$$

$$\lambda_{module} = \frac{d_{module}}{R_{module}} \quad \textit{( Equation 2. 6 )}$$

Where: $R_{module}$ is the summation of the thermal resistances of each of the module's layers $R_{glass}$, $R_{cell}$ and $R_{EVA}$. The term $\lambda_{module}$ is the module's equivalent thermal conductivity and $d_{module}$ is the overall thickness of the module including all the layers. The same thermal resistance of the module ($R_{module}$) was assumed for all PVR on the façade as the thermal conductivity of the solar cell is very high and the layer is also very thin consequently having negligible thermal resistance (see Table 2.11).

The resulting overall thermal conductivity of the module is equal to 0.51 W/ (m·K).

The total solar transmittance of the external skin (at the parts with solar cells) was thereafter calculated in IDA-ICE, for each PVR.

Figure 2.10 shows the calculated g-value as a function of PVR. The g-values corresponding to the PVRs used in this study are noted. The 0% PVR case represents a structure with two layers of low iron glass with an encapsulated layer of EVA. The g-value of a single low iron glass is also shown as it represents the total solar transmittance of the external skin with a single low – Iron glass without any PV integration.

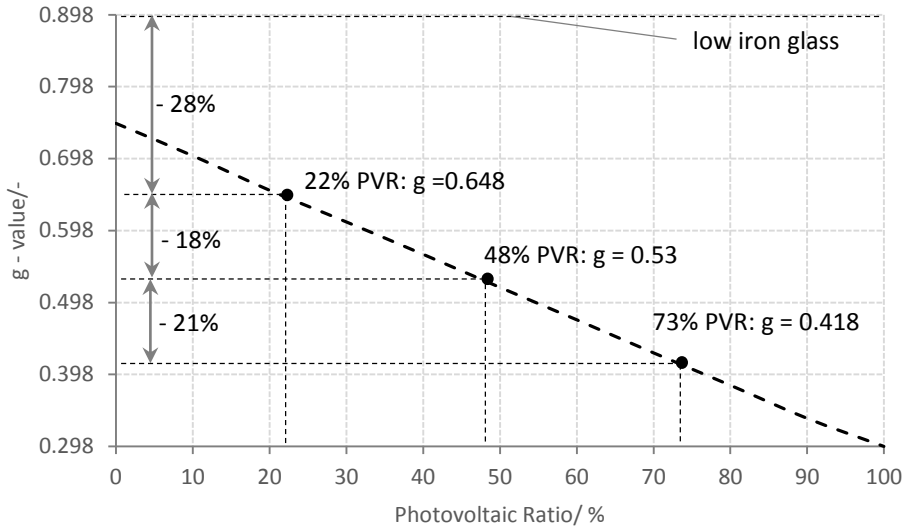


*Figure 2.10: G-value of the system as a function of the PVR.*

The effect of having a lower g-value when there is a load connected to the system was neglected based on the studies of [26], who found little variation of the g-value (absolute decrease of 0.01 – 0.03, see section 1.1.4.2) due to this factor.

### *2.4.6.2 Modelling of the semitransparent solar glazing in IDA-ICE*

The double façade model in IDA-ICE takes as input the properties of a glazing (or a combination of glazing systems) covering the whole façade. The semitransparent PV modules, however, were assumed to be placed on the upper and lower zones of the external skin as already shown in Figure 2.10. This means that the total solar transmittance of the façade is different between the lower and upper parts (due to PV integration) and the viewing area (single low-Iron glass).

In order to model the geometric position of the semitransparent PV modules as already seen in Figure 2.11, an external shading screen was positioned at a distance of 0.05m in front of the external glazing at the lower and upper zones of the façade. Figure 2.11 shows a picture of the shadings as positioned in IDA-ICE.

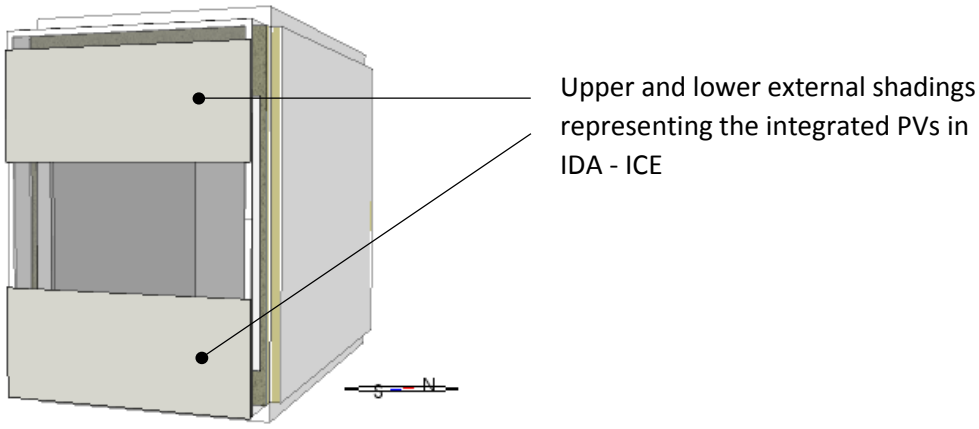


*Figure 2.11: Model of PVs in IDA-ICE.*

The input for the external shading consists only of transmittance which is defined as shading transparency. In order to get the g-value calculated for each PVR, the shading transparency was calculated as:

$$\tau_{external\ shade} = \frac{g_{PVR}}{g_{low\ Iron}} \quad \textit{( Equation 2. 7)}$$

Where: $\tau_{external\ shade}$ is the external shading transmittance, $g_{PVR}$ is the g-value calculated for each PVR and $g_{low\ Iron}$ is the g-value of a single low-Iron glass.
Table 2.18 summarizes the transparency of the shadings used to model each PVR.

*Table 2.13: Transparency of shadings for each PVR.*

| PVR | $\tau_{external\ shade}$ | $g_{low\ Iron}$ | $g_{PVR}$ |
|---|---|---|---|
| 22% | 0.72 | 0.90 | 0.648 |
| 48% | 0.59 | 0.90 | 0.531 |
| 73% | 0.465 | 0.90 | 0.418 |

The thermal transmittance of the outer skin was not changed in the simulations as the layers of the PV module are very thin and the overall thermal resistance is very low (see Table 2.12).

### 2.4.7 Alternative initial window

This study examined the performance of the ventilated façade in terms of energy use and thermal comfort when combined with a triple clear initial window. This window was considered another possible startup scenario for the base case. The geometry, shading and glazing characteristics chosen for the ventilated facades in this case (when combined with a triple clear initial window) were based on the previous studies (ventilated façade and double clear window). At first, an alternative base case was defined and thereafter two ventilated façade options with the glazing types presented in section 2.4.2 (low-Iron and low-E).

Table 2.14 summarizes the basic solar and thermal properties of the triple clear window, and its combination with the low-Iron and the low-E coated external skins. The properties are given without and with shading (effective values). The reflective shading screen presented in section 2.4.3 was assumed as solar protection for all the cases. For the triple clear unit it was positioned inside the room while for the double façade cases it was positioned in the ventilated cavity.

*Table 2.14: Solar and thermal properties of triple clear window and outer skins.*

| | g | Tsol | Ug ($W/(m^2K)$) | $g_{eff}$ | $Tsol_{eff}$ | $Ug_{eff}$ ($W/(m^2K)$) |
|---|---|---|---|---|---|---|
| triple clear + Reflective shading | 0.608 | 0.472 | 1.867 | 0.237 | 0.03 | 0.996 |
| low-Iron + Reflective shading + triple clear | 0.587 | 0.424 | 1.375 | 0.1 | 0.029 | 0.843 |
| low-E + Reflective shading + triple clear | 0.459 | 0.317 | 1.08 | 0.086 | 0.022 | 0.794 |

The frame U-value was assumed equal to $2W/m^2K$. The following settings were chosen for the ventilated façade options:

The cavity depth and opening were set to 0.2 m. The cavity was ventilated when the room air temperature exceeded 24.5 °C (See also section 2.3.2). The shading devices were used when the room air temperature exceeded 24.5 °C for both the alternative base case and the ventilated options.

### 2.4.8 Highly insulated triple glazed units

This study examined the option of refurbishing the base case room with highly insulated modern triple glazed units. Two window types were assumed according to the window to wall ratio. The aim for the 30% WWR was to achieve a low U-value and retain high light transmission due to the small window area. The aim for the 70% WWR was primarily a very low U-value as the increased window area can provide sufficient daylight. For both windows, a reflective shading screen was assumed positioned in the outermost gap between the panes.

The glazing combinations of the highly insulated triple glazed windows chosen for each WWR are described in the following table: The detailed properties for each glazing used in the thesis are also summarized in Appendix A.

*Table 2.15: Properties of the different layers of the chosen highly insulated TGUs for each WWR.*

| WWR | Outer pane | Gap | Middle pane | Gap | Inner pane |
|---|---|---|---|---|---|
| 30% | Optiwhite 6mm low-Iron glass | air / argon 10/90 32mm | clear 6mm | air / argon 10/90 - 16mm | low-E ** |
| 70% | Ipasol Neutral 68/34* | air / argon 10/90 32mm | clear 6mm | air / argon 10/90 - 16mm | low-E ** |

*selective low-E glass: Ts = 0.383, Tvis = 0.748, $\varepsilon_{front}$ = 0.837 $\varepsilon_{back}$ = 0.025
**low-E soft coated: $\varepsilon_{front}$ = 0.0925, $\varepsilon_{back}$ = 0.84

Table 2.16 gives the solar and thermal properties for the chosen triple glazed units with (effective values) and without shading, for each WWR.

*Table 2.16: Solar and thermal properties of the triple glazed units.*

| Window | g | Tsol | Ug | geff | $Tsol_{eff}$ | $Ug_{eff}$ |
|---|---|---|---|---|---|---|
| TGU 30% WWR | 0.602 | 0.472 | 0.993 | 0.1 | 0.033 | 0.657 |
| TGU 70% WWR | 0.285 | 0.212 | 0.662 | 0.064 | 0.017 | 0.559 |

For both window options the frame U-value was set to 1.5 W/m$^2$K.'

## 2.5 Performance on a component level

This section presents the parametric studies conducted in WIS in order to examine some of the key design parameters of a double skin façade. The geometrical characteristics, the glazing type and the shading influence were studied. The analysis is divided in two parts related to the performance during winter and summer conditions.

It should be noted that WIS is a software for studying glazing systems. Therefore the inner skin in these studies was fully glazed (100%) and was configured as for the base case window (double clear pane).

### 2.5.1 Winter conditions

The aim of this study was to understand the possibilities of the double façade acting as a thermal barrier and its potential on improving the inner layer temperatures of the base case. Therefore the temperature profile across the façade was studied for the following cases:

The base case window was combined with the two glazing types presented in section 2.4.2 for the external skin (low-Iron glass and a low – E hard coated glass with the coating facing the cavity). To extend the comparison the highly insulated TGU presented in Table 2.17 for the 70% WWR was additionally simulated. For all double skins the gaps between the panes were assumed completely sealed. Table 2.17 summarizes the studied cases.

*Table 2.17: Cases studied in WIS for the winter period.*

| Glazing Description | Cavity depth | Inner skin | Ug / W/m$^2$K |
|---|---|---|---|
| Low-Iron glass* | 0.2 | Double clear window | 1.81 |
| Low - E hard coated* | 0.2 | Double clear window | 1.34 |
| Triple glazed unit with 2 low - E coatings ** | - | - | 0.662 |

*Detailed properties are given in section 2.4.2

** Detailed properties are given in section 2.4.8 (70% WWR case)

The simulations were conducted for a sunny and a cloudy winter day. The boundary conditions for irradiation, internal and external air temperatures were chosen based on the climate file presented in section 2.1. Two days, with high and low solar irradiation were chosen from February, which is the coldest month of the year in the climate file.

Figure 2.12 presents the chosen days. The room temperature was set to 22°C. The inner and outer radiant temperatures were assumed equal to the respective air temperatures. The internal and external heat transfer coefficients were set to 3.6 W/m$^2$K and 20 W/m$^2$K according to [15] for winter conditions.

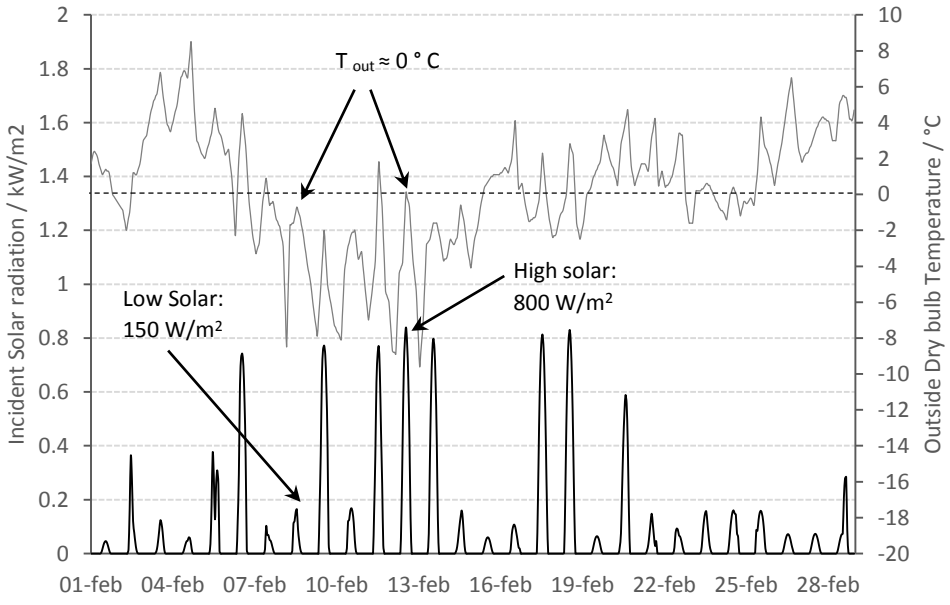


*Figure 2.12: Winter period examined.*

### 2.5.2 Summer conditions

The aim of this study was to understand the impact of ventilation and the different shading options on the temperature profile across the ventilated facade. Moreover, the influence of the shading devices in combination with different cavity depths and opening sizes was examined in terms of airflow, total solar transmittance, inner layer temperatures, and the vertical temperature profile of the air in the cavity

The temperature profile across the façade was studied with and without the three shading devices presented in section 2.4.3, for the low-Iron and the low–E coated external skins (section 2.4.2). The cavity depth and opening were set to 0.2 m.

The airflow through the cavity, the g-value and the inner layer temperatures were studied for the low-Iron and the low-E coated external skins and the three shading options (section 2.4.3), as a function of the cavity depth. Two ratios between opening height and cavity depth were assumed, namely 0.5 and 1, i.e. openings equal to half of the cavity depth and openings equal to the cavity depth. The examined cavity depths were: 0.05m, 0.1m, 0.2m and 0.4m.

The vertical temperature profile of the air in the cavity was studied only for the low-E hard coated façade, the three shading options (section 2.4.3) and cavity depths of 0.05m, 0.1m, 0.2m and 0.4m. The ratio between opening height and cavity depth was set to 1.

All the temperature profile studies across the façade were performed on the basis of the boundary conditions of ISO 15099 for summer conditions [15]. An extreme summer day based on [9] was assumed for all the analyses on the airflow, the g-value, the inner layer temperatures and the vertical temperature profile of the air in the cavity.

The conditions with respect to outdoor and indoor air and radiant temperatures and the convective heat transfer coefficients are summarized in Table 2.18. The presented conditions are the same between the ISO 15099 and the assumed extreme summer day. However the standard assumes incident solar radiation of 500 W/m$^2$ while for the extreme summer day this parameter was set to 900 W/m$^2$.

*Table 2.18: Temperature conditions and convective coefficients for the extreme summer day and the summer day of ISO 15099.*

| Outside convection coefficient $h_c$/ (W/(m$^2$K)) | Inside convection coefficient $h_c$/ (W/(m$^2$K)) | Outside air temperature/ °C | Inside air temperature/ °C | Outside radiant temperature/ °C | Inside radiant temperature/ °C |
|---|---|---|---|---|---|
| 8 | 2.5 | 30 | 25 | 30 | 25 |

An analysis of the main parameters affecting the airflow rate through the cavity and the vertical air temperature profile, as calculated in WIS is presented in Appendix D.

## 2.6 Annual energy and thermal comfort performance

This section presents the parametric studies performed in IDA-ICE with focus on the energy use for heating and cooling and the thermal comfort performance of the room. As a first step the overall thermal transmittance of the facade (including wall, window frame and glazing) with the addition of the ventilated façade was estimated. This study is presented in section 3.6.1. Sections 3.6.2 – 3.6.5 present the simulations performed for the analysis of the annual energy and comfort performance of the chosen room.

### 2.6.1 Thermal transmittance of the ventilated facade

A methodology for calculating the overall thermal transmittance of the façade, when the two basic glazing options (low–Iron and low-E hard coated, see section 2.4.2) are applied on the base case, is hereby presented. Four U-values were estimated corresponding to the two glazing options and the two WWR (30% and 70%).

The aim was to gain an understanding of the magnitude of improvement of the overall thermal transmittance of the initial façade due to the addition of the external skins. Simulation results concerning the heating demand of the room with the double façade model of IDA-ICE were compared with results for single skin facades with overall thermal transmittances equal to the U – values estimated for each external skin and each WWR. All simulations were performed in IDA-ICE.

The estimated U-values were additionally used in heating demand calculations performed in Excel spreadsheets using the Degree Day method presented in [45] including solar gains. The aim was to test the validity of the simulated results.

#### *2.6.1.1 Thermal transmittance estimation*

The initial overall thermal transmittance (including frame, wall and window) for the 30% WWR and 70% WWR is equal to 1.38 W/m$^2$K and 2.17 W/m$^2$K respectively (see Appendix E). The thermal transmittances resulting from the addition of the low iron and the low-E hard coated external skins on the 30% and 70% WWR were calculated as follows: .

- Two glazing systems were made in WIS with thermal transmittances equal to the ones of the two WWR (30% and 70%) as specified above. These glazing systems can be considered equivalent to the initial façade for each WWR in terms of overall thermal transmittance.
- A low-Iron glass (Optiwhite) and a low-E hard coated glass (K-glass) (see section 2.4.2) were added to each of the equivalent glazing systems described above, at a distance of 200mm. Four thermal transmittances were thereafter calculated in WIS (for two external skins and two WWR).

Table 2.19 summarizes the initial overall U-value of the base case for each WWR, the equivalent window constructions made in WIS and their respective thermal transmittances, as well as the U-values estimated for each WWR after the addition of the low-Iron and the low – E hard coated external skins. The estimated U-values are highlighted in bold.

*Table 2.19: Overall U-values for the base case, equivalent to the base case facades in WIS and estimated U-values with the addition of a Low-Iron and a Low-E coated external skin, for WWR 30% and 70%..*

| | Windows equivalent to the facade of the base case | | | Estimated U-values / (W/ ($m^2$K)) | |
|---|---|---|---|---|---|
| WWR | Overall initial U-value W/$m^2$K | Equivalent construction in WIS | Resulting Equivalent U-value / W/$m^2$K | Low-Iron glazing | Low – E hard coated glazing |
| 30% | 1.38 | 6mm clear glass<br>11 mm air/argon mix10/90<br>6mm clear glass<br>10 mm air/argon mix10/90<br>6mm clear glass<br>10 mm air<br>6mm clear glass | 1.38 | **1.00** | **0.90** |
| 70% | 2.17 | 6mm clear glass<br>7.5 mm air<br>6mm clear glass<br>7 mm air<br>6mm clear glass | 2.17 | **1.52** | **1.21** |

### *2.6.1.2 IDA – ICE simulations with the Double Façade Model and with Equivalent Single Skin Facades*

A total number of 8 cases was simulated for each WWR (30% and 70%), each outer skin (Low-Iron and Low-E hard coated) and two orientations (south and north). The simulations were performed with the double façade model of IDA-ICE and with single skin facades for which the resulting overall thermal transmittances (including glazing, wall and frame) matched the estimated thermal transmittances. The configuration of the single skin facades is given below:

The window of the base case was alternated to a triple glazed window by adding an extra low-Iron or a hard coated Low - E glass depending on the case. The g – value achieved is the same as for a ventilated façade with closed cavity. Thereafter the thermal transmittance of the wall was modified by changing the thermal conductivity of the insulation layer in order to achieve the overall thermal transmittance estimated for each case (bold cases in Table 2.19). The frame was incorporated to the external wall.

Table 2.20 summarizes the thermal transmittance of the new window with the addition of low-Iron and low-E glass, the modified thermal transmittance and conductivity of the wall as well as the resulting overall thermal transmittance of the equivalent single skin facades. The detailed calculations of the presented values can be found in Appendix E.

*Table 2.20: Single skin facades with thermal transmittance equal to the values estimated for the different double skin options and WWR 30% and 70%..*

| WWR | External Skin | Window U-value / (W/(m$^2$K)) | Modified Wall U-value / (W/(m$^2$K)) | Modified wall λ / (W/(mK)) | Overall U-value / (W/(m$^2$K)) |
|---|---|---|---|---|---|
| 30% | Low -Iron | 1.81 | 0.86 | 0.0686 | 1.08 |
| | Low - E | 1.34 | 0.77 | 0.0586 | 0.9 |
| 70% | Low -Iron | 1.81 | 1.2 | 0.129 | 1.52 |
| | Low - E | 1.34 | 1.05 | 0.0985 | 1.21 |

The simulations were performed for constant heating setpoint at 22°C. All infiltration, ventilation and internal gains were removed and no shading devices were included in order to compare the results with the Excel based heating demand estimations performed with the CIBSE Degree Day Method [45], as described below.

#### *2.6.1.3 Heating demand estimation with the Degree Day method*

The following equations can be found in [45]. The method is based on calculation of a mean monthly balance temperature ($T_{bc}$) for the room. A balance temperature is the temperature where the heat losses equal the heat gains and therefore no input of heating power is required. It is calculated as:

$$T_{bc} = T_{sp} - \frac{Q_G}{U'} \quad \textit{( Equation 2. 8)}$$

Where: $T_{sp}$ is the heating setpoint, $U'$ is the overall heat loss coefficient and $Q_G$ stands for useful solar gains, i.e. the amount of solar gains that actually contribute to lowering the heating demand of the room.

The term $Q_G$ is calculated for each month based on the average hourly solar radiation incident on the façade. A utilization factor accounting for the thermal capacitance of the room and the type of heating (continuous or not) along with the window's total solar transmittance (g-value) are used to estimate the amount of the useful solar gains$Q_G$.

By knowing the balance temperature the heating power for every hour $(i)$ of the month can be calculated as:

$$Q_{(i)} = U' \cdot (T_{bc} - T_{out(i)}) \quad \textit{( Equation 2. 9 )}$$

In the case considered in this study i.e. no ventilation or infiltration losses, the overall heat loss coefficient is:

$$U' = U_{ov} \cdot A_{facade} \quad \textit{( Equation 2. 10 )}$$

Where: $U_{ov}$ is the overall thermal transmittance of the room including wall, frame and window $A_{facade}$ is the area of the external wall, $T_{bc}$ is the balance temperature and $T_{out(i)}$ is the outdoor dry bulb temperature at the specific hour (i). The sum of all the hourly power values for the month gives the monthly heating demand.

The heating demand was calculated for every month and the monthly values were summed to give the annual heating need. The hourly incident solar radiation on the façade for south and north orientation was calculated in IDA-ICE and was used to calculate the useful solar gains

and the balance temperature for each month. For a full description of the method the reader should refer to [45]

### 2.6.2 Annual heating demand

The parametric studies that examined the performance of the ventilated facade in terms of annual heating demand are hereby presented. The influence of the external skin glazing type the WWR and the inner wall cladding on the heating performance was examined. The cavity behavior as a heat buffer was analyzed and thereafter the heating demand was evaluated.

For the 30% WWR the low-Iron and the low-E coated external skins (section 2.4.2) were combined with the different cladding options presented in section 3.4.5 (base case cladding, reflective cladding, concrete and brick). For the 70% WWR only the cladding of the base case was assumed.

All simulations were performed for a cavity depth of 0.2 m with openings of the same height. The cavity was ventilated when the room air temperature exceeded 24.5 °C. Only the reflective shading screen was used as the shading type has little influence on the annual heating demand. This is because in all examined cases the shading was used when the room air temperature exceeded 24.5 °C, i.e. that the room was almost in need for cooling.

The simulations were performed for south, east, west and north orientations. However the north orientation was not studied in terms of inner skin cladding because it is not affected by direct solar radiation.

The temperature rise in the cavity and its performance as a heat buffer zone was studied for a period in February (14/02 – 21/02) including cold sunny and cold cloudy days, as can be seen in Figure 2.13. The period for which the cavity temperatures were studied is noted (light green).

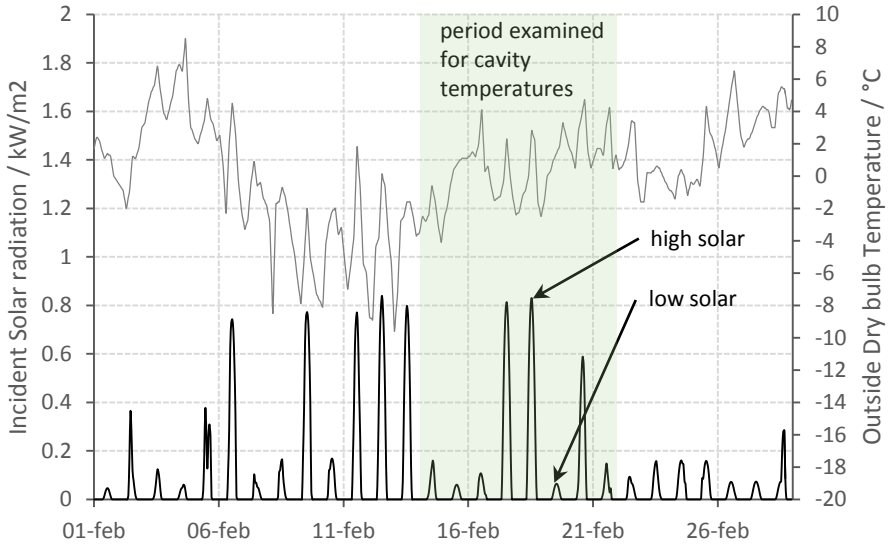


*Figure 2.13: Solar radiation incident on a south façade and Outdoor Dry bulb Temperature for February. The period for which the cavity temperature was examined is noted with light green color.*

Table 2.21 summarizes the parameters studied for the heating demand.

*Table 2.21: Parameters examined for the cavity temperatures and the annual heating demand.*

| External Skin Glazing | | Low - Iron glass DSF1 | | | | | | | | Low - E hard coated glass DSF2 | | | | | | | |
|---|---|---|---|---|---|---|---|---|---|---|---|---|---|---|---|---|---|
| window to wall ratio (WWR) | | 30% | | | | 70% | | | | 30% | | | | 70% | | | |
| Orientation | | S | E | W | N | S | E | W | N | S | E | W | N | S | E | W | N |
| Inner wall cladding | Base case | | | | | | | | | | | | | | | | |
| | Reflective (5% absorptance) | | | | | | | | | | | | | | | | |
| | Concrete | | | | | | | | | | | | | | | | |
| | Brick | | | | | | | | | | | | | | | | |
| Shading | 80% absorptance | | | | | | | | | | | | | | | | |
| | 57 %absorptance | | | | | | | | | | | | | | | | |
| | 20% absorptance | | | | | | | | | | | | | | | | |
| Cavity depth and opening / m | 0.1 | | | | | | | | | | | | | | | | |
| | 0.2 | × | × | × | × | × | × | × | × | × | × | × | × | × | × | × | × |
| | 0.4 | | | | | | | | | | | | | | | | |

Inner Wall cladding
× Cavity depth and opening
Shading Device

### 2.6.3 Annual cooling demand and specific energy use

The parametric studies that examined the performance of the room with the addition of a ventilated façade in terms of cooling energy use as well as the specific energy use are hereby presented. The influence of the shading type, the cavity depth and opening and the Photovoltaic ratio (PVR) on the cooling performance and the specific energy use of the room was analyzed.

As already seen in section 1.1.2.1 the specific energy use should include heating, cooling DHW and facility electricity (fans etc.). In this study the DHW was assumed to be a constant value of 2 kWh/$m^2$ per year according to [42]. The electricity for fans was calculated in IDA-ICE and was the same for all cases as the delivered airflow is the same for all rooms. Consequently this value was constantly set to 6 kWh / $m^2$ per year (as calculated in IDA-ICE).

The low-Iron external skin was combined with the three shading options (reflective, medium absorptive and absorptive), the three PVR (22%, 48% and 73%) and the case without solar cells. The cavity depths and openings examined were 0.1, 0.2 and 0.4 m. Detailed information on each of the above parameters are given in sections 2.4.2 – 2.4.4 and 2.4.6

The low–E coated façade was only combined with the reflective shading option due to limitations in IDA-ICE (see section 1.4.2). No solar cells covered this case, since the PVs were

assumed encapsulated between two layers of low-Iron glass (see Section 2.4.6). The depth and opening of the cavity were set to 0.2 m.

All studies regarding the cooling demand of the room and the specific energy use were performed for south, east, west and north orientations, for 30% and 70% window to wall ratios (WWR). No shading devices, and no solar cells, were assumed for north oriented facades, due to the lack of direct solar radiation.

The cavity performance in terms of air and shading temperatures was additionally analyzed for a low–Iron façade at a 70% WWR. The studies were performed for a south oriented room for a warm day during August.

The temperature of the air in the cavity was analyzed for the reflective and the absorptive shading options, for all cavity depths and openings (0.1m, 0.2m and 0.4m). The aim was to evaluate the influence of the cavity geometry on the air temperature rise.

The temperature of the shading device was studied for the reflective and the absorptive shading options with 73% PVR as well as without solar cells (0% PVR). In the former case less energy is transmitted though the outer skin due to the PV cells whereas in the latter most energy passes through the outer low-Iron glass and is absorbed or reflected by the shading behind. The temperature of the shading affects both the airflow through the cavity and the longwave radiation exchange with the inner skin, consequently affecting the secondary transmittance and the cooling demand.

Table 2.22 summarizes the parameters combined for the studies of the annual cooling performance and the specific energy use.

*Table 2.22: Parameters examined for the cavity and shading temperatures, the annual cooling demand and the specific energy use.*

| External Skin Glazing | | Low -Iron glass | | | | | | | | Low-E hard coated glass | | | | | | | |
|---|---|---|---|---|---|---|---|---|---|---|---|---|---|---|---|---|---|
| window to wall ratio (WWR) | | 30% | | | | 70% | | | | 30% | | | | 70% | | | |
| Orientation | | S | E | W | N | S | E | W | N | S | E | W | N | S | E | W | N |
| Inner wall cladding | Base case | | | | | | | | | | | | | | | | |
| Shading type | 80% absorptance | | | | | | | | | | | | | | | | |
| | 57 %absorptance | | | | | | | | | | | | | | | | |
| | 20% absorptance | | | | | | | | | | | | | | | | |
| Cavity depth and opening / m | 0.1 | × | × | × | | × | × | × | | | | | | | | | |
| | 0.2 | × | × | × | × | × | × | × | × | × | × | × | × | × | × | × | × |
| | 0.4 | × | × | × | | × | × | × | | | | | | | | | |
| PVR | 0% | | | | | | | | | | | | | | | | |
| | 22% | | | | | | | | | | | | | | | | |
| | 48% | | | | | | | | | | | | | | | | |
| | 73% | | | | | | | | | | | | | | | | |

Inner Wall cladding

× Cavity depth and opening

Shading Device

PV coverage ratio

### 2.6.4 Thermal comfort

The same parameters presented in section 2.6.3 (Annual cooling demand and Specific energy use) were analyzed in terms of their effects on thermal comfort quality. The operative temperature was studied for 30% and 70% WWR. The target performance was to achieve the Belok 25 °C or 26 °C requirement, i.e. that the operative temperature should not exceed 25°C or 26°C for more than 10% of the occupied time during the months April to September.

The inner layer temperatures (inner pane or inner shading) were additionally studied for the 70% WWR due to the high view angle between the occupant and the window (see Figure 1.5). It was assumed that the inner layer temperature should not be below 18°C and above 27°C for more than 10% of the occupied time.

### 2.6.5 Alternative refurbishment options

The best cases defined through sections 3.6.2 -3.6.4 for the low–Iron and the low–E coated facades were selected and compared with the option of adding the same external skins to a base

case with an initial triple clear pane window (section 2.4.7) as well as the option of refurbishing the room with non-ventilated highly insulated triple glazed units (TGU). The highly insulated triple glazed units were chosen specifically for each WWR and were combined with the reflective screen (section 2.4.3) which was positioned in the outermost gap of each TGU (see section 2.4.8).

In the cases with ventilated facades the cavity depth was set to 0.2 m and the reflective shading was positioned inside the cavity. No solar cells were assumed. The cavity was open when the room air temperature exceeded 24.5 °. For all cases the shading was used when the room air temperature exceeded 24.5 °.

The main aim of this study was to assess the improvement potential in terms of energy use and thermal comfort when the ventilated facade is integrated at a base case with better initial window, and to compare the ventilated options with modern highly insulated triple glazed units that comprise a simpler, than the ventilated façade, refurbishment possibility.

The energy use for heating and cooling as well as the operative temperatures were studied for both 70% and 30% WWR. The inner layer temperatures were studied only for the 70% WWR.

# 3 Impact of the ventilated facade on PV performance

This section describes the methodological approach taken, in order to calculate the annual electricity output from the façade in the case of integrated photovoltaics. The main aim of this study was to evaluate the impact of the cavity's ventilation on the annual electricity output. The chapter is divided in two subsections.

The first describes a method developed for calculating the cell temperature in IDA-ICE. The validity of the obtained results was examined through a comparison with cell temperatures obtained from System Advisor Model (SAM) for a BIPV module.

The second part describes the methodology for calculating the annual electricity output with and without ventilation of the cavity.

## 3.1 Estimation of solar cell temperature

### 3.1.1 Cell temperature in IDA-ICE

The estimation of the cell temperature rise was performed in IDA-ICE. The program does not offer any model for calculating cell temperatures of building integrated photovoltaics.

The integrated cells were modelled as an equivalent glazing with 100% Photovoltaic ratio (PVR) as the external skin of the Double Façade. The solar and thermal properties of the different layers of the PV module as already presented in Table 2.11 of section 2.4.6 were used in order to calculate an overall solar transmittance, reflectance and absorptance equivalent for the whole module. The exact methodology is described in detail in chapter 2.4.6.1.

The equivalent solar properties for the module with 100% PVR, as can be seen in Table 3.1 were used as input for the glazing that described the module in IDA-ICE. Although no radiation would be transmitted, a transmittance ($\tau$) of 1% was assumed as IDA-ICE cannot take values of 0% for the transmittance of a glazing.

*Table 3.1: Solar properties of PV module at 100% PVR.*

| PVR | τ | r | α |
|---|---|---|---|
| 100% | 0.01 | 0.10 | 0.89 |

A certain part of absorbed energy by the cell is converted into electricity and does not contribute to the cell's temperature increase. An external shading device was modeled outside of the equivalent glazing in order to reduce the amount of the absorbed radiation and account for the conversion of electricity. The transmittance of the shading was set to 0.865 considering a cell efficiency of 0.135. The temperature of the inner surface of the equivalent glazing was calculated by IDA-ICE and was assumed equal to the cell temperature. The cavity was assumed to be non-ventilated, which corresponds to a negligible amount of airflow over the back of the module. The hourly cell temperatures obtained with the above method were compared with hourly cell temperatures calculated in the program System Advisor Model (SAM) for a BIPV structure.

### 3.1.2 Cell temperature in System Advisor Model

The cell temperature was calculated in SAM with the use of simple efficiency mathematical model. According to [36], a simple method can be used for preliminary estimations of the power output when a specific module type is not yet chosen.

The method accounts for decrease of a module's efficiency due to high solar cell temperatures, based on maximum power temperature coefficients, determined empirically for different types of solar cells. Such coefficients state a percentage of efficiency loss per degree °C due to deviation of the solar cell's temperature from the nominal operating temperature of 25°C.

Table 3.2 gives maximum temperature correction coefficients for different cell types according to SAM [36].

*Table 3.2: Maximum temperature coefficients for different cell types.*

| Type of cell | γ - Maximum Power Temperature Coefficient / (%/ °C) |
|---|---|
| Monocrystalline silicon | -0.49 |
| Polycrystalline silicon | -0.49 |
| Amorphous silicon | -0.24 |

An analytical description of the method is given below. All of the following equations are presented in the help file of SAM which can be found in [36].

The calculation of the power output is based on a chosen cell efficiency and the area covered by solar cells. A corrected electricity conversion efficiency is estimated for every hour with the use of temperature correction factors.

The hourly direct current power output of the PV module is calculated as:

$$P_{mp\ Module} = E_{\ incident} \cdot A_{module} \cdot \eta_{module} \cdot F_{Temp\ corr} \quad \textit{( Equation 3. 1)}$$

Where: $E_{incident}$ is the hourly incident solar radiation on the module's surface including beam, diffuse and ground reflected radiation, $A_{module}$ is the area covered by the PV cells, $\eta_{module}$ is the module efficiency at a given incident global radiation level, calculated by extrapolating values from the radiation level and efficiency tables and $F_{Temp\ corr}$ is the temperature correction factor based on the temperature of the solar cells at the specific hour.

The hourly value of $F_{Temp\ corr}$ is given as:

$$F_{TempCorr} = 1 + \gamma \cdot (T_{cell} - T_{Ref}) \quad \textit{( Equation 3. 2)}$$

Where: $\gamma$ is the maximum temperature correction coefficient based on the module and can be found in Table 3.2, $T_{cell}$ is the cell temperature at the specific hour and $T_{Ref}$ is the reference temperature at which the nominal efficiency is calculated, i.e. at standard test conditions (STC) of 25 °C for 1000W/m$^2$ incident solar radiation.

The cell temperature depends on the hourly wind speed specified in the climate file, the hourly outdoor dry bulb temperature and empirical coefficients determined for different types of module structures and type of module mounting. It is calculated as:

$$T_{Cell} = T_{Back} + \frac{E_{incident}}{E_0} \cdot dT \text{ and} \quad \textit{( Equation 3. 3)}$$

$$T_{Back} = E_{Incident} \cdot e^{a+b \cdot V_{wind}} + T_{out} \quad \textit{( Equation 3. 4)}$$

Where: $T_{Cell}$ is the cell temperature, $T_{Back}$ is the module's back surface temperature, $E_{Incident}$ is the incident solar radiation, $E_0$ is the reference total irradiation equal to 1000 W/m$^2$ and $T_{out}$ and $V_{wind}$ are the outdoor dry bulb temperature and wind speed respectively as stated in the

climate file. The parameters $a$ and $b$ are empirically determined coefficients for different module structures and mounting options and account for convective heat losses due to wind.

$dT$ is the temperature difference between the cell temperature and the module's back surface temperature at $E_0$. This parameter depends on the mounting type of the module which determines the amount of airflow on module's back surface.

Table 3.3 gives typical values of the parameters $a$, $b$ and $dT$ for different module types and mounting options according to SAM [36].

*Table 3.3: Typical values for parameters a, b and dT according to SAM.*

| Module structure and mounting | a | b | | dT |
|---|---|---|---|---|
| Glass/ Cell / Polymer Sheet Open Rack | -3.56 | -0.0750 | | 3 |
| Glass/ Cell / Glass Open Rack | -3.47 | -0.0594 | | 3 |
| Glass/ Cell / Polymer Sheet Insulated Back | -2.81 | -0.0455 | | 0 |

The two first types refer to modules mounted on an open rack construction allowing air to flow freely around the module while the third refers to BIPV types of construction preventing airflow at the back surface of the module.

Monocrystalline cells were considered for this study with an efficiency of 13.5%. The maximum temperature coefficient was set to -0.49%/ °C. The module area was set to 1.46 $m^2$ which corresponds to 73% WWR and the parameters $a$, $b$ and $dT$ were chosen for an "insulated back" structure in order to account for limited airflow over the module's back surface. The climate file used was for Copenhagen. The simulations were performed for south, east and west orientations.

The input parameters in SAM are summarized in the Table 3.4 below:

*Table 3.4: Input Parameters in SAM.*

| | |
|---|---|
| Module area / $m^2$ | 1.46 |
| Module efficiency (η) | 13.5% |
| maximum temperature coefficient γ / (%/ °C) | -0.49 |
| module structure and mounting | Glass/ Cell / Polymer Sheet Insulated Back |
| climate file | Copenhagen |
| reference irradiation/ ($W/m^2$) | 1000 |
| Nominal Operating temperature / °C | 25 |

## 3.2 Ventilation impact on annual electricity output

After evaluating the above defined methodology, simulations were performed in IDA-ICE to calculate the cell temperatures with and without ventilation of the cavity. In order to evaluate the maximum possible benefit of ventilation on the electricity output, the cavity was assumed either always closed either always open.

The annual electricity output was calculated with an Excel spreadsheet based on the above equations of the simple efficiency model [36]. However, the hourly cell temperatures used in the calculations were obtained by IDA-ICE. The simulations were performed for three orientations namely south, east and west.

# 4 Results

This section gives the results for the different parametric studies presented in chapter 2 as well as the results related to the PV performance with and without ventilation. The subsection 4.1 gives the results from the steady state simulations in WIS, followed by the annual energy and comfort performance of the room in subsection 4.2. The results for the PV performance are given in section 4.3.

## 4.1 Performance on a component level

The results from the steady state simulations performed in WIS are hereby presented.

### 4.1.1 Winter conditions

Figure 4.1 and Figure 4.2 show the temperature profiles across the façade for a cloudy and a sunny winter day respectively. The black line stands for the low-Iron external skin, the grey line for the low-E coated façade and the dotted line for a highly insulated triple glazed unit (TGU) with two low-E coatings, one on the inside of the outer pane and one at outside of the inner pane. The grey line with red squares stands for base case double clear window. The detailed properties of all glazings and window units are summarized in Appendix A and Appendix B respectively.

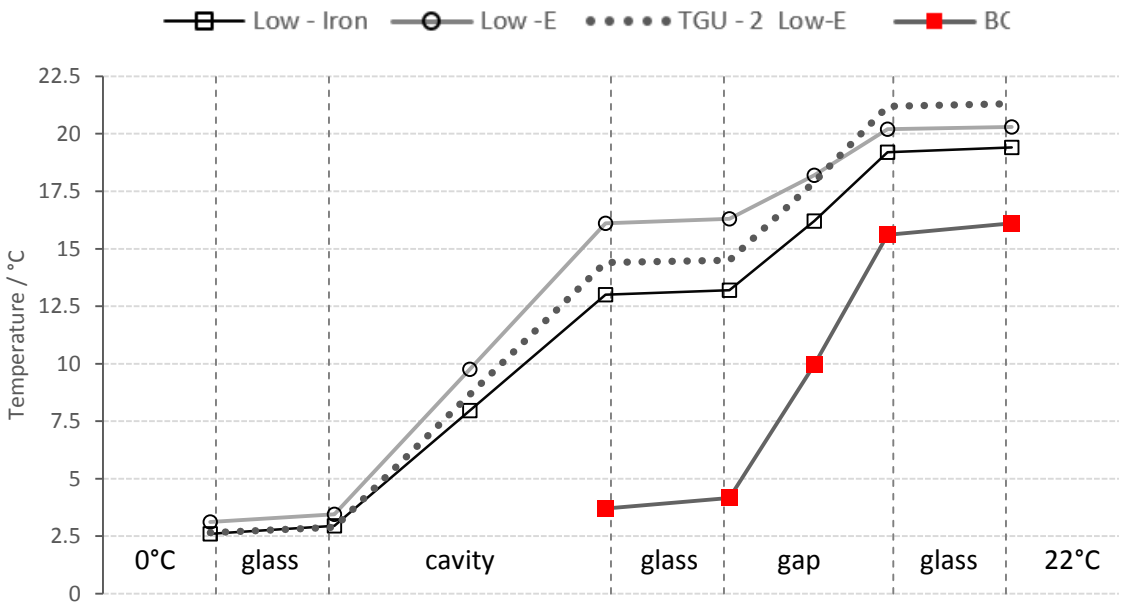


*Figure 4.1: Temperature profile across the double facade for a cloudy winter day. Closed cavity and incoming radiation of 150 W/m². The cavity depth is set to 0.2m for all the double skin façade cases.*

When a third pane is added to the base case (double clear window), the temperature of the inner window layer increases for 3.5 °C to 5 °C from a starting point of 16 °C. The highest inner pane temperature (21.3°C) is observed for the highly insulated TGU, followed by the low-E coated façade (20.3 °C). The façade with the low-Iron external skin has the lowest temperature of the different alternatives (19°C). For a day with limited solar radiation the highest inner pane temperatures are observed for the units with the lowest thermal transmittance, i.e. the highly insulated TGU (dotted line).

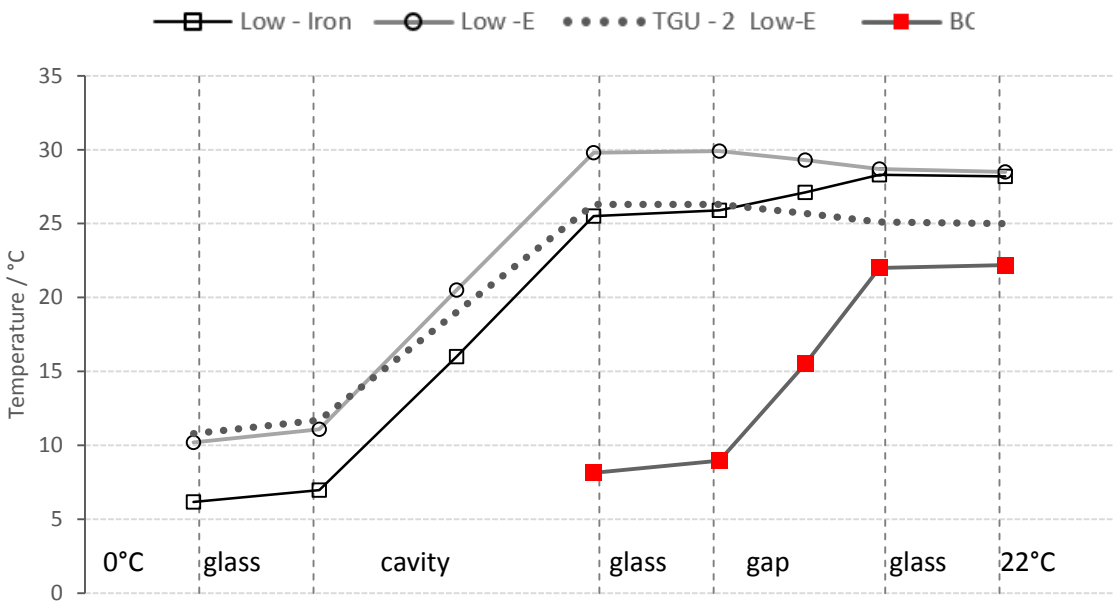


*Figure 4.2: Temperature profile across the double facade for a sunny winter day. Closed cavity and incoming irradiation of 800 W/m$^2$. . The cavity depth is set to 0.2m for all the double skin façade cases.*

In a sunny winter day, all the refurbishment options (double skins and highly insulated TGU) have higher inner pane temperatures than the base case. The latter has an inner temperature close to the inside air (22 °C), due its high thermal transmittance (2.80 W/m$^2$K). The highly insulated TGU has an inner pane temperature of 25°C which is also close to the air temperature of the room. The solar selective outer pane of this unit blocks more solar radiation than the low-Iron or the low- E facades and therefore the inner pane remains in lower temperature than the double skin alternatives. The latter have almost the same inner layer temperature (28.5°C). The low-E coated façade blocks solar radiation on the outer pane, while the low-Iron façade allows more radiation to be absorbed at the inner panes. On the other hand, the low-E façade has lower heat losses to the outside than the low-Iron case, due to its lower thermal transmittance. This results in similar inner pane temperature for the two cases. The cavity air temperatures are 16°C - 20°C higher than the outdoor, which demonstrates high insulation potential for specific climatic conditions and orientations.

### 4.1.2 Summer conditions

Figure 4.3 shows the temperature profile across the façade for the low-Iron (black line) and the low-E (light grey line) coated external skins with and without ventilation (solid and dashed lines respectively). The cavity depth and opening are 0.2m.

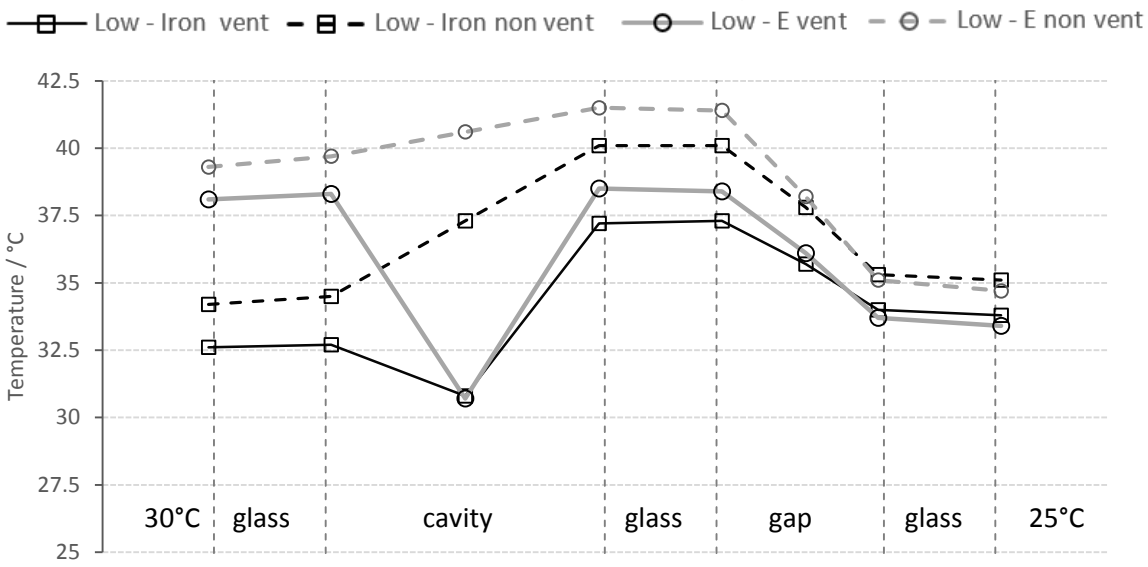


*Figure 4.3: Temperature profile across the ventilated facade for sunny summer day for open and closed cavity, incoming radiation of 500W/m$^2$ and cavity depth of 0.2m.*

Compared to the non-ventilated cases, the ventilation of the cavity brings about a decrease on air temperature of 7°C and 10°C for the cases with a low-Iron and a low-E coated external skin respectively. The ventilation results in general in colder panes. The most notable pane temperature decrease (3°C), when ventilation is introduced, can be observed for the middle pane for both cases. The inner layer temperature of the ventilated cases is lower by only 1.3 °C, compared with the non-ventilated facades for both skins.

In all cases, the low-E coated external skin is warmer than the low-Iron one because the former absorbs more solar radiation than the latter. Moreover in all cases the middle pane is warmer than the inner pane as more solar radiation is absorbed in this layer (than the inner pane). It is interesting to note that the mid pane of the low-E façade (both ventilated and not) is warmer than the respective pane of the low-Iron case for approximately 1°C. This can be attributed to the low-E coating of the external skin which keeps the mid pane warmer. On the other hand, the low-E coated façade has slightly lower inner layer temperature because less solar radiation reaches this layer compared to the low-Iron case. Nevertheless, both cases have almost the same temperature at the inner layer.

Figure 4.4 shows the temperature profile across the façade with a low-E coated external skin and an absorptive (black line), medium absorptive (red line) and a reflective (grey line) shading device. The cavity depth is and opening is 0.2m.

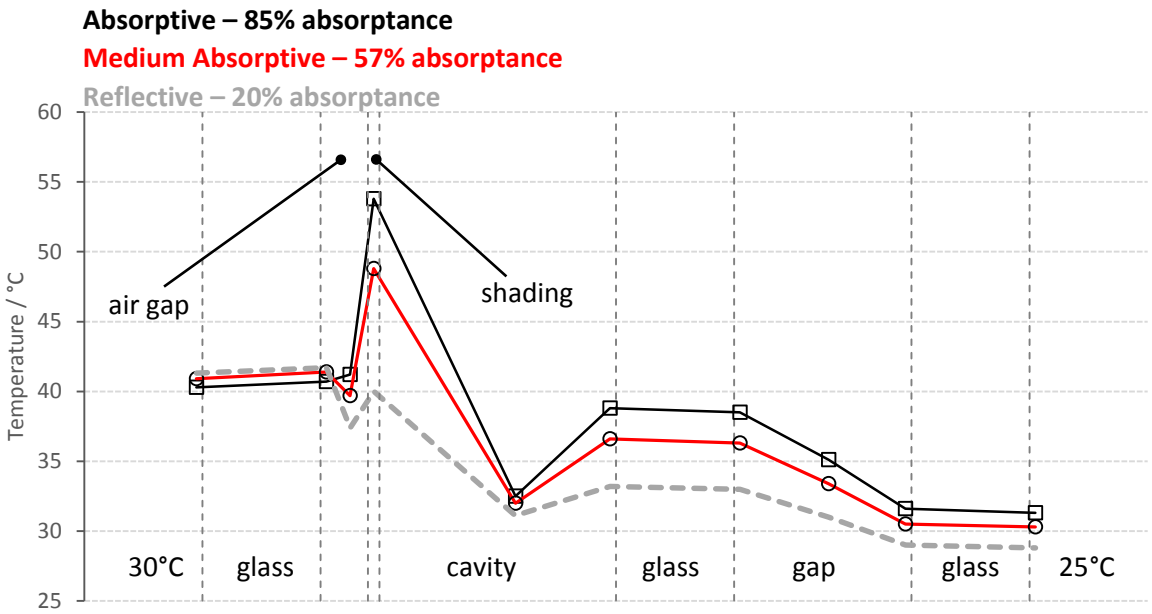


*Figure 4.4: Temperature profile across the ventilated façade for sunny summer day for different shading devices. Open cavity with Low - E hard coated external glazing, for incoming radiation of 500W/m² and cavity depth of 0.2m.*

Compared to the low-E coated case without shading devices (Figure 4.3), the addition of shading in the cavity results in lower inner layer temperatures with a range of reduction between 2°C and 4.6°C. The highest inner pane temperature is observed for the absorptive shading with 31.3°C, followed by the medium absorptive with 30.3°C and the reflective with 28.8°C. The temperature of the absorptive shading is 15°C higher than the one of the reflective, which in turn results to the highest inner surface temperature.

Figure 4.5 shows the airflow rate (per meter of cavity width) through the cavity as a function of cavity depth, for reflective (light grey lines), medium absorptive (red lines) and absorptive (black lines) shading devices, for different ratios between cavity opening to cavity depth. A ratio of 0.5 (dashed lines) means that the opening is equal to half of the cavity depth, and a ratio of 1 (solid lines) means that the opening is equal to the cavity depth. The results are for a façade with a low- E coated external glazing.

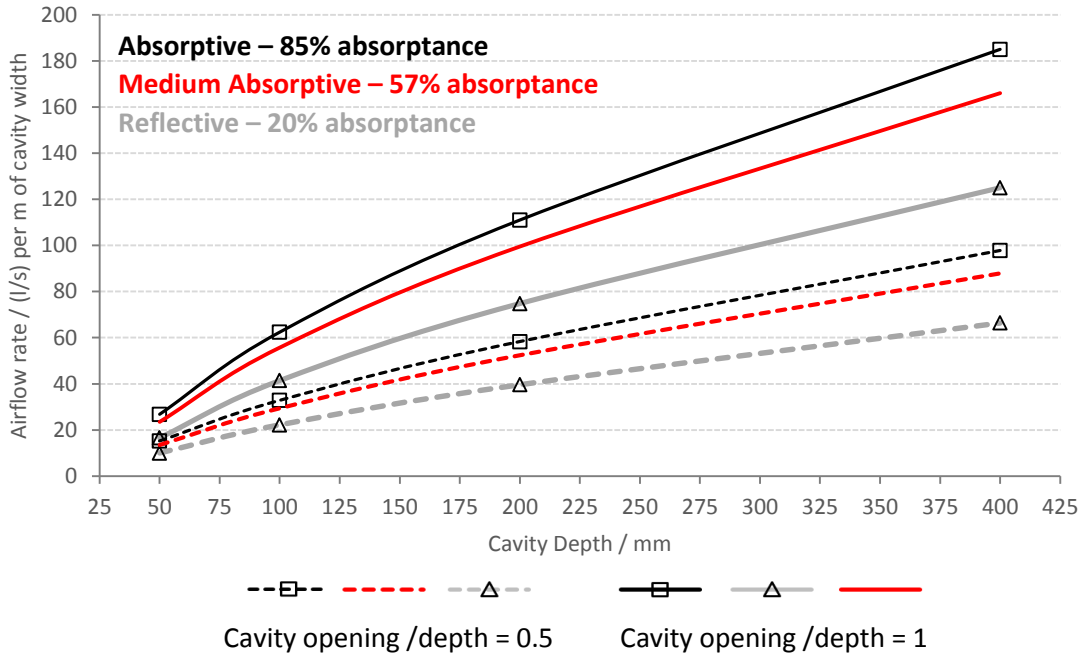


*Figure 4.5: Airflow rate per meter of cavity width for different shading devices and ratios of opening width to cavity depth, for an extreme summer day ($T_{out}$ = 30°C and $T_{in}$ = 25°C, I = 900 W/m$^2$). Low-E coated glass as external skin.*

The airflow rate through the cavity is higher for absorptive shadings than reflective ones. More absorptive shadings result in higher temperature difference between the layers bounding the cavity and the outside air (see also Figure 4.4), which in turn results in an increased airflow rate. The airflow rate increases as the cavity depth and opening size increases. However, cavities which have the equal opening size to the cavity depth (opening/depth = 1) have higher airflow rate than cases with the same opening size at a wider cavity (opening/depth = 0.5). For example, in the case of absorptive shading with 0.2m opening and 0.4m cavity depth, the airflow rate is lower than for the one with an equal depth and an opening of 0.4m. All the cases with openings equal to the cavity depth result in higher airflow rate than the cases with the same depth but smaller openings.

Figure 4.6 shows the g-value as a function of cavity depth, for reflective (light grey lines), medium absorptive (red lines) and absorptive (black lines) shading devices, for different ratios between cavity opening to cavity depth. A ratio of 0.5 (dashed lines) means that the opening is equal to half of the cavity depth, and a ratio of 1 (solid lines) means that the opening is equal to the cavity depth. The results are for a façade with a hard coated low-E external skin and a double clear inner window.

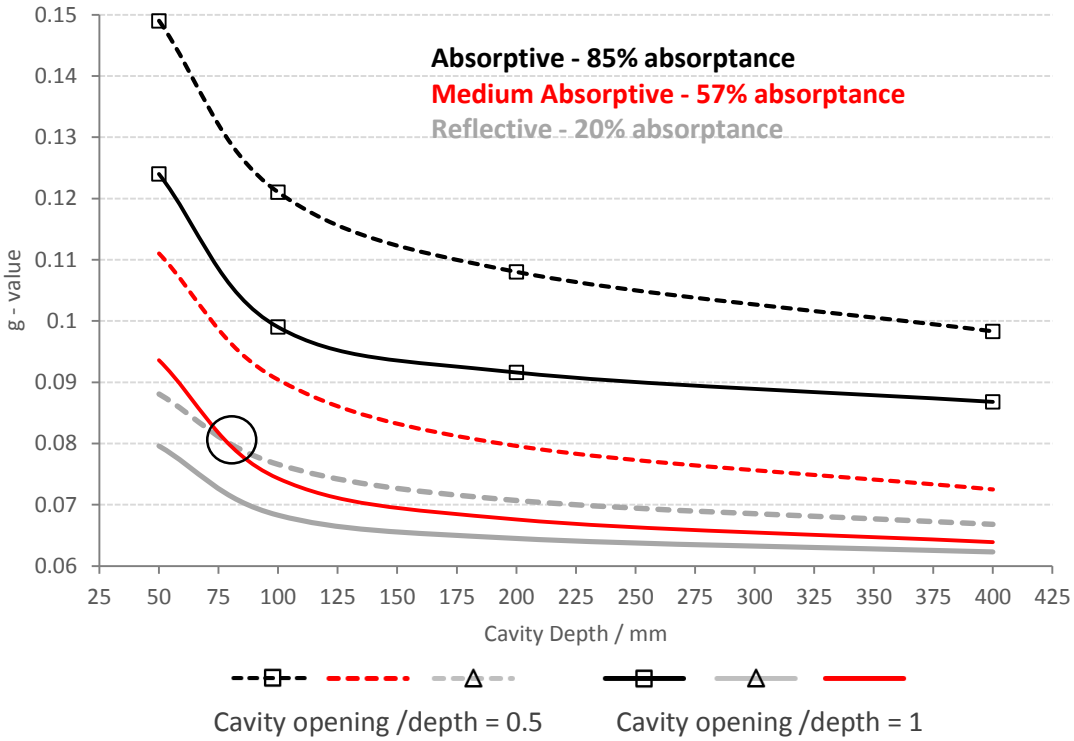


*Figure 4.6: Impact of cavity and opening sizing on the g-value of the system for an extreme summer day ($T_{out}$ = 30°C and $T_{in}$ = 25°C, I = 900 W/m$^2$). Low-E hard coated glazing as external skin.*

The g-value of the façade system decreases as the cavity opening and depth increases. This can be attributed to the simultaneous increase of the airflow rate through the cavity (see also Figure 4.5). For the same reason the g-value of the system for each shading type is lower in fully open cavities (opening/depth =1) than half open ones (opening/depth = 0.5). The highest reductions of the g-value are obtained for the absorptive shadings which have higher secondary transmittance. However, the reflective shading gives in general lower g-values than the rest of the cases, despite of the ventilation. Nevertheless, the following case should be noted: the medium absorptive shading positioned in a fully open cavity (opening/ depth =1) starts with a higher g-value than the reflective shading positioned in a half open cavity (opening/depth = 0.5). However, the g-value of the former case becomes lower than the latter as the cavity depth and opening size increases (black circle in the graph). This means that the higher airflow rate of the medium absorptive case (see also Figure 4.5) removed enough heat from the system to result in a lower total heat gain in the room.

Figure 4.7 shows the inner layer temperature as a function of cavity depth, for reflective (light grey lines), medium absorptive (red lines) and absorptive (black lines) shading devices, for different ratios between cavity opening to cavity depth. A ratio of 0.5 (dashed lines) means that the opening is equal to half of the cavity depth, and a ratio of 1 (solid lines) means that the opening is equal to the cavity depth. The results are for a façade with a hard coated low-E external skin and a double clear inner window.

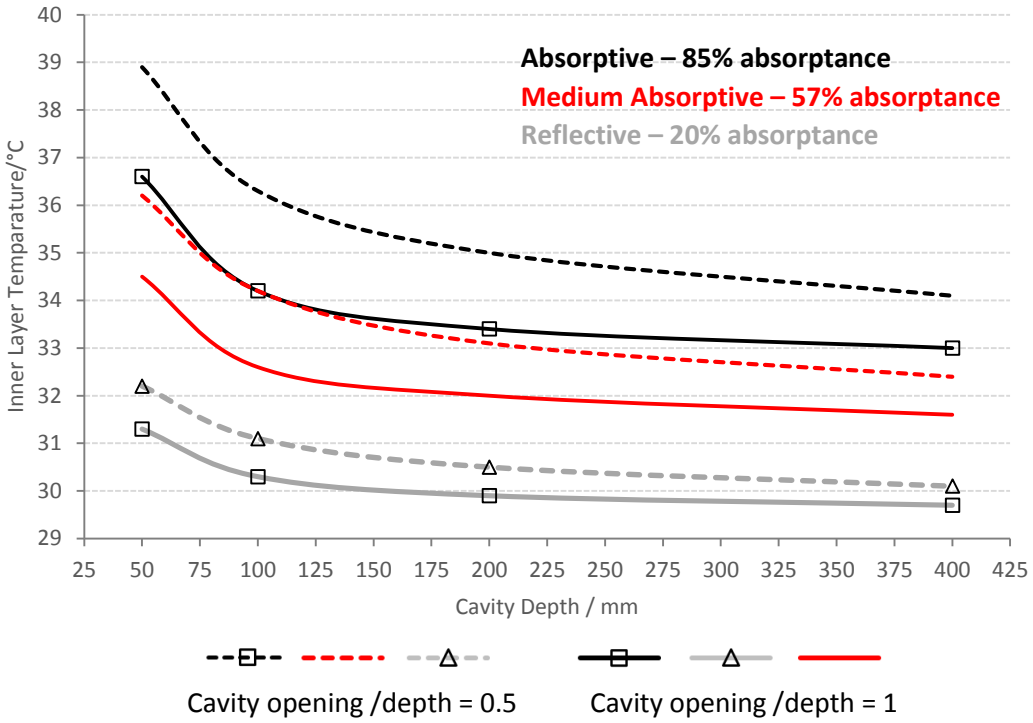


*Figure 4.7: Impact of cavity and opening sizing on inner layer temperatures for an extreme summer day (outside T = 30°C and inside T = 25°C, incoming radiation = 900 W/m$^2$). Low-E hard coated glazing as external skin.*

The inner layer temperature decreases as the cavity opening and depth increases. Moreover fully open cavities (opening/depth=1) result in lower inner layer temperatures than half open ones (opening/depth=0.5). This is an effect of the higher airflow rates through cavities with large openings which reduce the secondary transmitted energy and consequently the inner layer temperature. The absorptive shading is affected more by the changes of the cavity geometry (and consequently the airflow rate) and has a temperature decrease of 6°C when comparing a half open cavity (opening/depth=0.5) of 0.05m to a fully open cavity (opening/depth=1) of 0.4m. Interesting to note that in contrast to the g-value relationship seen in Figure 4.6 for the cases of totally open cavity with medium absorptive shading (opening/depth=1) and half open cavity with reflective shading (opening/depth=0.5), Figure 4.7 shows that the inner layer temperature of the first case is 1.5 °C higher than the second.

Figure 4.8 shows the vertical air temperature profile in the cavity of a ventilated façade as a function of cavity height for a façade with a low-E coated external skin for an absorptive (upper left graph), medium absorptive (upper right graph) and a reflective shading (lower graph), for different cavity depths and opening sizes. In all cases the opening size is equal to the cavity depth.

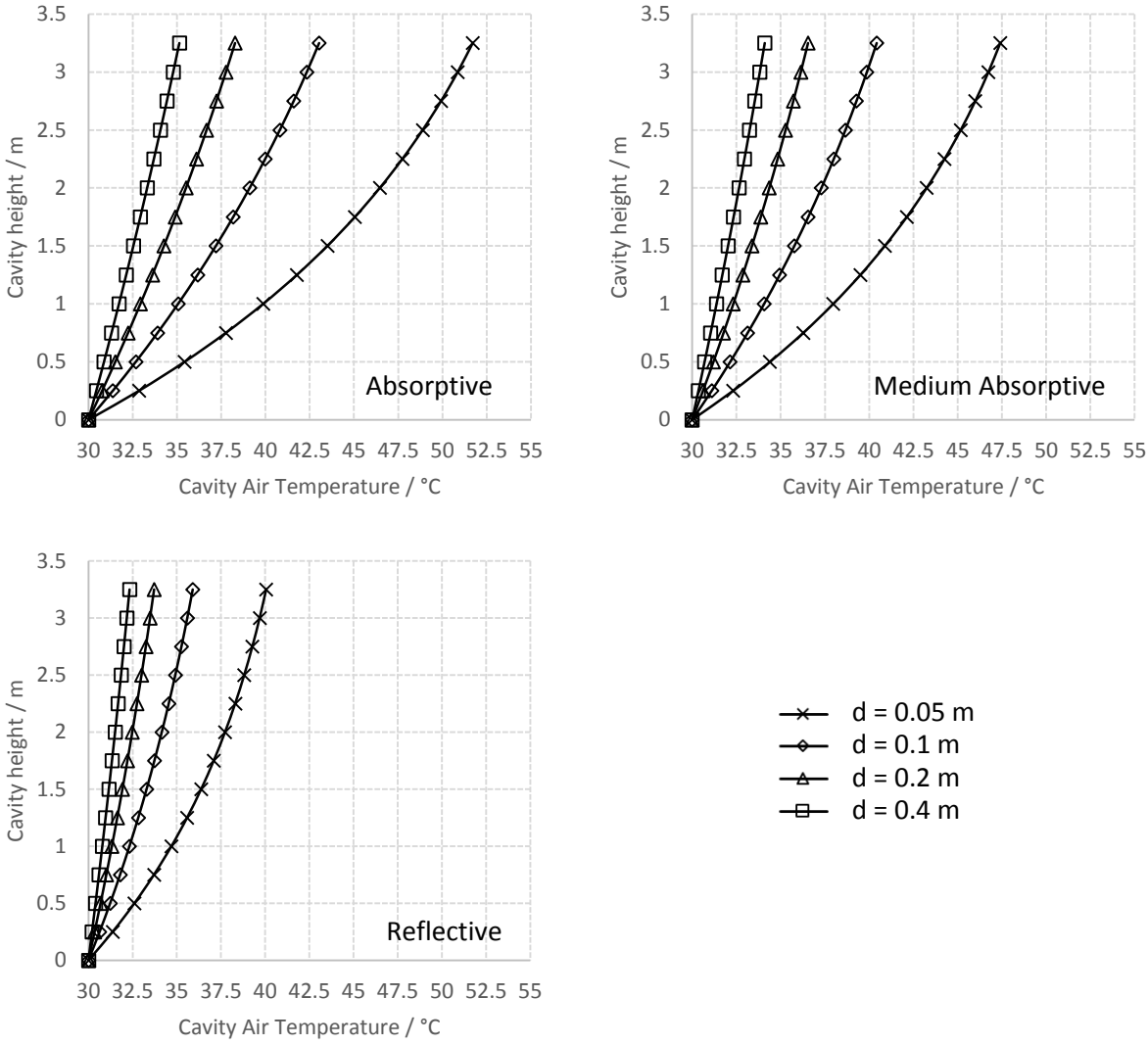


*Figure 4.8: Vertical air temperature profile for a low-E coated external skin for different shading options at different cavity depths and openings. The ratio of cavity opening to cavity depth is 1.*

All three graphs show that small cavities (0.05m opening and depth) result in significant increase of the cavity air temperature along the façade height. For a cavity depth of 0.05 m and for the reflective shading the temperature at the top of the cavity is 10°C higher than the outdoor, while for the absorptive shading the same temperature difference is more than 20°C. When increasing the cavity depth and opening, consequently providing higher airflow rate (see also Figure 4.5), the cavity air temperature rise decreases. For the absorptive shading the temperature drop of the cavity air at the top of the cavity is approximately 10°C when moving from a cavity depth of 0.05m to 0.1 m. The temperature drop of the cavity air at the top of the cavity is 5°C for a reflective shading, for the same change in geometry.

## 4.2 Annual energy and thermal comfort performance

The results from the annual dynamic simulations performed in IDA-ICE are hereby presented. The estimation of the thermal transmittance of the ventilated façade is presented in section 4.2.1. The annual heating energy demand, the cooling energy demand and the specific energy use as well as the performance of the studied room in terms of thermal comfort are thereafter analyzed for the different parameters presented in chapters 2.4. These results are presented in

sections 4.2.2– 4.2.4. The best cases of these simulations are then compared with the alternative refurbishment scenarios described in chapters 2.6.5. These results are given in section 4.2.5.

### 4.2.1 Thermal transmittance of the ventilated façade

Figure 4.9 shows the heating energy demand of a north oriented room for 30% and 70% window to wall ratio (WWR), for facades with low-Iron and low-E coated external skins. The light grey bars refer to simulations performed with the double façade model of IDA-ICE. The white bars refer to simulations performed in IDA-ICE with single skin facades with thermal transmittance equal to the one estimated for the ventilated options (when they are closed). The dark grey bars refer to Excel based estimations of the heating demand of the room with the CIBSE degree day method [45]. The base case is presented as a single skin façade. Figure 4.10 shows the same results for a south oriented room.

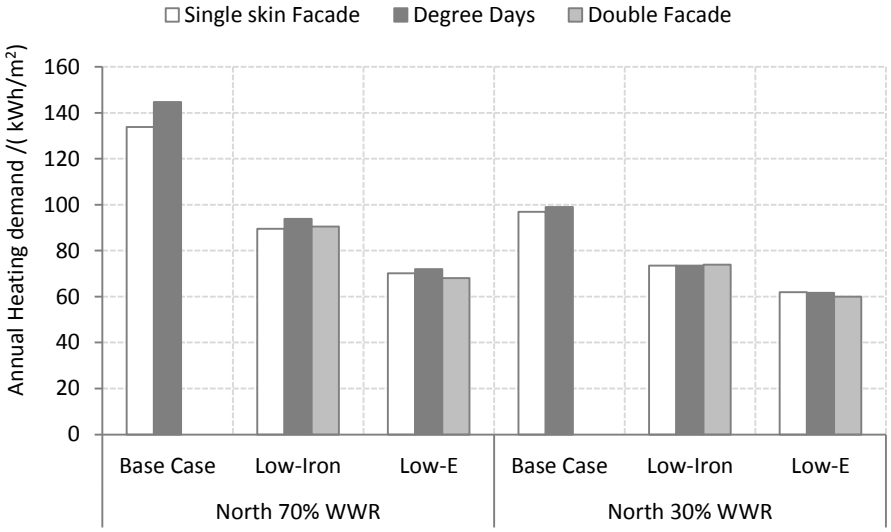


*Figure 4.9: Annual heating demand for north orientation for 30% and 70% WWR, for different calculation and modelling methods.*

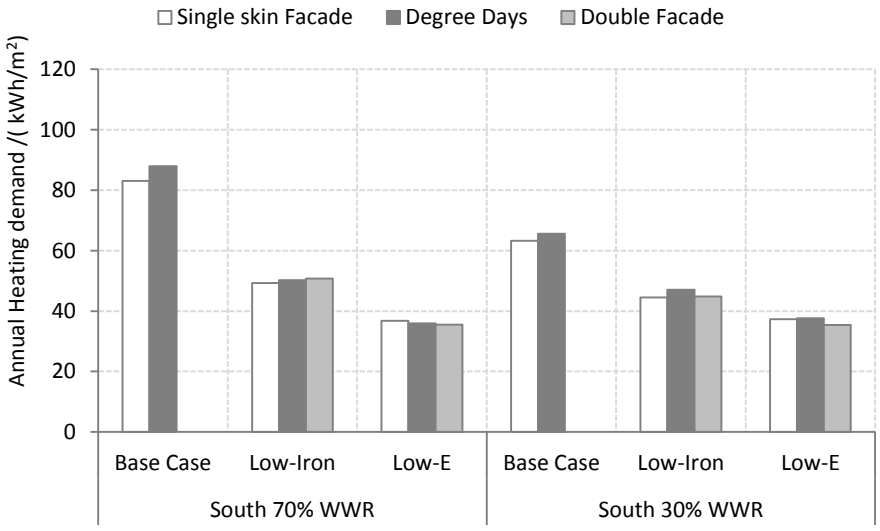


*Figure 4.10: Annual Heating demand for south orientation for 30% and 70% WWR, for different calculation and modelling methods.*

At both north and south orientations (Figure 4.9 and Figure 4.10 respectively), the results for the heating demand of the room obtained by the different methods are similar, i.e. that the U-values estimated for the different external skin options (low-Iron and low-E) are fairly correct. In most cases the Excel based calculations predict slightly higher heating demand than the single skin or the double façade alternatives. The maximum difference is observed for the base case of the north oriented room at 70% WWR, where the energy demand with the degree day method is by 8% higher than the simulated single skin alternative. In most cases however the differences between the predicted energy demands do not exceed 6%. Small differences can be also seen in the cases with the low-E coated external skin which in both examined orientations and WWR result in slightly lower heating demand for the double façade model than the single skin alternatives or the Excel cases. Despite these discrepancies it can be concluded that the addition of the ventilated facades results in a significant reduction of the thermal transmittance for all cases as summarized in Table 4.1.

*Table 4.1: Reduction of U-value for the low –Iron and low – E façades compared to the base case.*

| | U-value/ (W/(m$^2$K)) | | Low -Iron reduction of U-value compared to Base Case / % | U-value/ (W/(m$^2$K)) | Low-E reduction of U-value compared to Base Case / % |
|---|---|---|---|---|---|
| WWR | Base Case | **Low Iron** | | **Low – E Coated** | |
| 30% | 1.38 | **1.08** | 22 | **0.9** | 35 |
| 70% | 2.17 | **1.52** | 30 | **1.2** | 45 |

The reductions of the heating demand of the base case due to the addition of the external skins follow closer the reduction of the U-value in north orientation than in south, as north orientation is not affected that much by solar gains. For north orientation the heating demand is reduced by 35% and 46% for the low-Iron and low-E facade respectively at 70% WWR and 25% and 37% at 30% WWR. On south the reduction is higher, between 38% and 56% for the low-Iron and the low-E façade respectively at 70% WWR and 28% to 41% at the smaller window (30% WWR).

### 4.2.2 Annual heating demand

This section gives the results regarding the performance of the examined room in terms of annual heating energy demand. At first the temperature rise in the cavity is examined in order to understand the influence of the glazing type, the window to wall ratio (WWR) and the solar and thermal properties of the inner skin on the cavity as a heat buffer zone. Thereafter the resulting annual heating demand is given.

Figure 4.11 demonstrates the outdoor and the cavity temperature for the base case with low-Iron and low-E external skins at 30% WWR (dashed, grey and black lines respectively). The presented cases are with a double clear initial window and the cladding presented for the base case (see section 2.2).

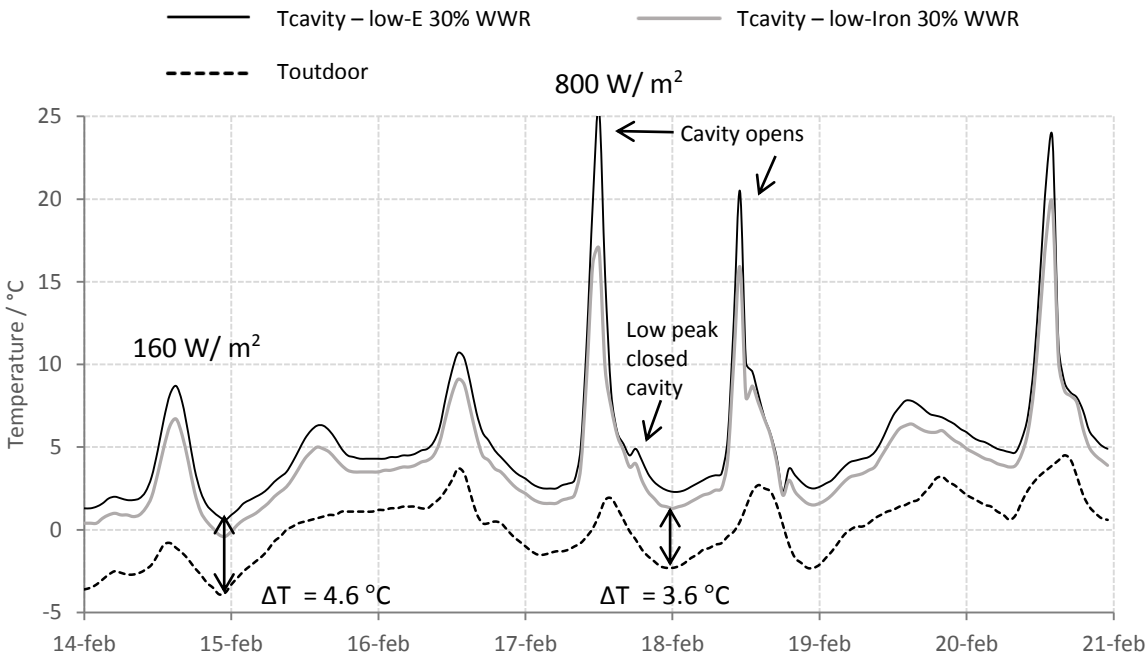


*Figure 4.11: Outdoor temperature and cavity temperatures at 30% WWR for low-Iron and low-E coated external glazing.*

According to Figure 4.11, the cavity is warmer for the low-E coated case. The low-E coating of the outer skin reduces heat losses, by reflecting longwave radiation from the inner skin back to the cavity. The temperature difference between the outdoor temperature and the cavity temperature during nights is 4.6°C and 3.6°C for the low-E coated and the low-Iron facade respectively. During days with low amount of solar radiation (eg. 14/02) the peak temperature is 8.7 °C and 7.7°C for the low-E and the low-Iron external skin respectively while the outdoor temperature is below 0 °C.

During the examined period, the cavity temperature reaches its highest values on 17/02 and 18/02, due to high solar radiation. A steep drop of the cavity temperature is observed during these two days and on 20/02. This happens since the space becomes ventilated and the heat is removed, i.e. the setpoint $T_{air,room}$ = 24.5°C is reached. The low peak of the curve corresponds to the first value calculated after the cavity closes and the temperature rises slightly.

Figure 4.12 shows the outdoor and the cavity temperature for the base case with low-Iron façade for 30% and 70% WWR (dashed, black and grey lines respectively). The graph also includes the cavity temperature for a case with reflective inner cladding (absorptance=5%, red line in the graph) at 30% WWR.

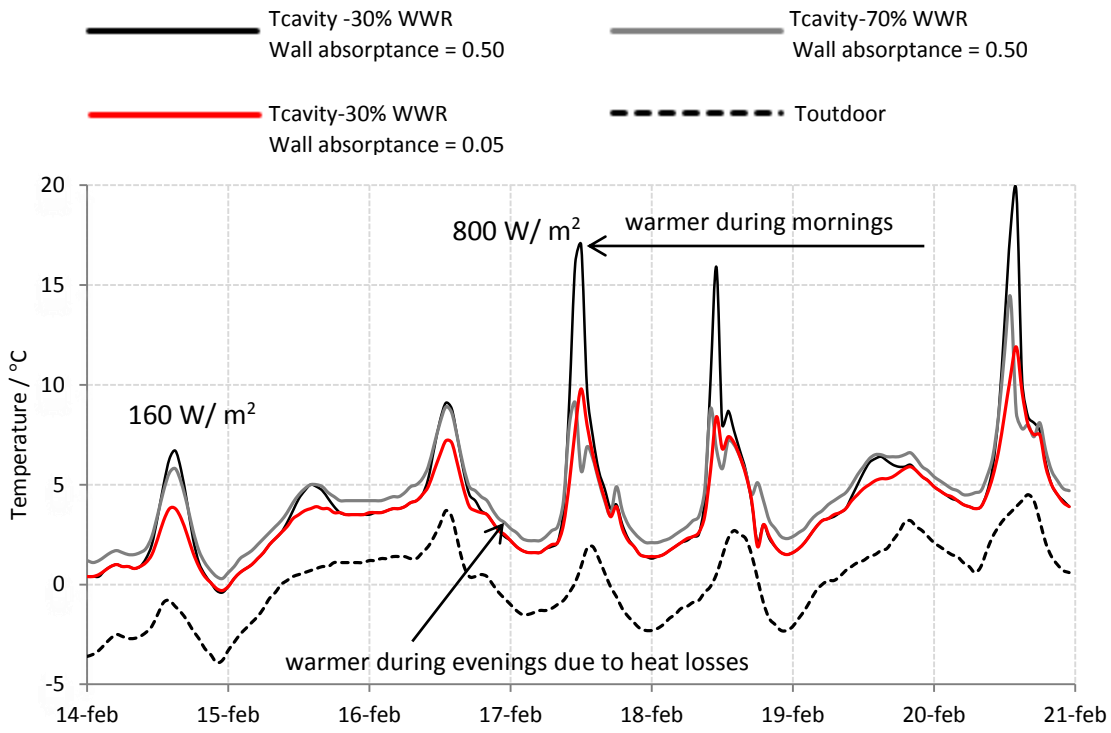


*Figure 4.12 Outdoor temperature and cavity temperature for WWR 30% and 70% and a wall with low absorptance at 30% WWR. External glazing of low-Iron.*

By comparing the fluctuation of the cavity temperature of the two WWRs combined with the base case inner wall cladding (grey and black lines), it can be seen that the 30% WWR case is warmer during daytime and colder during nighttime.

The curve which corresponds to a wall of low absorptance (α = 5%) at 30% WWR shows that the cavity is colder than the base case's one (α =50%) during daytime. The temperature difference between these cases is 2-3°C and 6-8°C on days with low and high solar radiation respectively (ex. 14/02 and 17/02 respectively). The wall of low absorptance results into lower cavity temperature during daytime, since the highest part of radiation is reflected, as opposed to the initial wall, where the 50% of the incoming radiation is absorbed.

Figure 4.13 demonstrates the outdoor and cavity temperature for a 30% WWR case with a low-Iron outer skin and the inner wall cladding of the base case (black line), as well as concrete (grey line) and brick claddings (red line).

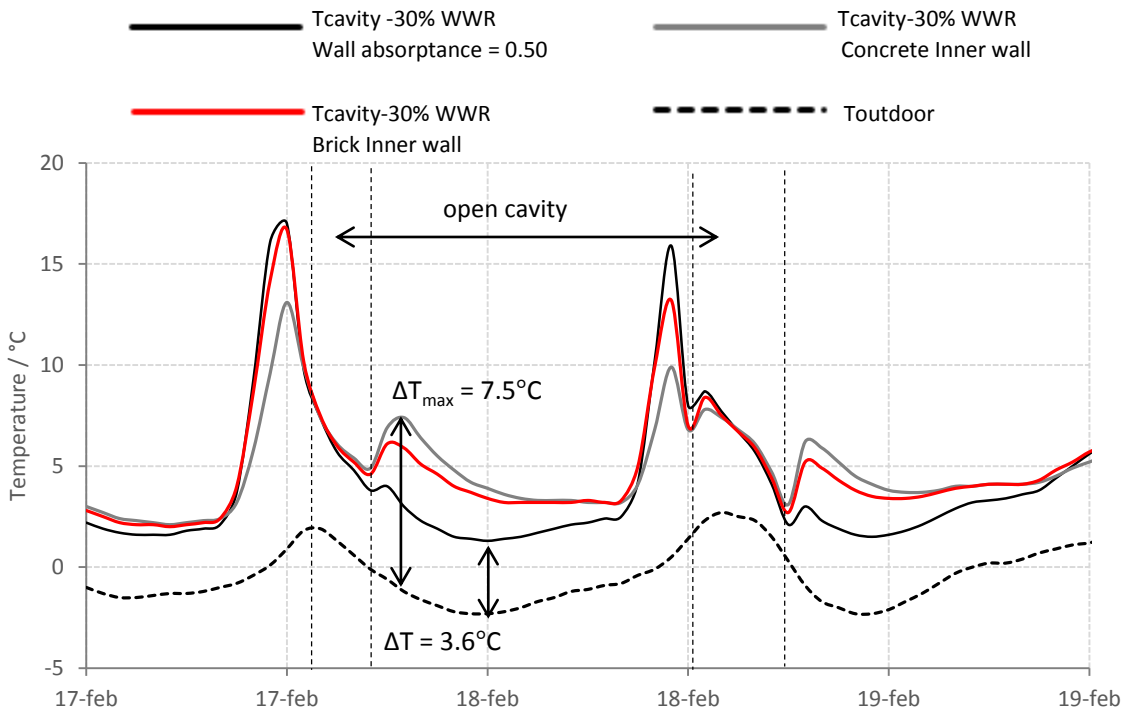


*Figure 4.13: Cavity Temperature with the base case cladding, concrete and brick for a low-Iron external glazing.*

The temperature fluctuation of the air in the cavity is smoother when the inner cladding changes from the base case cladding to a more thermally massive construction (brick and concrete). The cavity temperature is lower during daytime for the concrete and the brick wall, because the two materials absorb solar radiation and store the heat. During nighttime the cavity temperature of both massive walls is higher than in the case of the initial wall, as the stored heat is released to the cavity. This explains the higher temperature peak for the massive walls after the cavity closes. At this point the temperature difference between the cavity and the outdoor space becomes maximum for all the cases and it is found 4°C, 7°C and 7.5°C for the base case, the brick and concrete wall respectively. In general, the temperature difference is higher with concrete cladding as it has higher thermal capacity than brick.

Figure 4.14 shows the annual heating demand of the 30% WWR case with low-Iron and Low-E external skins with the base case cladding as well as concrete and brick claddings for south, west, and east orientations. The heating demand for the north oriented rooms is only presented for the base case cladding. The type of cladding is noted in the parentheses.

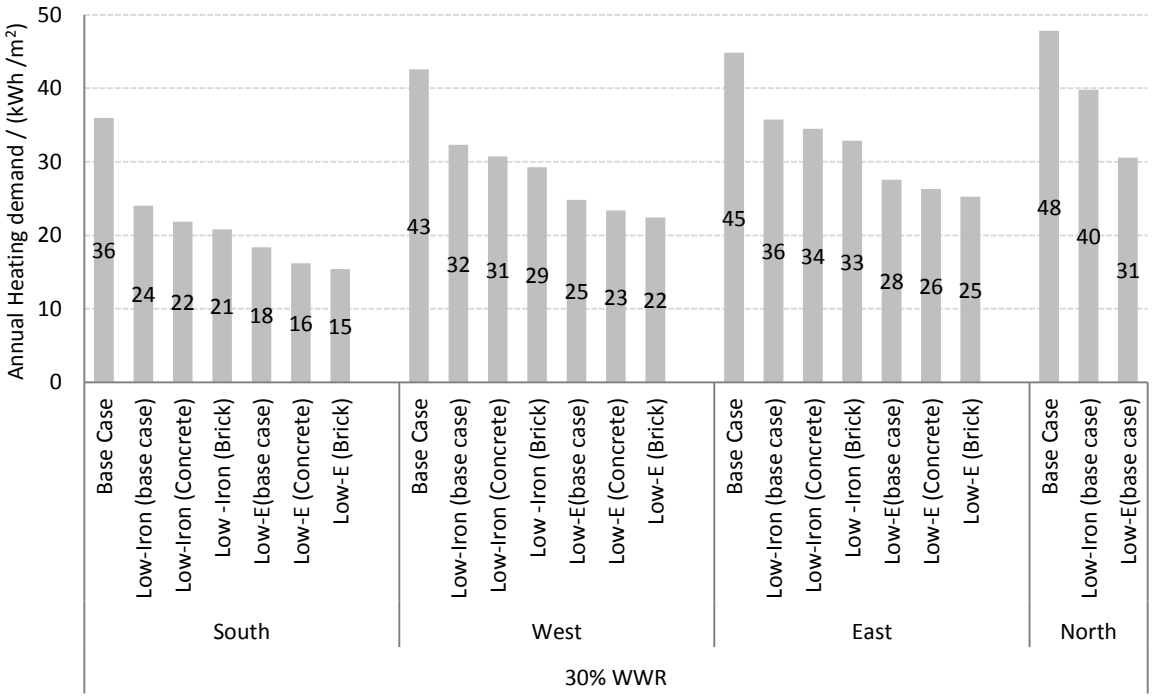


*Figure 4.14: Annual Heating Demand at 30% WWR for base case and different external skins and cladding materials at different orientations, for cavity depth and opening of 0.2m.*

Figure 4.15 shows the annual heating demand of the 70% WWR case with low-Iron and low-E external skins for south, west, east and north orientations.

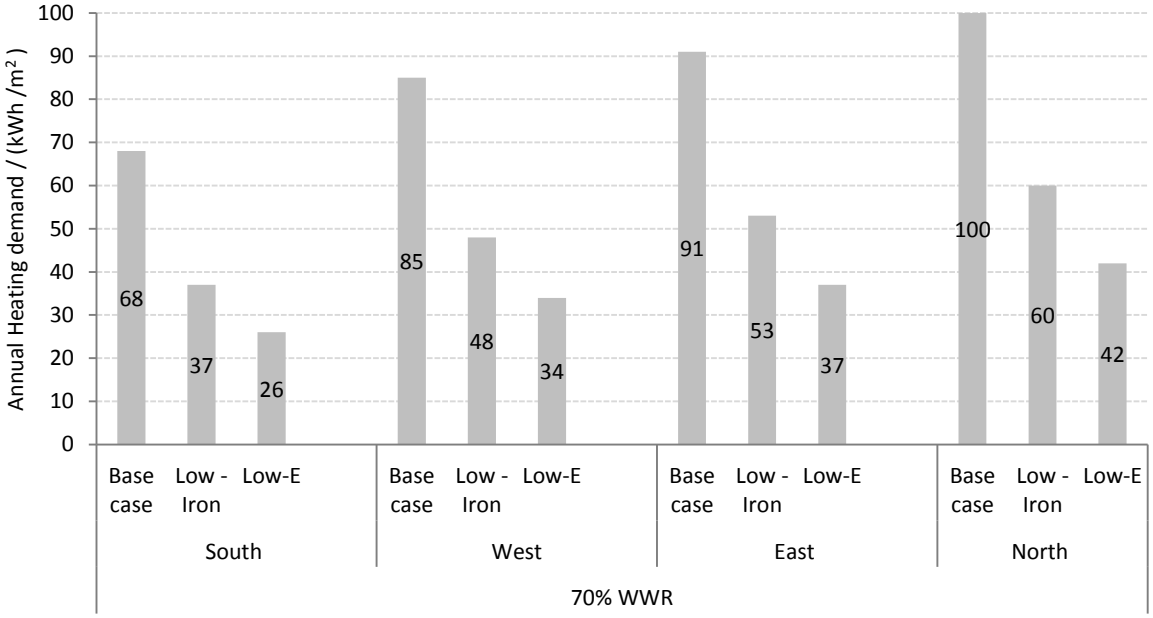


*Figure 4.15: Annual Heating Demand at 70% WWR for base case and different external skins at different orientations, for cavity depth and opening 0.2m.*

The annual heating demand of the base case ranges from 36 kWh/m$^2$ to 48 kWh/m$^2$ for the 30% WWR and 68 kWh/m$^2$ to 100 kWh/m$^2$ for the 70% WWR at south and north orientation respectively. The impact of improving the U-value, on the heating energy demand of the room with the addition of any of the ventilated options is significant. Table 4.2 summarizes the reduction of the heating energy use at 30% and 70% WWR for the examined outer skins at

different orientations. Table 4.3 shows the reduction of the heating demand for concrete and brick cladding with low-Iron and low-E external skins from the base case cladding, at south, east and west orientations for 30% WWR.

*Table 4.2: Reduction of heating demand of the base case for low-Iron and low-E external glazings at different orentations.*

| 30% WWR | | | | | | | | 70% WWR | | | | | | | |
|---|---|---|---|---|---|---|---|---|---|---|---|---|---|---|---|
| Low-Iron | | | | Low-E | | | | Low-Iron | | | | Low-E | | | |
| S | W | E | N | S | W | E | N | S | W | E | N | S | W | E | N |
| 33% | 24% | 20% | 17% | 49% | 42% | 39% | 36% | 46% | 44% | 42% | 40% | 62% | 60% | 59% | 58% |

S = south, W = west, E = east, N = north

*Table 4.3: Reduction of the heating demand from base case cladding, for the cases of concrete and brick cladding, for south, east and west orientations and WWR 30%*

| Low-Iron | | | | | | Low-E | | | | | |
|---|---|---|---|---|---|---|---|---|---|---|---|
| S | | W | | E | | S | | W | | E | |
| Brick | Con-crete | Brick | Con-crete | Brick | Con-crete | Brick | Con-crete | Brick | Con-crete | Brick | Con-crete |
| 13% | 9% | 9% | 5% | 8% | 4% | 16% | 12% | 10% | 6% | 8% | 5% |

S = south, W = west, E = east

The highest heating demand reductions are obtained for the 70% WWR, due to the larger glazing area that corresponds to higher heat losses. Regarding the outer skin, the low-E coated façades bring the highest heating reductions for all the cases. With respect to the orientations, the highest reduction is noted for the south orientated room, which is affected the most by solar radiation. The rest of the reductions follow the solar exposure for each room (Figure 2.2) and therefore the lowest heating decrease is obtained for the north oriented room followed by the east and west.

Concerning the influence of thermal mass in the cavity, there is an improvement in the heating demand with concrete and brick claddings at both double skin options. The improvement is higher in south orientation due to higher irradiation. Brick performs better bringing another 13% of reduction in the heating demand of the low-Iron case. Even though concrete presented higher temperatures in the cavity during nighttime compared to the brick case (see Figure 4.13), the latter results in higher heating demand reduction due to its slightly lower U-value (see Table 2.10).

The cases with low-E outer skin and massive walls result in higher decrease of heating demand of the low-E case with the base cladding compared to the respective low-Iron options. The highest decrease of 16% is again noted on south orientation for brick cladding.

### 4.2.3 Annual cooling demand and specific energy use

The results regarding the cooling performance of the room with the different shading options are hereby presented. The influence of ventilation and photovoltaic ratio (PVR) on the external skin in terms of cavity air and shading temperatures is analyzed. The cooling demand and the specific energy use of the different cases examined is thereafter presented.

Figure 4.16 shows the cavity temperature during a warm summer day for the 30% WWR case with a reflective (upper figure) and an absorptive (lower figure) shading for cavity depths and openings of 0.1m, 0.2m and 0.4m. A low-Iron glazing is used at the outer skin.

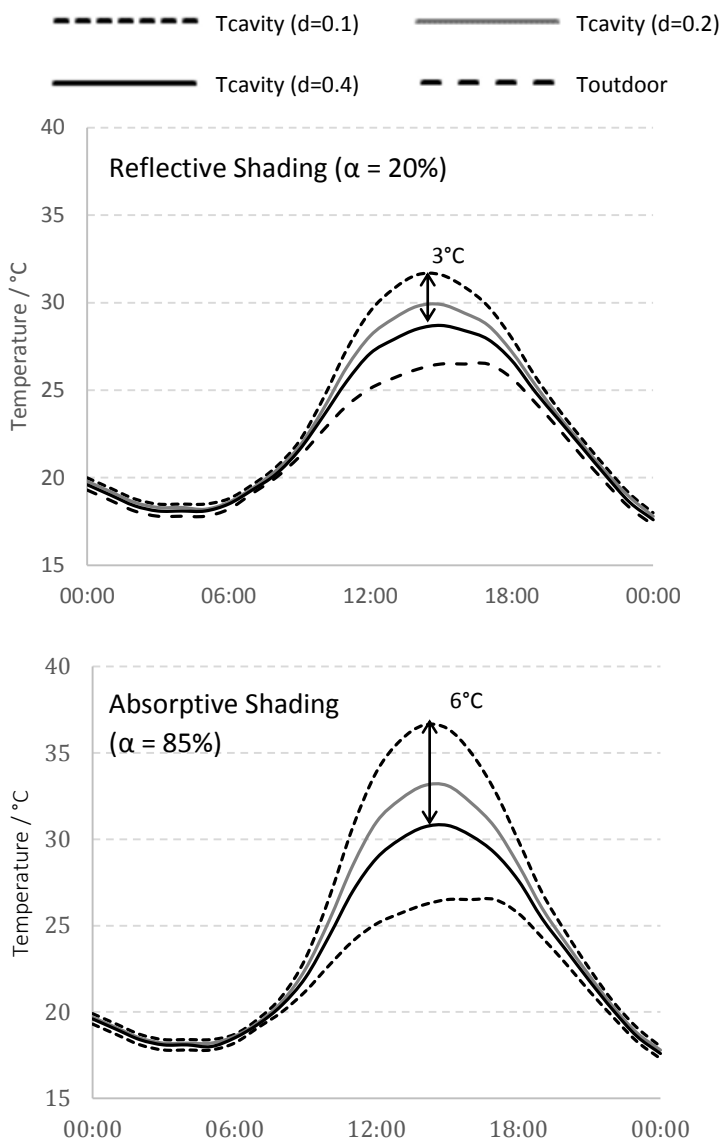


*Figure 4.16: Cavity Temperature for a reflective (left) and an absorptive (right) shading device during a warm summer day at different cavity depths and openings. The openings are equal to the cavity depths.*

The lowest cavity temperatures are obtained for the cavity depth and opening of 0.4m. At this depth the air temperature in the cavity is 2°C and 4°C higher than the outdoor temperature for the reflective and absorptive shading respectively. The difference of the peak cavity temperature (at 15:00) between the cases of 0.1m and 0.4 m is 3°C and 6°C for the reflective and absorptive shading respectively.

Figure 4.17 shows the temperature of a reflective and an absorbing shading during a warm summer day, with 0% and 73% PVR on the external skin. A low- Iron glazing is used at the external skin and the cavity depth is set to 0.2m. The results are presented for the 30% WWR.

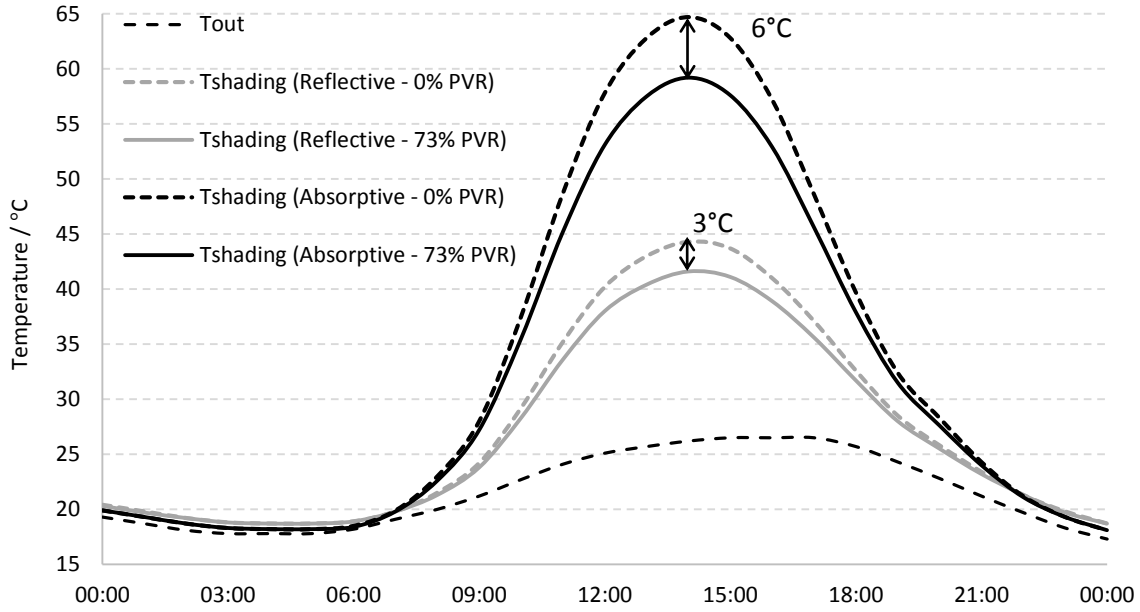


*Figure 4.17: Shading Temperature for reflective and absorptive shading for 0% and 73% PV coverage ratio.*

It can be seen that the integrated PVs affect the temperature of the shading. For the reflective shading the temperature difference is 3°C between the cases of PVR 0% and 73%. For the absorptive shading the maximum temperature decrease is 6°C for the same PVRs. The integrated PVs prevent an amount of the incident radiation from reaching the shading behind them. The temperature drop due to PV integration is lower (3°C) for the reflective shading which anyway does not absorb as much solar radiation as the absorptive case.

Figure 4.18 shows the cooling demand for 30% WWR for an absorptive, medium absorptive and a reflective shading with low-Iron external skin, for a reflective shading with a low-E coated external skin and for the base case with a reflective screen in internal position. The cavity depth and opening of the ventilated options is set to 0.2 m. Figure 4.19 shows the same results for the 70% WWR.

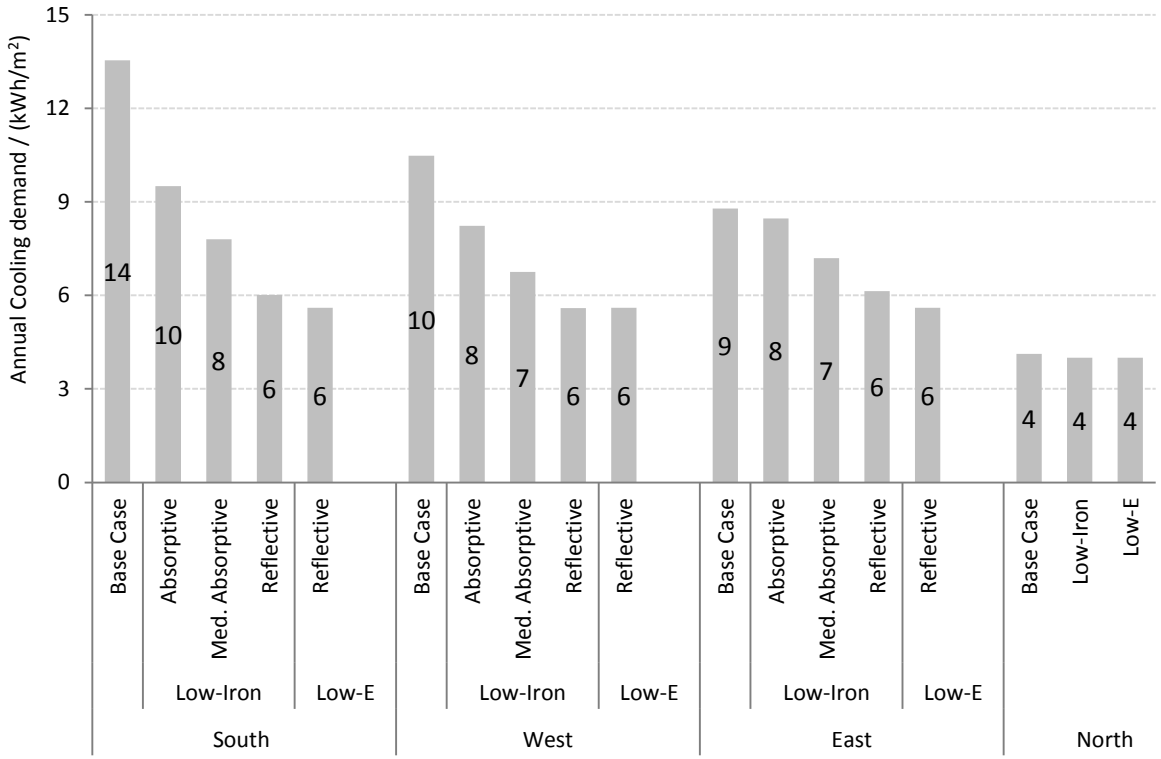


*Figure 4.18: Cooling demand at 0.2m cavity for 30% WWR and different shading devices.*

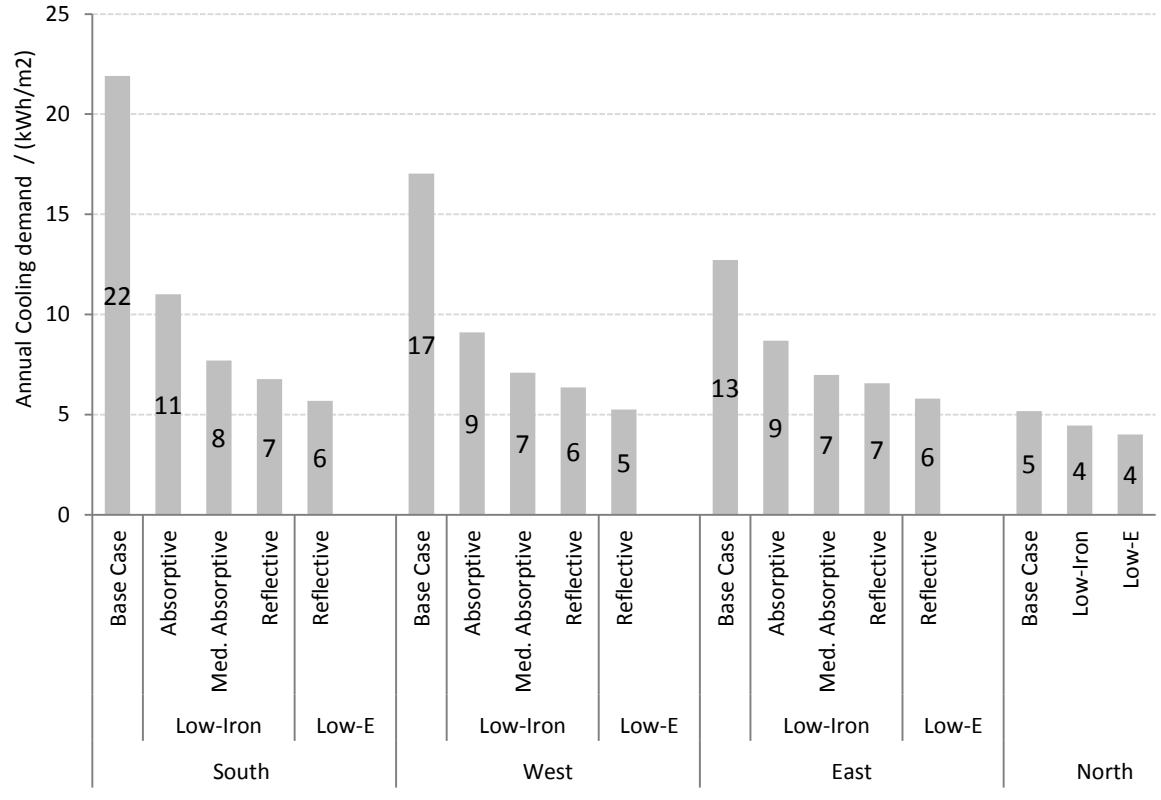


*Figure 4.19: Cooling Demand at 0.2m cavity for 70% WWR and different shading devices.*

Table 4.4 and Table 4.5 summarize the reduction in the cooling demand of the base case at different orientations for both WWRs and the different shading options.

*Table 4.4: Reduction of the cooling demand of the base case at 30% WWR for low-Iron and low-E external skins with different shadings at different orientations.*

| Low-Iron | | | | | | | | | | Low-E | | | |
|---|---|---|---|---|---|---|---|---|---|---|---|---|---|
| Absorptive | | | Medium Absorptive | | | Reflective | | | | Reflective | | | |
| S | W | E | S | W | E | S | W | E | N | S | W | E | N |
| 30% | 21% | 4% | 42% | 36% | 18% | 56% | 47% | 30% | 3% | 59% | 47% | 36% | 3% |

S = south, W = west, E = east, N = north

*Table 4.5: Reduction of the cooling demand of the base case at 70% WWR for low-Iron and low-E external skins with different shadings at different orientations.*

| Low-Iron | | | | | | | | | | Low-E | | | |
|---|---|---|---|---|---|---|---|---|---|---|---|---|---|
| Absorptive | | | Medium Absorptive | | | Reflective | | | | Reflective | | | |
| S | W | E | S | W | E | S | W | E | N | S | W | E | N |
| 50% | 47% | 32% | 65% | 58% | 45% | 69% | 63% | 48% | 14% | 74% | 69% | 55% | 23% |

S = south, W = west, E = east

Figure 4.18 and Figure 4.19 show that the base case results in higher cooling demand than all the ventilated options, due to the internally positioned shading. The results show a significant cooling reduction compared to the base case, for all the ventilated options and all WWR. For the absorptive screen at south orientation, the cooling demand decreases by 30% and 50% at 30% and 70% WWR respectively. The same reductions are 56% and 69% for the reflective ventilated case.

The decrease of cooling demand from the base case with the addition of the different facades is higher for south and west orientations for both WWRs, as these cases have initially higher cooling need, due to higher solar exposure. This is also the case for the two WWR, where the 70% case is affected more than the 30% one with the addition of the double skins with shading.

For all the cases, the Low-Iron façade with reflective shading results in the lowest cooling demand, as this case has the lowest g-value.

Figure 4.20 shows the annual cooling demand on the x-axis and the specific energy use on the y-axis of the 70% WWR case at south (squares), east (triangles) and west (circles) orientations, for different cavity depths and openings, as well as percentages of PVR on the external skin for absorptive (black points), medium absorptive (red points) and reflective (grey points) shadings. Each point represents a combination of PVR and cavity depth as noted on the graph. The increase in PVR can be discriminated by the cases falling vertically or moving parallel to the x- axis towards the right. The increase of cavity opening and depth can be discriminated by the cases moving parallel to the x–axis and to the left. A low-Iron glass is used at the external skin of all cases. The dashed vertical line notes the current BBR requirement in terms of specific energy use. Figure 4.21 shows the same results for the 30% WWR.

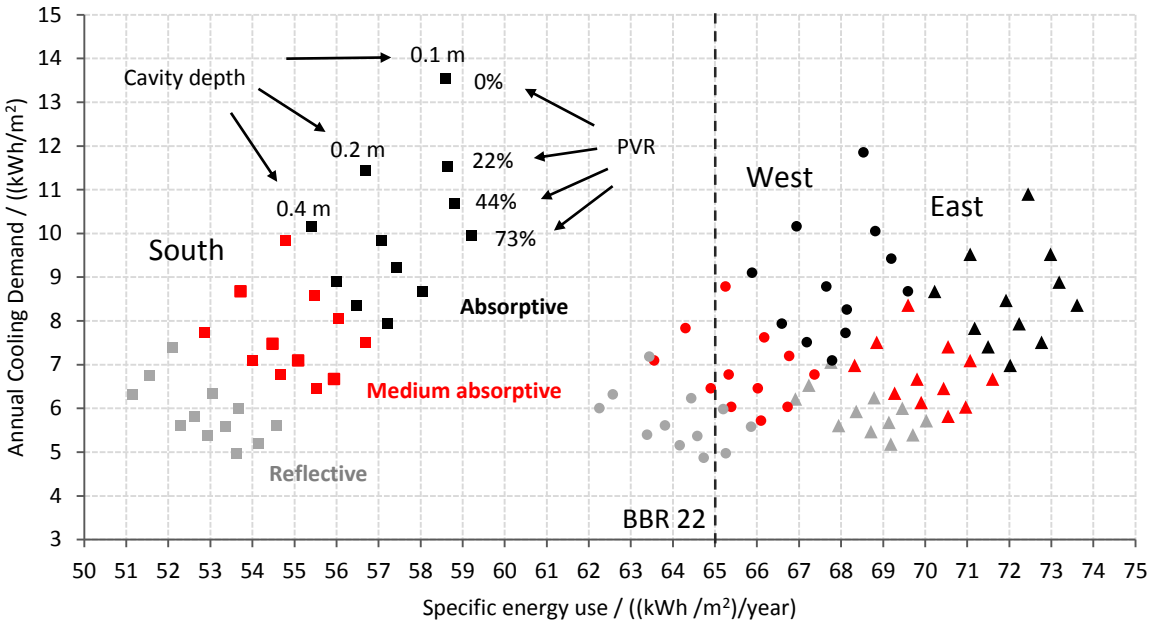


*Figure 4.20: Annual cooling demand and specific energy use for 70% WWR and different shadings, cavity depths, PV ratios and orientations. Low-Iron façade as external skin.*

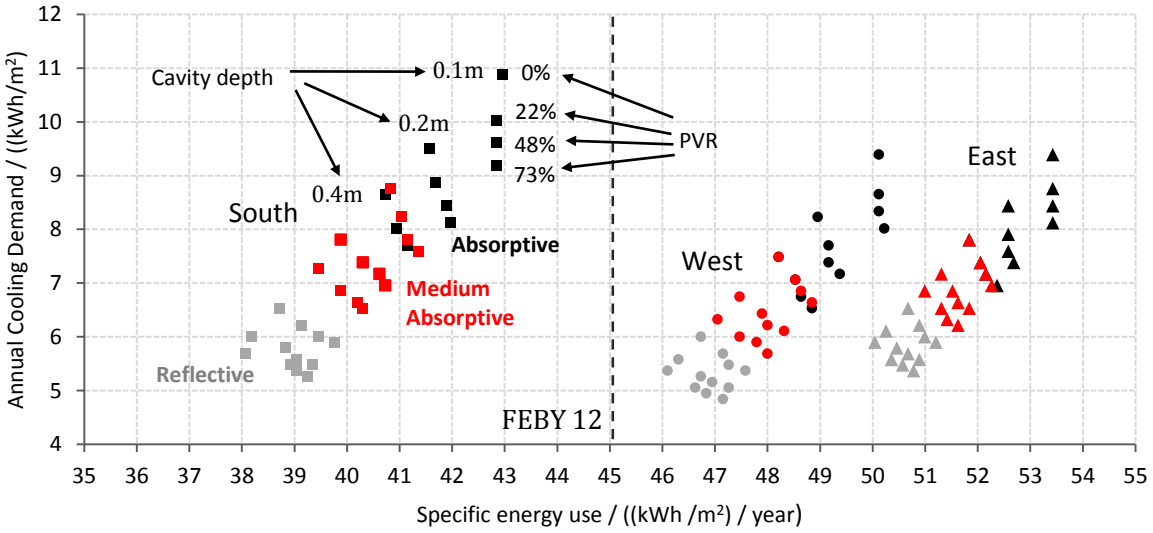


*Figure 4.21: Annual cooling demand and specific energy use for 30% WWR and different shadings, cavity depths, PV ratios and orientations. Low-Iron façade as external skin.*

According to Figure 4.20 and Figure 4.21, the integration of PVs leads to a reduction of the cooling demand for most cases and both WWRs. However, the energy use increases. The latter includes heating, cooling, fans and domestic hot water (DHW). Any increase of the specific energy use reflects an increase of the heating demand, as the part of the energy for fans and DHW is constant (8 kWh/m$^2$ per year – sees section 2.6.3). Consequently the results show that any savings in cooling are lower or equal to the heating increase which is an outcome of the integrated PVs acting as a fixed shading throughout the year. On the other hand, the cooling demand decreases for larger cavity depths and openings, which is also the case for the specific energy use.

Concerning the integrated PVs, the highest reduction of cooling is again observed for the absorptive shading, which is the case with the highest secondary gains to the room. The

decrease of cooling demand is in general larger when moving from 0% PVR to 22% than from 22% to 44% or 44% to 73%.

Table 4.6 summarizes the reduction of the cooling demand of a south oriented room at different cavity depths and openings and different PVR for the different shading options. The relative reduction of cooling is always compared to the case without integrated PVs (0% PVR) at 0.1m cavity and opening.

*Table 4.6: Cooling demand reduction for each combination of depth and PVR, from the case of d=0.1m and PVR 0%, for all the shadings.*

| Absorptive | **WWR** | **30%** | | | **WWR** | **70%** | | |
|---|---|---|---|---|---|---|---|---|
| | **Depth** / **PVR** | 0.1m | 0.2m | 0.4m | **Depth** / **PVR** | 0.1m | 0.2m | 0.4m |
| | 0% | 0% | 13% | **20%** | 0% | 0% | 16% | **25%** |
| | 20% | 8% | 18% | 26% | 20% | 15% | 27% | 34% |
| | 50% | 12% | 22% | 29% | 50% | 21% | 32% | 38% |
| | 80% | **16%** | 25% | 30% | 80% | **27%** | 36% | 41% |

| Medium Absorptive | **WWR** | **30%** | | | **WWR** | **70%** | | |
|---|---|---|---|---|---|---|---|---|
| | **Depth** / **PVR** | 0.1m | 0.2m | 0.4m | **Depth** / **PVR** | 0.1m | 0.2m | 0.4m |
| | 0% | 0% | 11% | **17%** | 0% | 0% | 12% | **22%** |
| | 20% | 6% | 16% | 22% | 20% | 13% | 24% | 28% |
| | 50% | 11% | 18% | 24% | 50% | 18% | 28% | 31% |
| | 80% | **13%** | 21% | 25% | 80% | **24%** | 32% | 34% |

| Reflective | **WWR** | **30%** | | | **WWR** | **70%** | | |
|---|---|---|---|---|---|---|---|---|
| | **Depth** / **PVR** | 0.1m | 0.2m | 0.4m | **Depth** / **PVR** | 0.1m | 0.2m | 0.4m |
| | 0% | 0% | 8% | **13%** | 0% | 0% | 9% | **14%** |
| | 20% | 5% | 11% | 16% | 20% | 14% | 21% | 24% |
| | 50% | 8% | 15% | 18% | 50% | 19% | 24% | 27% |
| | 80% | **10%** | 16% | 19% | 80% | **24%** | 30% | 33% |

The tables indicate that the highest reduction of cooling demand at the 30% WWR cases occurs when the cavity depth and opening increase. On the other hand the 70% WWR cases are affected more by the increase of PVR. The lower WWR has higher opaque surface, and a significant amount of the solar gains are accumulated in the cavity, which becomes warmer. Heat is thereafter removed by convection and therefore ventilation becomes significant.

On the other hand, the room with 70% WWR is affected more by solar radiation, due to its higher glazing area. Since PVs cover a part of this transparent area, an amount of the incoming shortwave radiation does not reach the room and consequently, the cooling demand decreases.

Nevertheless, the combined effect of PVR and ventilation results in a significant relative decrease of the cooling demand. The maximum cooling reduction obtained is 41% for the absorptive shading at 70% WWR.

### 4.2.4 Thermal comfort

The operative temperatures during occupied hours were evaluated against Belok classes 25°C and 26°C for the 30% and 70% WWR. The inner pane temperatures were evaluated only for the 70% WWR.

Table 4.7 and Table 4.8 summarize the percentage of occupied hours when the operative temperature exceeds 25°C or 26°C in the period between April and September, for the different double skin options examined, for 30% and 70% WWR respectively. The peak operative temperature ($T_{op, max}$), is additionally presented. All the cases correspond to 0.2m cavity with no integrated PVs.

*Table 4.7: Percentage of occupied hours when the operative temperature exceeds 25 or 26 °C and maximum operative temperature for 30% WWR and double clear initial window for different external skins and shadings at different orientations.*

| 30% WWR | South | | | | | East | | | | | West | | | | |
|---|---|---|---|---|---|---|---|---|---|---|---|---|---|---|---|
| Outer skin | BC | Low-Iron | | | Low E | BC | Low-Iron | | | Low E | BC | Low-Iron | | | Low E |
| Shade | R | R | MA | A | R | R | R | MA | A | R | R | R | MA | A | R |
| Top >25 °C | 40% | 32% | 34% | 36% | 31% | 42% | 34% | 36% | 37% | 33% | 37% | 28% | 29% | 31% | 27% |
| Top >26 °C | 0% | 0% | 0% | 0% | 0% | 0% | 0% | 0% | 0% | 0% | 0% | 0% | 0% | 0% | 0% |
| $T_{op,max}$ /°C | 26.5 | 25.7 | 25.8 | 25.9 | 25.6 | 25.6 | 25.6 | 25.6 | 25.6 | 25.5 | 25.8 | 25.6 | 25.6 | 25.6 | 25.5 |

BC = Base Case, R = Reflective, MA = Medium Absorptive, A = Absorptive

*Table 4.8: Percentage of occupied hours when the operative temperature exceeds 25 or 26 °C and maximum operative temperature for 70% WWR and double clear initial window for different external skins and shadings at different orientations.*

| 70% WWR | South | | | | | East | | | | | West | | | | |
|---|---|---|---|---|---|---|---|---|---|---|---|---|---|---|---|
| Outer Skin | BC | Low-Iron | | | Low E | BC | Low-Iron | | | Low E | BC | Low-Iron | | | Low E |
| Shade | R | R | MA | A | R | R | R | MA | A | R | R | R | MA | A | R |
| Top >25 °C | 52% | 31% | 35% | 38% | 27% | 48% | 34% | 35% | 36% | 31% | 42% | 27% | 30% | 32% | 24% |
| Top >26 °C | 2% | 0% | 0% | 0% | 0% | 0% | 0% | 0% | 0% | 0% | 1% | 0% | 0% | 0% | 0% |
| $T_{op,max}$ / °C | 26.5 | 25.7 | 25.8 | 25.9 | 25.7 | 26.3 | 25.7 | 25.8 | 25.9 | 25.6 | 26.6 | 25.6 | 25.7 | 25.8 | 25.5 |

BC = Base Case, R = Reflective, MA = Medium Absorptive, A = Absorptive

According to the above tables, Belok-25°C is not achieved for any of the cases. However, Belok-26°C is reached, since the maximum operative temperature does not exceed 26°C, except for a few cases of the 70% WWR (south and west for absorptive and medium absorptive shading). For these cases the percentage of hours when the operative temperature is higher than 26°C is below 10% of the occupied time.

Figure 4.22 shows the percentage of occupied hours when the inner layer temperature is below 18°C or above 27°C for south, east, west and north orientations for the base case, as well as for the low-Iron and low-E facades in combination with the different shading options. The cavity depth is set to 0.2m. The grey triangles and dots indicate the maximum and minimum inner layer temperature respectively at the right axis.

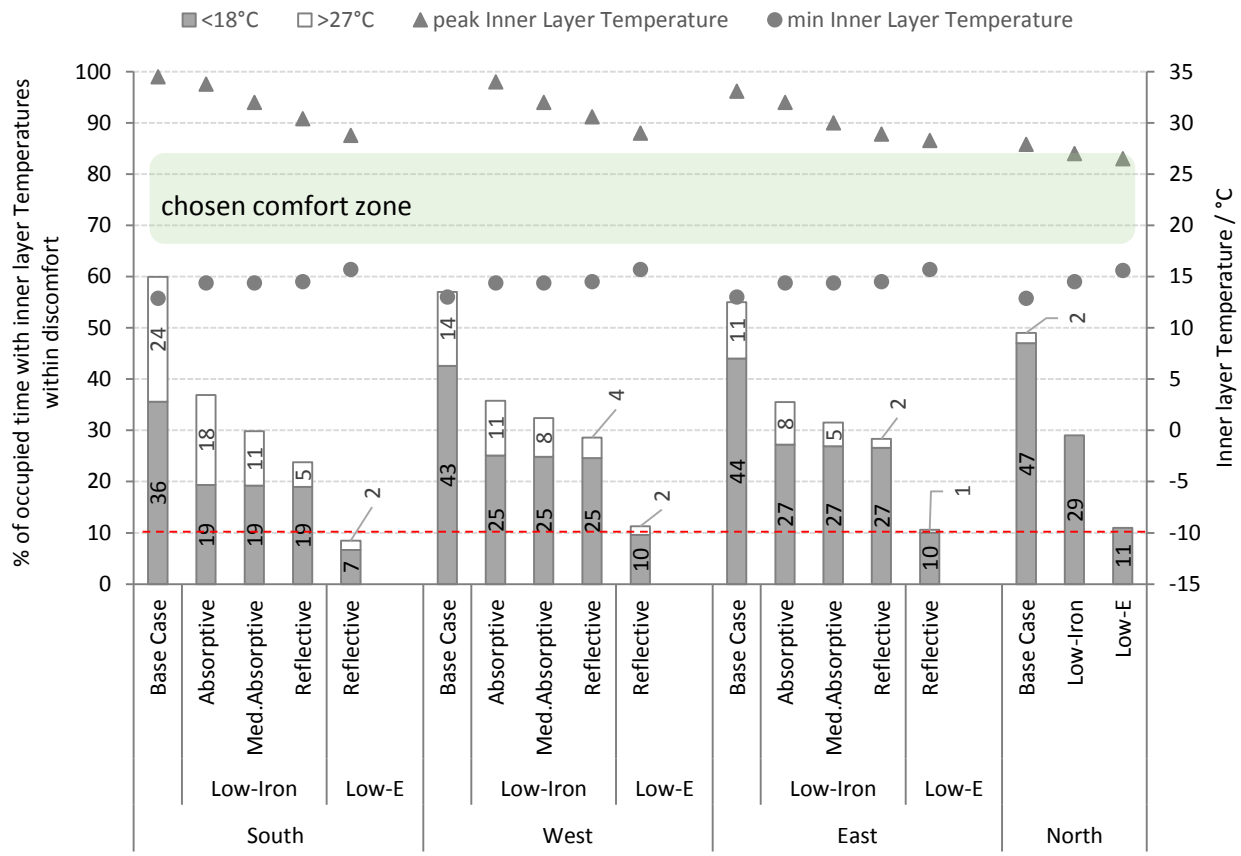


*Figure 4.22: Percentage of occupied time with inner layer temperatures within discomfort, as well as peak and minimum inner layer temperatures, for double clear initial window with different external skins and shadings at different orientations.*

For all the double skin options, the percentage of occupied time with inner layer temperatures below 18 °C is reduced compared to the base case. The obtained reductions are at least 38%, which is the case for north orientation with low-Iron skin. The percentage of occupied time with inner layer temperatures below 18 °C drops below 10% for the low-E coated façade at south orientation and is around 10% for the rest orientations at the same outer skin. The low-E façade has also the highest minimum temperature which is 15.7°C. For the low-Iron façade the percentage of time with inner layer temperatures below 18 °C varies between 19% - 29% depending on the orientation.

Among the different shading options, the reflective case results in the lowest amount of time with inner layer temperatures over 27 °C, as for this case a large amount of incoming radiation is reflected without reaching the inner skin. The best performance is achieved for the low-E façade with reflective shading which also has the lowest peak temperature at 29°C. The rest of the cases result in radiant temperatures higher than 31°C. Excluding the base case, the maximum inner layer temperature is obtained for the absorptive shading which peaks at 34 °C at south orientation.

Figure 4.23 presents the specific energy use on the x –axis and the percentage of occupied time with inner layer temperatures exceeding 27 °C of the 70% WWR case at south (squares), east (triangles) and west (circles) orientations, for different cavity depths and openings, as well as percentages of PVR on the external skin for absorptive (black points), medium absorptive (red points) and reflective (grey points) shadings. Each point represents a combination of PVR and cavity depth as noted on the graph. The increase in PVR can be discriminated by the cases falling vertically or moving parallel to the x- axis towards the right. The increase of cavity opening and depth can be discriminated by the cases moving parallel to the x–axis and to the left. The outer skin is a low-Iron glazing. The vertical dashed line shows the current BBR requirement for specific energy use and the horizontal dashed line the shows the percentage of occupied time for which the inner layer temperatures are allowed to exceed 27 °C.

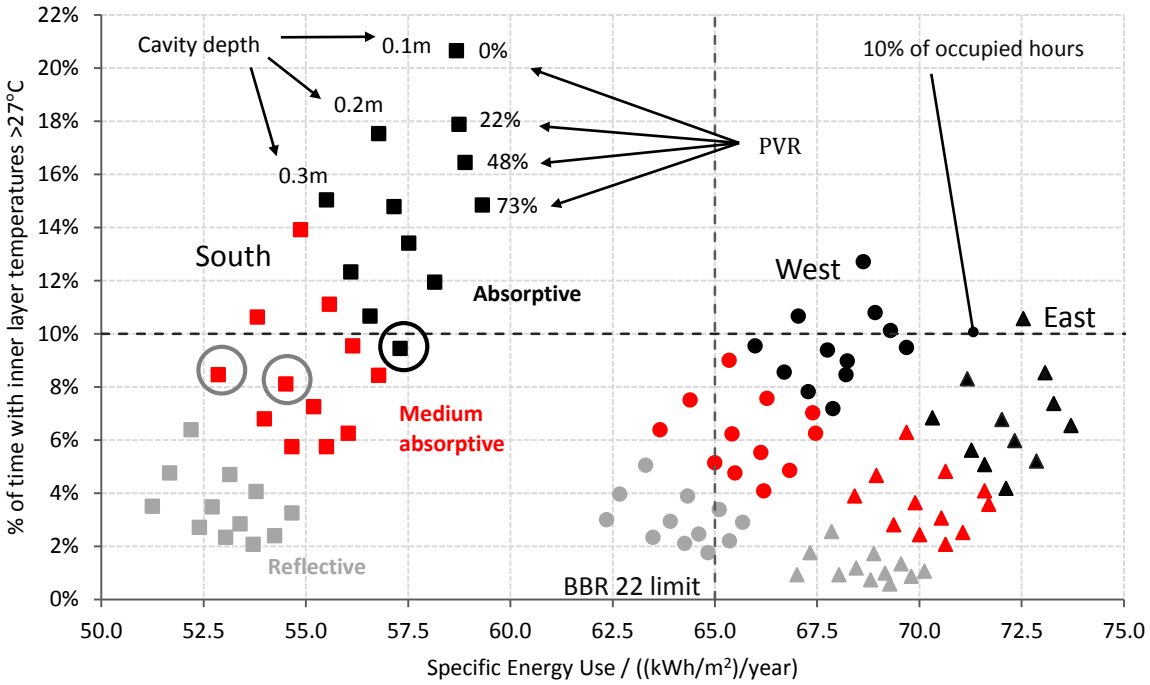


*Figure 4.23: Percentage of occupied time with inner layer temperatures over 27 °C and specific energy use for 70% WWR and different shadings at different cavity depths, PV ratios and orientations. Low-Iron façade as external skin.*

The above graph indicates that only the south and some of the west oriented cases fulfill the current BBR limits. However for an absorptive shading at south orientation the percentage of occupied time with inner layer temperatures over 27 °C exceeds 10% of the working hours except for a combination of 73% PVR at a 0.4m cavity (black circle). For a shading with 57% absorptance (medium absorptive) a 0.2m cavity with 22% PVR or a 0.4 m cavity alone reduce the percentage of time exceeding 27 °C to about 8% (grey circles). The inclination of the points at a specific cavity depth and different PVR is steeper for the absorptive shading than the medium absorptive or the reflective. This shows that the more reflective the shading the less is the improvement gained from the PVR in terms of thermal comfort. The same is also the case for orientations with lower solar exposure as the drop of the over temperature time in south oriented cases is larger than east and west.

### 4.2.5 Alternative refurbishment options

This section presents the results for the simulations where the two glazing options (low-Iron and low-E) were added to a base case with an initial triple clear window and the cases with highly insulated triple glazed units. The results were analyzed in terms of specific energy use, operative temperatures and inner layer temperatures.

Figure 4.24 shows the specific energy use (heating, cooling, DHW and fan electricity) for the base case with double clear initial window and the addition of a low-Iron and a low-E coated façade, for the alternative base case with triple clear window and the addition of the same skins, as well as for the highly insulated triple glazed units presented in chapter 2.4.8. The graph is presented for the 30% WWR (black outline) and the 70% WWR (grey outline) for south and north orientation. The limits specified by FEBY 12 and BBR 22 are also noted. All the ventilated options have a reflective shading inside a 0.2 m cavity. The base cases have the same shading inside the room and the highly insulated cases have the reflective shading inside the outermost gap.

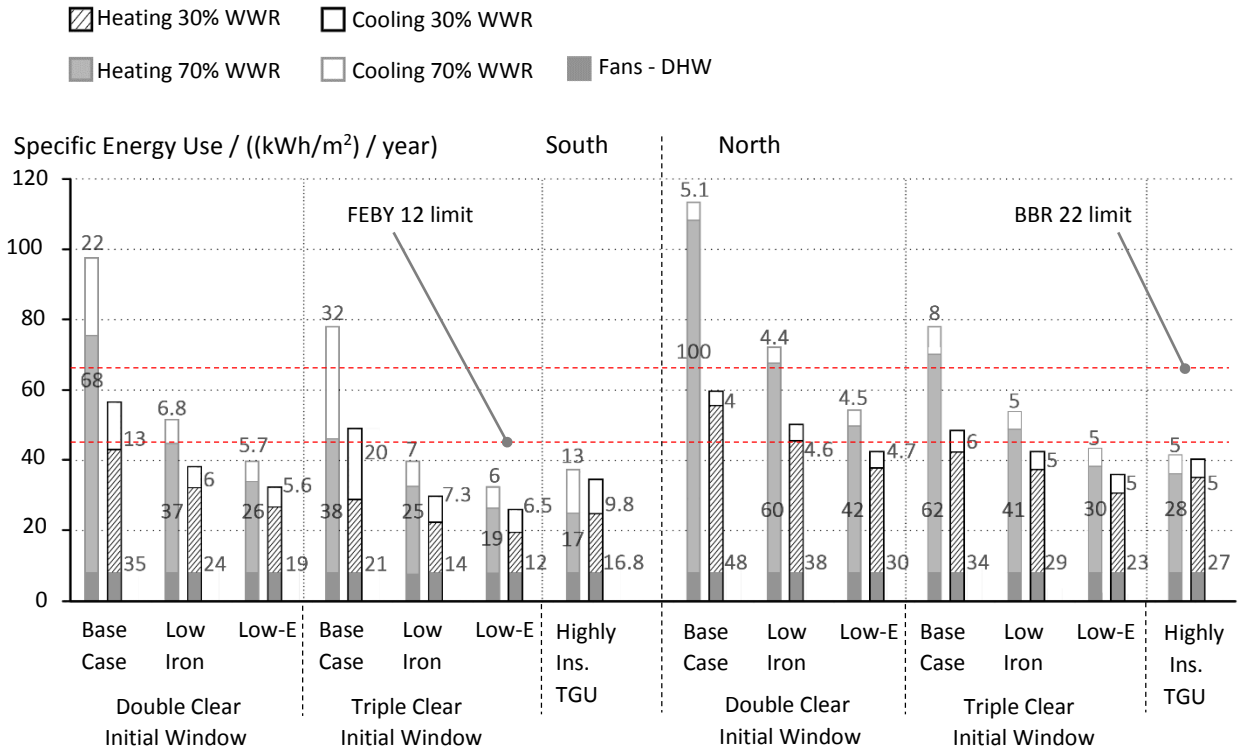


*Figure 4.24: Specific energy use for double and triple clear initial windows with different outer skins as well as for highly insulated TGUs, for 30% and 70% WWR at south and north orientations.*

The case with triple clear initial window at both orientations has a heating performance similar to the initial base case with a low-Iron facade. The addition of both external skins at the alternative base case with the triple window, brings significant heating savings. For a south oriented room with 70% WWR the heating reduction is 34% for the low-Iron façade and 50% for the low-E coated façade. For the 30% WWR the same reductions are 33% and 43%.

The alternative base case in south orientation results in higher cooling demand compared to the initial base case. The increase is counted at 45% for the 70% WWR and 54% for the 30% WWR. The ventilated options however bring significant reduction of the cooling demand of the alternative base case. The reduction is calculated at 78% and 81% for the low-Iron and the low-E coated façades respectively at 70% WWR. For the 30% WWR the reduction is around 65% for both external skins.

In south orientation the highly insulated triple glazed units result in very low heating demands for both WWR. The cooling demand however is higher than the ventilated cases due to the interstitial position of the shading. For the same orientation and double clear initial window at 70% WWR a low-E façade achieves the passive house requirements (FEBY). In the case of a triple clear initial window and 70% WWR a low-Iron façade is enough to fulfill the FEBY standard. This is also the case for the highly insulated TGUs at any WWR. At 30% WWR all the ventilated cases achieve passive criteria.

For the north orientation, the heating demand is the dominant part of the total energy use, due to lack of solar gains. Therefore, more insulated cases result in lower energy demand for heating. The highly insulated TGU results in the lowest energy use for the 70% WWR. For the 30% WWR however, the alternative base case with the low-e coated façade results in slightly lower heating demand than the highly insulated TGU case. The heating savings for the alternative base case and 70% WWR are 34% and 52% for the low-Iron and the low-E coated façade respectively. For the 30% WWR the same savings are 15% and 32%.

None of the ventilated options achieves the FEBY requirements at north orientation with double clear window and 70% WWR. In the case of a triple clear initial window a low-E façade is needed to achieve the standard. The passive criteria are achieved with the highly insulated TGUs. At 30% WWR the low-Iron façade fulfills the passive criteria only when combined with a triple clear window, while a low-E façade always achieves the standard.

Figure 4.25 shows the specific energy use including heating, cooling, DHW and fan electricity for the base case with double clear initial window and the addition of a low-Iron and a low-E coated façade, for the alternative base case with triple clear window and the addition of the same skins, as well as for the highly insulated triple glazed units presented in chapter 2.4.8. The graph is presented for the 30% WWR (black outline) and the 70% WWR (grey outline) for east and west orientation.

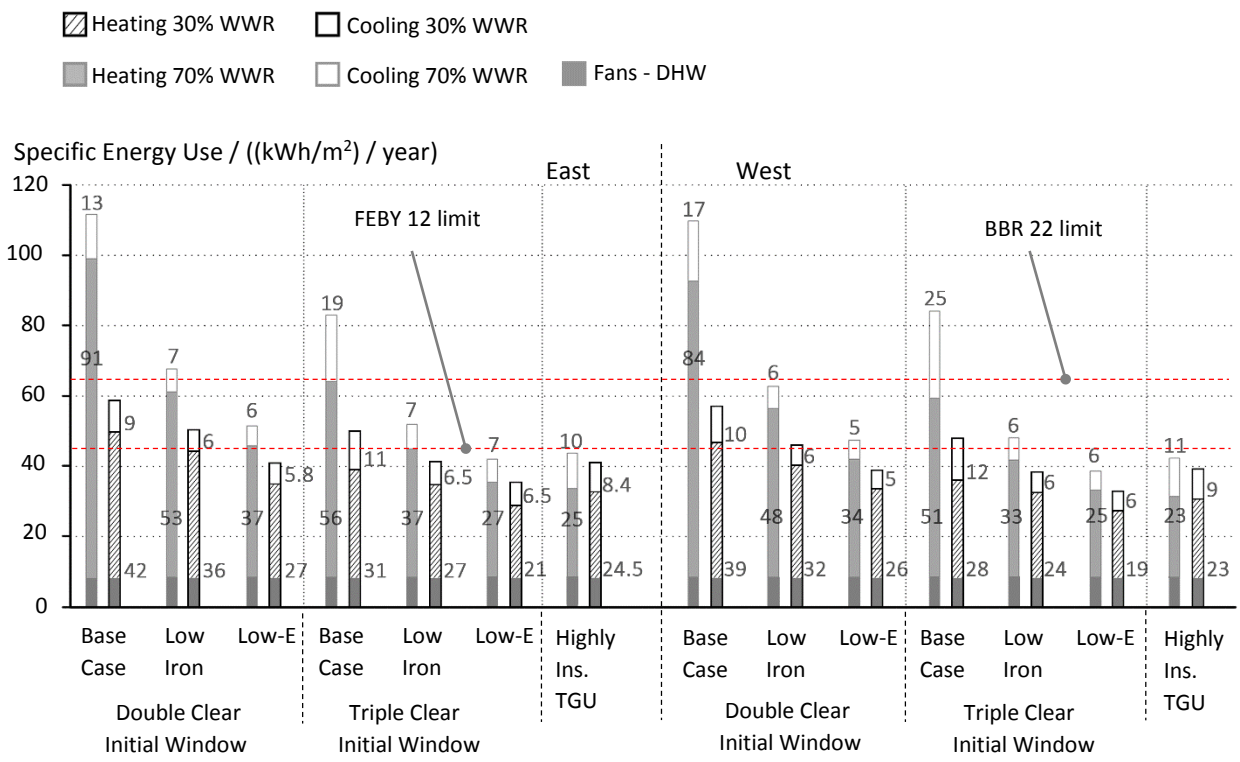


*Figure 4.25: Specific energy use for double and triple clear initial windows with different outer skins as well as for highly insulated TGUs, for 30% and 70% WWR at east and west orientations.*

The heating demand savings at east and west oriented rooms with a triple clear initial window at 70% WWR are counted to approximately 35% for the low-Iron façade and 50% for the low-E coated option. For the 30% WWR the same savings are 15% and 32%. The highly insulated triple glazed units result in slightly higher cooling demand compared to the ventilated options.

None of the ventilated options achieves the FEBY criteria at 70% WWR with double clear initial window. For the triple clear initial case the standard is achieved with a low-E coated façade. At the 30% WWR the low-E coated is needed to achieve passive criteria while for the triple clear case a low-Iron skin is enough. The highly insulated TGUs fulfill the passive requirements in all cases.

Table 4.9 shows the analysis of operative temperatures of the south oriented room for 30% and 70% WWR for the base case with double clear initial window and the addition of a low-Iron and a low-E coated façade, for the alternative base case with triple clear initial window and the addition of the same skins, as well as for the highly insulated triple glazed units presented in chapter 2.4.8. The table includes the peak operative temperature and the percentage of occupied time that the latter exceeds 25°C and 26°C within April to September. The south oriented room was chosen since south orientation experiences the highest amount of solar gains (see section 2.1). The remaining orientations are presented in Appendix C.

*Table 4.9: Percentage of occupied hours when the operative temperature exceeds 25°C or 26 °C and maximum operative temperature for double and triple clear initial windows with different outer skins as well as for highly insulated TGUs, for 70% and 30% WWR at south orientation.*

| | Double clear initial window | | | Triple clear initial window | | | |
|---|---|---|---|---|---|---|---|
| **South 70% WWR** | Base Case | Low-Iron | Low-E | Base Case | Low-Iron | Low-E | Highly Ins. TGU |
| max Op.Temp / °C | 26.5 | 25.9 | 25.7 | 26.5 | 25.8 | 25.7 | 26 |
| Top >25°C / (%) | 51.8% | 30.6% | 27.4% | 61.9% | 37.0% | 33.0% | 56.0% |
| Top >26°C / (%) | 2% | 0% | 0% | 3% | 0% | 0% | 1% |
| **South 30% WWR** | | | | | | | |
| max Op.Temp / °C | 25.8 | 25.7 | 25.6 | 25.8 | 25.7 | 25.6 | 25.8 |
| Top >25°C / (%) | 40.4% | 31.8% | 30.6% | 54.9% | 36.8% | 38.4% | 54.9% |
| Top >26°C / (%) | 0% | 0% | 0% | 0% | 0% | 0% | 0% |

For both WWR, when moving from a double clear initial window to a triple clear one the over temperature time with respect to Belok – 25 °C increases, due to the lower thermal transmittance of the window. This is also the case with the highly insulated triple glazed units for which in both WWR, the higher g-values and the lower thermal transmittances compared to the double skin options result in longer over temperature times than any of the ventilated cases. Interesting to note that with the low –E coated facades the operative temperature of the 30% WWR remains over 25°C for slightly longer time than the respective cases of the 70% WWR. Nevertheless it should be noted that the Belok – 26 °C requirement is achieved, for all the examined cases, even the ones with internal shading.

Figure 4.26 shows the analysis of the inner layer temperatures of the 70% WWR for the base case with double clear initial window and the addition of a low-Iron and a low-E coated façade, for the alternative base case with triple clear initial window and the addition of the same skins, as well as for the highly insulated triple glazed units presented in section 2.4.8. The graph is presented for south and north orientations and includes the amount of time with inner layer temperatures lower than 18°C (grey bars) and higher than 27 °C (white bars), as well as the minimum (circles) and maximum (triangles) inner layer temperatures at the right y-axis. The assumed comfort zone between 18°C and 27°C is also noted. Figure 4.27 shows the same results for east and west orientations. All the ventilated options have a reflective shading inside a 0.2 m cavity. The base cases have the same shading inside the room and the highly insulated cases have the reflective shading inside the outermost gap.

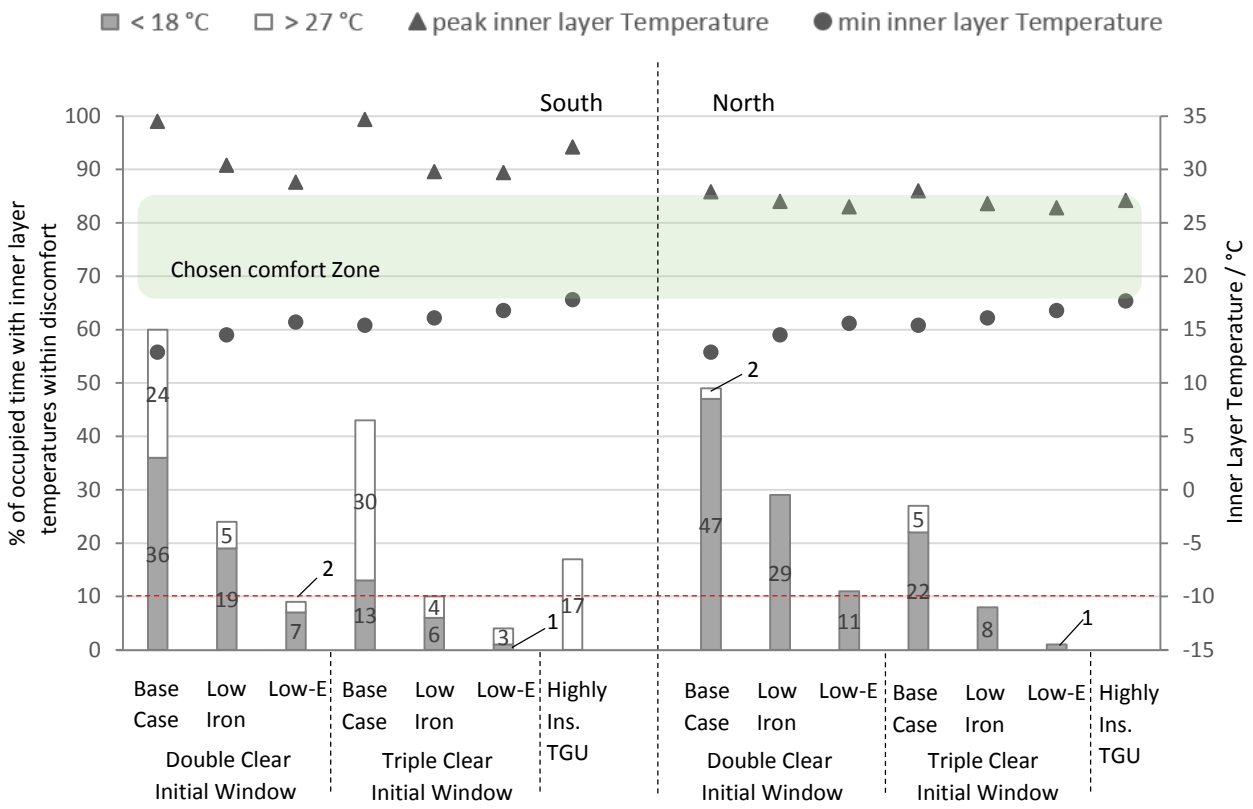


*Figure 4.26: Percentage of occupied time with inner layer temperatures within discomfort, as well as peak and minimum inner layer temperatures, for double and triple clear initial window with different external skins at south and north orientations.*

For south orientation, the alternative base case results in longer time with inner layer temperature higher than 27 °C compared to the initial base case. The addition of any of the outer skins along with the placement of the shading in the cavity improves significantly this performance, limiting the over temperature time to about 4% of the occupied hours. When adding any of the external skins to the triple clear window, the amount of time with inner layer temperatures below 18 °C is limited to a maximum of 6% and 8% for the south and north oriented room respectively. For the low-E coated skin, these numbers are counted to 1% of the time. The inner layer temperatures of the highly insulated triple glazed unit are never below 18 °C which is the best performance of all cases. However, in the south oriented room this glazing option results in temperatures higher than 27°C for 21% of the occupied time and a peak temperature of 32.1°C. The north oriented room has no problem in terms of high (>27°C) inner layer temperatures. For both orientations, the total percentage of time within discomfort with the addition of any of the external skins to a triple clear window does not exceed 10% (red line limit).

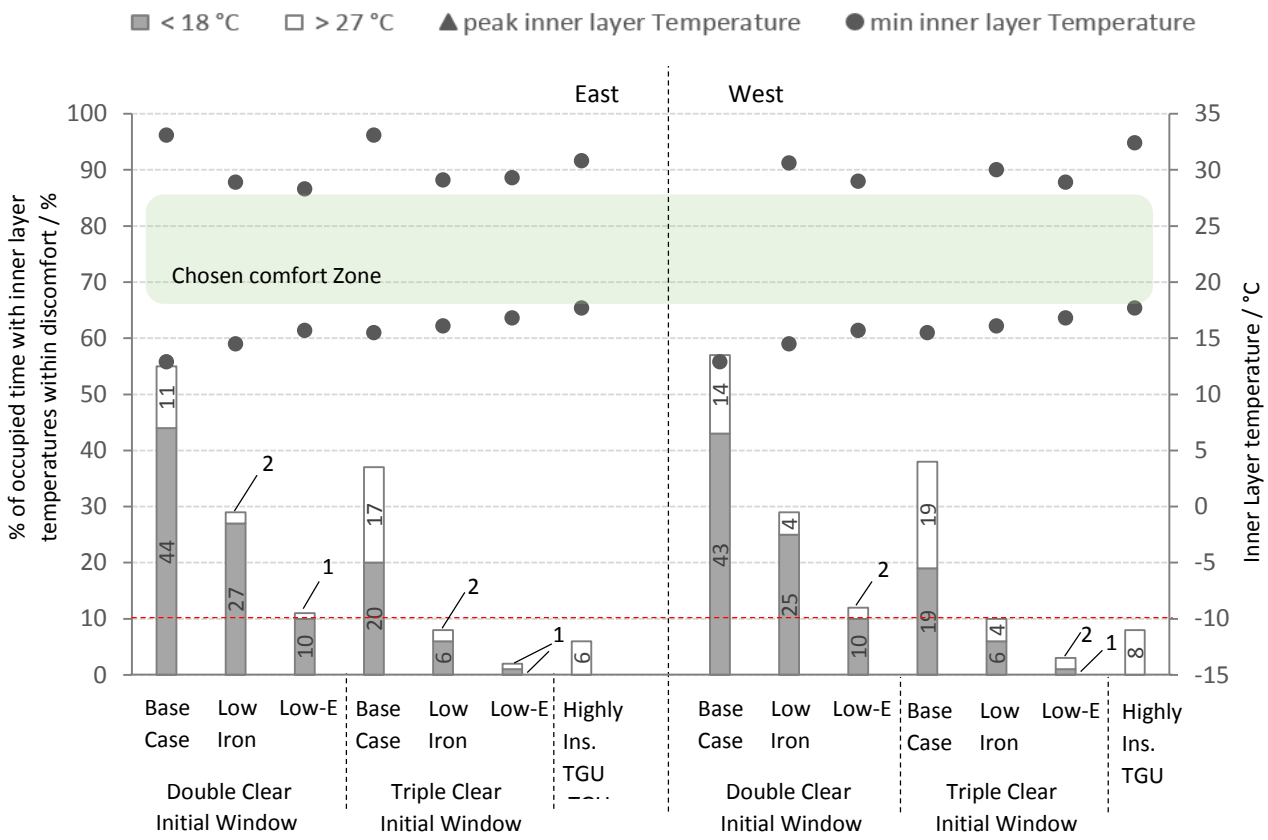


*Figure 4.27: Percentage of occupied time with inner layer temperatures within discomfort, as well as peak and minimum inner layer temperatures, for double and triple clear initial window with different external skins at east and west orientations.*

The results for the inner layer temperatures at east and west orientation show similar trends as for the south and north (Figure 4.26). The amount of time with inner layer temperatures higher than 27°C with the highly insulated triple glazed unit are counted to 8% at the east and 10% at the west orientation. The total amount of time with discomfort temperatures, however, does not exceed 10% due to the very good performance in terms of temperatures below 18 °C (0% of time). As for the south and north orientation, the total percentage of time within discomfort does not exceed 10% with the addition of any of the external skins to a triple clear window (red line limit).

## 4.3 Impact of the ventilated façade on PV performance

This section presents the results related to the influence of cavity ventilation on the operative temperature of the PV cells.

Figure 4.28 shows the hourly cell temperatures calculated in SAM at the x-axis and the cell temperatures calculated in IDA-ICE at the y-axis. The results are presented for east, south and west orientations. The results from IDA-ICE are for a closed cavity and the results from SAM are for a BIPV structure with limited airflow at the back of the module. The same climate file for Copenhagen was used in both simulations.

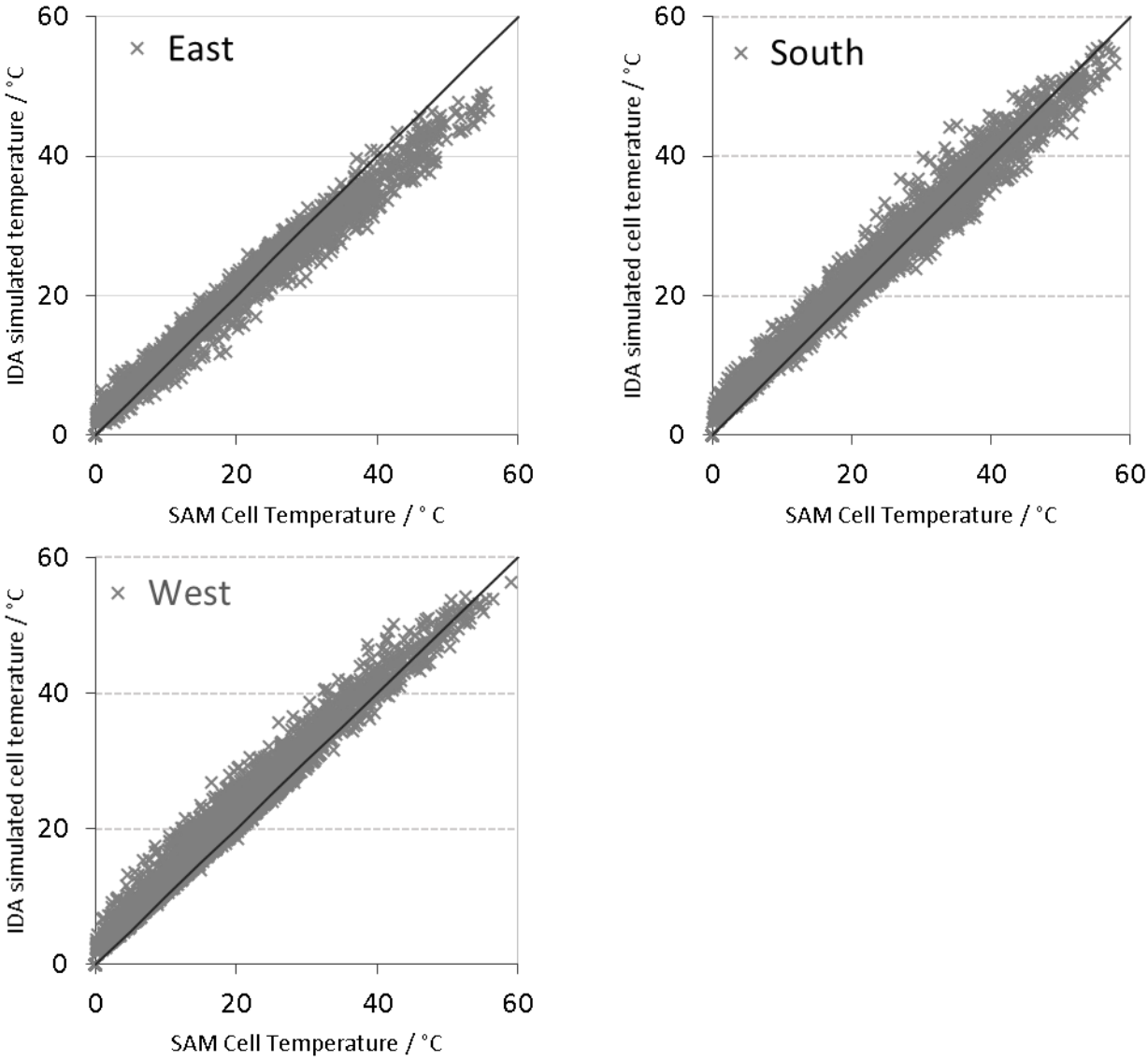


*Figure 4.28: Comparison between cell temperatures calculated in IDA-ICE for closed cavity with cell temperatures from SAM for a non-ventilated BIPV, for different orientations.*

The results show that there are some discrepancies between the temperatures calculated in IDA-ICE and the ones in SAM. For all orientations the maximum difference attained was between 9°C - 10°C. However, a large amount of the calculated temperatures are in good agreement between the two methods as they follow the diagonal line that separates the graph.

The cell temperatures calculated in SAM are higher for east orientation. This is more obvious at temperatures higher than 30°C, which drop below the separating line. On the other hand the temperatures for west orientation are higher in IDA-ICE. For the south orientation the values that the two software calculate have higher proximity. The peak temperatures are closer between the two programs for both south and west orientations.

The left y-axis of Figure 4.29 shows the annual electricity output of a façade with 73% PVR for SAM (black bars) and for Excel calculations (grey bars) based on cell temperatures from IDA-ICE, at different orientations. The right y – axis shows the total annual irradiation incident on each façade as calculated by the two programs (black triangles are for SAM and grey squares for IDA-ICE). The results are for the same simulations presented in Figure 4.28.

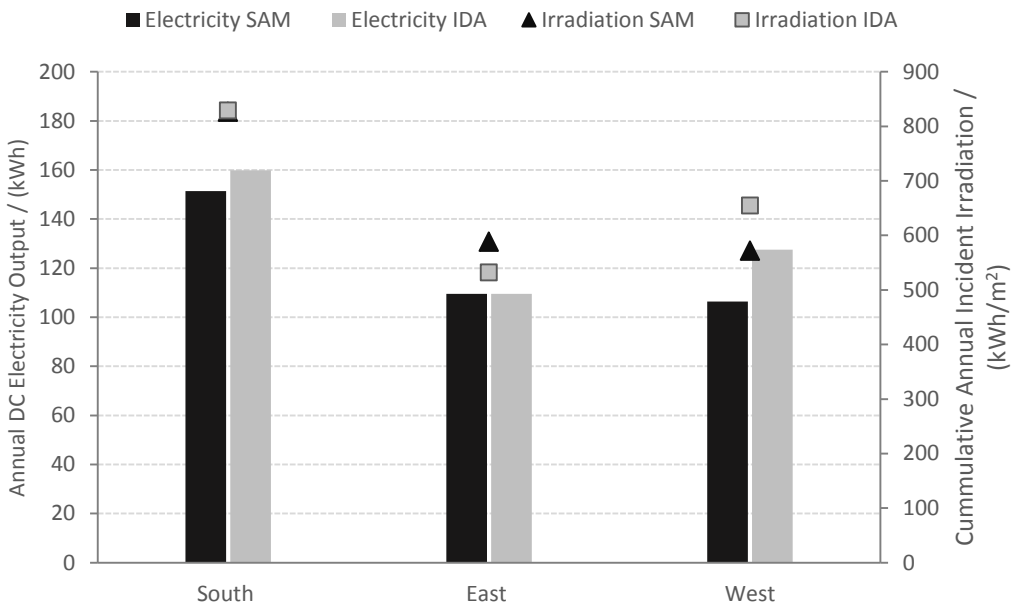


*Figure 4.29: Annual Electricity output and annual incident solar radiation for south, east and west facades from SAM and based on IDA-ICE cell temperatures.*

The irradiation calculated for west orientation in IDA-ICE is higher than the one obtained from SAM by 12%. This results in higher annual electricity production for the calculations performed based on IDA-ICE cell temperatures at west orientations. On east the annual irradiation is lower for IDA-ICE than in SAM for about 9% while there is good agreement between the two methods for south orientation. The difference between the two methods in terms of the annual electricity output is counted to 6% at south, 16% at west while there is not difference in east orientation.

Figure 4.30 shows the cell temperature calculated in IDA-ICE with (black line) and without ventilation (black dashed line) for a warm summer day at south orientation.

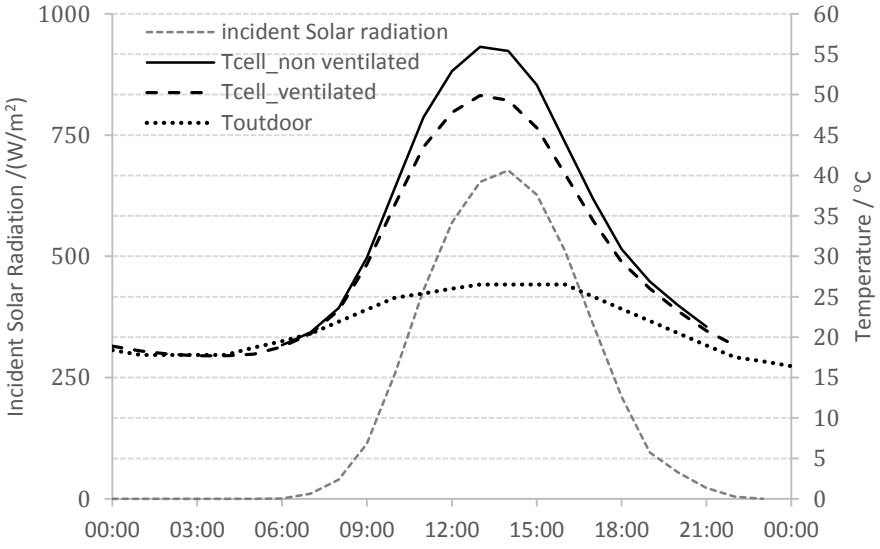


*Figure 4.30: Incident solar radiation and cell temperature during 06/08, for a ventilated and a non-ventilated cavity at south orientation.*

The case with ventilated cavity results in 6°C lower cell temperature than the non – ventilated case.

Figure 4.31 shows the relative increase of the PV cell efficiency as a function of the temperature decrease (ΔT) of the cell temperature due to ventilation for a south oriented façade.

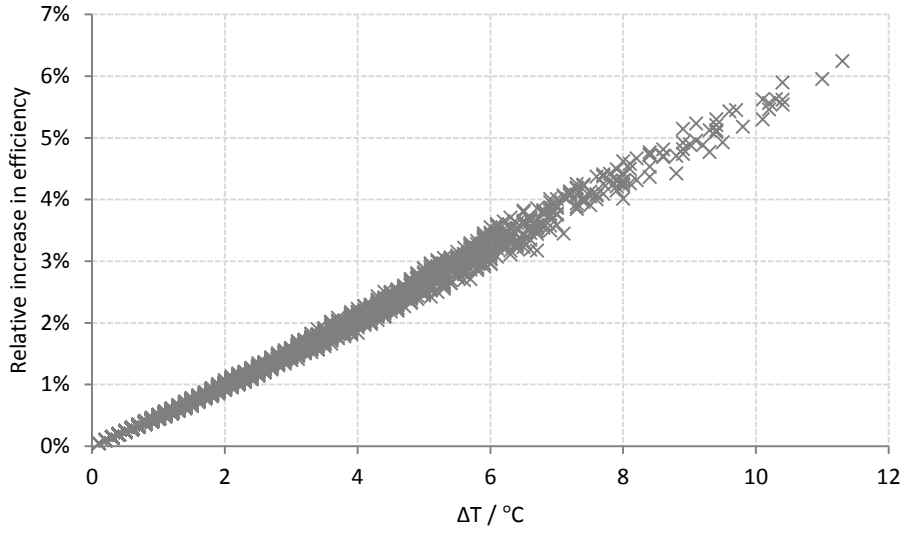


*Figure 4.31: Relative increase in PV cell efficiency as a function of the decrease in cell temperature due to ventilation of the cavity for a south oriented façade.*

The increase in efficiency is between 3% - 3.5% at a temperature decrease of 6° C, i.e. also at the warm day seen in Figure 4.30. However the highest relative increase in the efficiency is between 6% - 6.5% when the temperature drop is around 10°C - 11°C. Nevertheless these values are not as many as the ones gathered at 3% - 4% and below, i.e. that the efficiency improvement due to ventilation is not very significant.

Figure 4.32 shows the annual electricity output for a non – ventilated (black bars) and a ventilated cavity (grey bars) at different orientations. Results for a "glass /cell/ glass-open rack" ventilated case based on SAM's simple efficiency model are also included in order to evaluate the ventilation impact on the annual output.

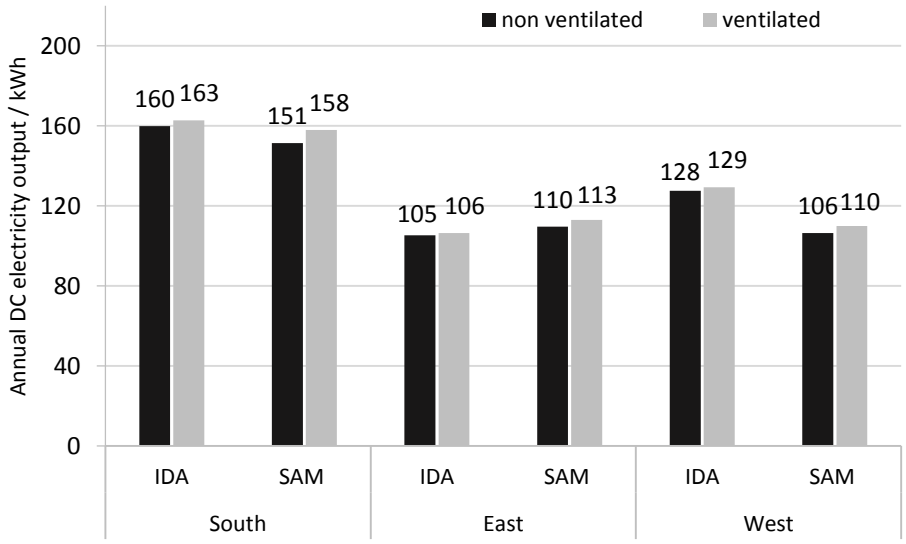


*Figure 4.32: Annual electricity output for a ventilated and a non-ventilated façade based on IDA-ICE cell temperatures, as well as for a ventilated and a non-ventilated BIPV from SAM, for different orientations.*

For the cases simulated in IDA-ICE, the higher efficiency due to ventilation is translated into 2%, 1% and 0.8% higher annual output for the south, east and west orientations respectively. The results obtained by SAM show a slightly higher influence of ventilation on the annual output. The maximum increase of the annual electricity from the non-ventilated to the ventilated case in SAM is about of 4.6% at south orientation.

# 5 Discussion

## 5.1 Performance on a component level

For winter conditions with low solar irradiation (Figure 4.1), the addition of the low-Iron and the low-E facade at a double clear initial window resulted in a 3 °C to 4° C increase of the inner layer temperature respectively. This is of course a considerable improvement but quite expected due to the steep decrease of the base case's U-value from 2.8 W/m$^2$K to 1.81 W/m$^2$K and 1.34 W/m$^2$K for the low-Iron and low-E glazing respectively.

The position of the low-E coating is very important. In the case of the low-E coated façade, heat is lost from the inner pane towards the cavity resulting in a warmer inner skin and especially intermediate pane (2 °C higher than for the other cases). On the other hand, the use of the coating directly on the inner pane (highly insulated triple glazed unit) diminishes radiation losses from the inner layer resulting in the highest inner layer temperature of 21.3 °C, which is very close to the inner air temperature of 22 °C (Figure 4.1).

During a winter day with high solar radiation both double skin options resulted in similar inner layer temperature of approximately 28 °C (Figure 4.2). This behavior can be attributed to the balance between gains and losses for each case. The low-Iron skin allows more gains to be absorbed in the inner layers but has higher heat losses than the low-E option, which has less gains (due to the outer skin) but also less losses. On the other hand, during the same day, the low g-value of the highly insulated TGU resulted in an inner layer temperature of 25°C. Thus, the highly insulated TGU was optimum for both winter days.

The cavity temperature can be 16°C - 20°C higher than the outdoor during a winter day with solar radiation (Figure 4.2). This demonstrates high insulation potential for specific climatic conditions and orientations.

During a typical summer day, the difference between the inner layer temperature with an absorptive and a reflective shading was 2.5°C (Figure 4.4). The respective difference of the shading temperature was 15° C. This means that the high ventilation rates induced from absorptive shadings can improve their overall performance by removing absorbed heat which would otherwise transfer to the room as secondary heat gain. However, it should be noted that the lowest inner layer temperature (28.8°C) was still obtained for the reflective screen which makes questionable the choice of an absorptive shading for increasing the airflow rate. On the other hand, a larger opening and depth could possibly result in similar performance between the two shadings depending on the outdoor conditions.

With respect to the cavity geometry (Figure 4.5), it was seen that the size of the opening has a considerable influence on the airflow rate through the cavity. All the cases with half open cavities resulted in lower airflows, than the cases with fully open cavities, where the latter gave almost double airflow than the former. Moreover, cavities with depth equal to the opening result in higher airflow than larger cavities with the same opening. This is an effect of the air moving slower into deeper cavities consequently resulting in smaller airflow. Absorptive shadings resulted in higher airflow rates. The higher temperature of the absorptive shading (than the other examined options), strengthens the buoyancy due to temperature differences between the outdoor air and the cavity. Stronger buoyancy results in higher air flow rates.

The g-value (Figure 4.6) decreased as the opening area and depth increased i.e. as the airflow rate though the cavity increased. The airflow removes the heat absorbed in the different layers

(and especially the shadings) of the system, consequently reducing the secondary transmittance and therefore the g-value. The highest g-value reduction was obtained for the absorptive shading which has higher secondary transmittance and gives higher airflow rates than the reflective option which does not absorb as much solar radiation, and has lower secondary transmittance. Absorptive shadings require larger cavities and openings that give higher airflows in order to give lower g-values. Reflective shadings are not affected that much from the cavity geometry.

The same g-value does not necessarily mean similar inner layer temperatures (Figure 4.7). This was the case with a reflective shading in a half open cavity and a medium absorptive shading in a fully open cavity. Although the g-value was similar for the two cases, the latter had higher inner layer temperature by 1.6 °C (Figure 4.6 and Figure 4.7). This means that in terms of inner layer temperatures, the g-value alone cannot be indicative for the choice of shading and a careful analysis of all solar and thermal properties is required. Moreover, it should be noted that the inner layer temperature is not only affected by the g-value and more specifically the secondary part of it, but also by the thermal transmittance of the system.

The cavity geometry has a considerable impact on the vertical temperature profile of the air in the cavity (Figure 4.8). As expected, the cases with larger airflows (0.2m – 0.4m cavity and opening) resulted in smoother temperature profiles. The trends of the shadings were followed as expected with the reflective one having lower temperatures than the other options, even at narrower cavities (0.1m).

The cavity depth and opening combination after which the cavity air temperature does not decrease significantly can be considered optimum for cavity heat removal at specific boundary conditions. This means that an adequate analysis of the cavity temperature profile and correct selection of the design conditions are critical when designing a ventilated facade. On overall, for the studied cases, the optimum depth could be considered 0.2m – 0.4m for the absorptive shadings and 0.1m – 0.4m for the reflective.

## 5.2 Annual energy and thermal comfort performance

The investigation of cavity air temperatures during the winter period (Figure 4.12) showed that smaller window-to-wall ratios have warmer cavities than larger ones. This is reasonable as in the latter case, the solar radiation is transmitted in the room whereas in the former, a large amount of solar gains remain in the cavity, strengthening the buffer zone effect. It was also seen that the solar absorptance of the inner skin is significant for achieving high temperature rise of the air in the cavity, even in days with limited solar radiation.

Moreover, a low-E coated external glazing facing the cavity enhances the buffer zone effect. Indeed, the temperature rise between the low-E coated and the low-Iron cases differed for 2 °C to almost 10 °C depending on the amount of incident solar radiation (Figure 4.11 ). The cavity temperature investigation showed that even in February at south orientation, the cavity was ventilated in days with very high solar radiation (around 800W/m2 incident on the façade). This means that the room temperature exceeded 24.5 °C reaching almost the cooling setpoint. At the same time the temperature of the air in the cavity was around 25 °C for the low-E façade at 30% WWR. It can be speculated that such high cavity temperatures could lead to overheating problems even in February, but nevertheless a different control type of the cavity ventilation could possibly result in even better performance in terms of heating.

The investigation of the impact of thermal mass in terms of heating performance (Figure 4.13) showed that the inner skin's insulation is a more important factor for reducing the heating demand than the thermal mass of the cladding of the inner skin. This was the case for the brick cladding that gave better results in terms of annual heating than the concrete case which had higher temperatures during nights when the heat absorbed during the day was released.

On overall, the impact of thermal mass is small on reducing the heating for the cases with a low- Iron external skin. The performance with the massive cladding materials was better in combination with the low-E glazing.

With respect to the cooling demand of the room, it was seen that all the ventilated options resulted in lower cooling need than the base case (Figure 4.18 and Figure 4.19). This is reasonable as all the examined shadings resulted in lower g-values than the initial one (Table 2.8). For the absorptive shading, however, the g-value was closer to the base case, but the obtained cooling reductions were 40% - 50% at south orientation at 30% and 70% WWR respectively. This reveals that the impact of ventilation of the cavity is crucial for absorptive shadings as it removes secondary heat gains.

However, it should be also noted that the reflective shading examined had a low emittance surface, which results in a decrease of the U-value of the base case window when the shading is applied. Consequently, heat losses are reduced for the base case while the ventilated options have in general higher U-values when they are in ventilation mode. A reflective device with a high emittance would perform better as internal shading. The best cooling performance was in general obtained for the reflective shading combined with the low-E façade (Figure 4.18 and Figure 4.19), due to the lower g-value of this case (Table 2.8).

Concerning the cavity depth and opening, it was seen that the more absorptive the shading, the higher is the need for deeper cavities with larger openings in order to achieve better cooling performance. However, none of the absorptive shading options ($\alpha$>0.57) outperformed the reflective case.

The integration of PVs on the external skin resulted in lower cooling demands for the different shading options. The steeper decrease was obtained for the step of 0% PVR to 22% PVR as this change results in the larger reduction of the g-value of the outer skin (Figure 2.10). The obtained cooling reductions were more significant for the absorptive shading at south orientation as this option gives higher g-values and south oriented rooms have more solar gains (Table 4.5).

However, the specific energy use (Figure 4.20 and Figure 4.21) increased or remained the same in all cases as the fixed shading from the PVs decreases amount of useful solar gains and increases the heating demand. A positive impact on the overall energy balance could be obtained if the PVs were combined with more transmissive shadings than the ones examined in this study.

With respect to the window-to-wall ratio, the impact of the PVR on the cooling demand reduction was higher in the 70% WWR case than the 30% WWR (Table 4.6), as the former is more shaded than the latter due to the position of the PVs.

Regarding the operative temperatures (Table 4.7 and Table 4.8), all the examined cases achieved the Belok – 26°C requirement. This means that the obtained g-values for all the shadings examined and for all the ventilated options were sufficient together with the cavity depth of 0.2m. However, it should be noted that the vertical air temperature profile should be

considered. For example, the temperature of the air at the top of the cavity for the absorptive shading was 38°C, for an extreme summer day at a 0.2m cavity depth and opening (Figure 4.8).

The results for the inner layer temperatures (Figure 4.22) of the different shading options were not as similar as for the operative temperatures. The performance of the low-Iron façade in terms of thermally comfortable inner layer temperatures can be considered improved compared to the base case. The percentage of time with inner layer temperatures lower than 18 °C was 19% and 29% for south and north orientation respectively, while the lowest temperature was 14.4 °C. This means that the overall glazing U-value of 1.81 W/m$^2$K obtained for the low-Iron case is not enough from a thermal comfort perspective.

The low-E façade limited the period of time with temperatures below 18°C to a maximum of 11% at north orientation but resulted in a minimum temperature of 15.7 °C, which can still be considered low. In general, the position of the coating on the inner surface of the outer skin is not the best for improving the performance in terms of inner layer temperatures during cold periods, because the heat from inside reaches the cavity.

Among the different shading options, the reflective case results to the lowest amount of time with inner layer temperatures over 27 °C. The comparison of the amount of time with inner layer temperatures exceeding 27 °C between different orientations showed that the absorptive shading is more beneficial on East oriented rooms instead of south, due to the lower solar gains of this orientation.

With respect to an overall view including both high and low inner layer temperatures, the results clarify that the performance of the façade with the low-Iron external cladding is very poor resulting at discomfort temperatures at almost 40% of the occupied time. On the contrary, the low-E coated façade limits the total discomfort period to a maximum of 11% at west orientation and a minimum of 7% at south.

The integration of PVs on the external skin decreased the percentage of time with inner layer temperatures over 27°C from 15 % of the occupied time at a 0.4 m cavity without PVs to 9% of the occupied at the same cavity with 73% PVR (Figure 4.23). This is a considerable improvement but as already seen, it results in an increase of the overall energy use. A solution without an absorptive shading at south orientation is simpler than a case with integrated PVs and results to a better performance concerning both energy and thermal comfort.

The impact of having a larger cavity was also significant for reducing the amount of time with inner layer temperatures below 27°C, resulting in a reduction from 21% of the occupied time at a 0.1 m cavity to 15% at a 0.4 m cavity (Figure 4.23). However, the set target of 10% was not achieved for a shading absorptance of 87% at south orientation but was marginally achieved for the case with 57% absorptance (8% of the occupied time).

The results from the alternative refurbishment options showed that significant heating savings can be achieved when adding any of the examined external skins to a triple clear initial window (Figure 4.24 and Figure 4.25). The savings varied from 34% to 50% for the low-Iron and the low-E façade respectively at south orientation and 70% WWR. The same savings for the 30% WWR case where between 33% and 43%.

Therefore, the reduction of heating when the two outer skins are applied, is higher for the initial base case of WWR 70% (46% and 62%) and the same magnitude for WWR 30% (31% and 45%) (See also section 4.2.2). This implies that the outer skin is more beneficial for a high

WWR with high U-value, while for the low WWRs the magnitude of reduction is the same for different window U-values.

In general, in order to achieve passive criteria, a low-E coated façade was essential for all the 70% WWR cases with triple clear window except only for the south orientation where a low – Iron external glazing was enough due to the high amount of solar gains (Figure 4.24). This also means that for the double clear initial cases, the passive criteria were not achieved even with a low-E external glazing, as these cases have lower thermal transmittance than the respective triple ones. An exception to this is again the south oriented room with double clear inner pane and low-E facade. In general, the addition of a low-E coated façade to a double clear initial window resulted in similar results as the addition of a low-Iron façade to a triple clear window. This means that the U-value of the two cases is similar and that the low-E coating performs roughly as if adding one more clear glazing.

Concerning the 30% WWR and the passive criteria, the low-E façade was essential for the double clear initial case at east, north and west orientations except south (Figure 4.24 and Figure 4.25). For the triple clear initial case, however, the low-Iron case was enough.

The highly insulated triple glazed units achieved the passive criteria at all orientations and all WWR. The cooling demand was generally higher for the highly insulated TGUs compared to the ventilated options, although the former had lower effective g-values (0.11 for the 30% WWR and 0.064 for the 70% WWR) than the latter with closed cavity (0.12 and 0.08 for a double and triple clear unit respectively with a low-E outer skin). The better cooling performance of the ventilated options is attributed to the ventilation that lowers even more their g-values while increasing the heat loss rate from the room to the outside. On the contrary, the highly insulated TGUs have very low U-values that contribute to room overheating.

Regarding the inner layer temperatures, it was seen that the highly insulated TGUs resulted in the best performance during the colder periods, achieving the maximum lowest inner layer temperature of 18°C (Figure 4.26 and Figure 4.27). The low-E facade at triple clear window had also very good results achieving 1% of the occupied time with inner layer temperatures below 18°C.

With respect to inner layer temperatures higher than 27°C, the highly insulated TGUs resulted in an overall acceptable performance (< 10% of occupied time) at orientations with less solar gains, i.e. west, east and north. On south orientation, however, the amount of time with inner layer temperatures exceeding 27°C was 17% and the peak temperature was 32°C (Figure 4.26). As this was not the case for the ventilated options, which had peak temperatures below 30°C and over temperature times lower than 5%, it becomes clear that a ventilated façade can be useful for south orientation. This was generally noted throughout the thesis for both, comfort performance and energy use.

## 5.3 Impact of the ventilated façade on PV performance

The cell temperatures estimated with IDA-ICE at east orientation were lower than SAM, while this trend was reversed in west (Figure 4.29). These results follow the trends seen in the annual irradiation, which was higher in IDA-ICE for west orientation and lower for east (Figure 4.29). Nevertheless the annual electricity output calculated with the two software had a difference of 9% at south and 0% at east orientation (Figure 4.29), and therefore the method was considered reasonably accurate for estimating the cell temperature.

It should be noted that the cell temperature estimation conducted in IDA-ICE involves the main assumption that the solar cell temperature is independent of the coverage of PV cells on the module, i.e. the temperature is the same for all PV coverage ratios. However, in reality the solar cell packing factor, i.e. the amount of PV cells coverage on the module, is considered to have an impact on the cells' temperature [25]. In the case of small photovoltaic ratios, the transfer of heat would be towards several directions, due to unequal temperature distribution of the module between parts covered by cells and transparent parts. This could result in lower cell temperature than the one calculated in IDA-ICE. For larger PVR, however, the above assumption is likely to be more accurate as the temperature distribution would be more uniform.

The impact of ventilation on the annual PV output was found to be almost negligible as it resulted in a maximum annual output increase of 2% (Figure 4.32). Moreover the simulations of the ventilated case, assumed that the cavity was always open. This means that in a realistic performance of the façade, the influence would be even smaller as the cavity would be closed for long periods during the year.

On the other hand, the results obtained from SAM showed that a ventilated structure can result in 4.6% higher annual electricity output than a non-ventilated case (Figure 4.32). This is reasonable as the coefficients a and b (see section 3.1.2) used in the SAM model accounted for wind induced ventilation at the back of the module, which is in general stronger than the thermally driven natural airflow assumed in IDA-ICE. Nevertheless it can be said that the impact of ventilation on the PV output was insignificant in this climatic context, for both cases.

The whole issue of PV integration on the façade becomes highly questionable, considering that the annual electricity loss can reach up to 30% or more for vertically tilted modules compared to modules tilted at latitude angle [16] and that the cases with integrated PVs examined in this study resulted in higher energy use than the cases with no PVs. This means that from at least an energy and PV performance perspective, this façade design was not found reasonable, although other aspects such as economy aspects of the BIPVs should be considered to reach to a more general conclusion.

# 6 Conclusions

The main conclusions of this study are presented below.

- A ventilated façade can improve significantly the energy use of office buildings with outdated windows. For a low-E coated external glazing facing the cavity and an initial double clear window , the energy savings can reach 38% and 60% for a 30% and 70% WWR respectively. The same savings can be 32% and 52% for an initial triple clear window. South oriented room achieve even higher reductions.
- In large WWR (70%) and double clear initial windows, the specific energy use required from the current BBR is not achieved without a low-E coating on the external skin, except only for south orientation, where a clear glazing is enough.
- The Low-E coating is essential for the smaller WWR (30%) with a double clear inner window in order to fulfill the Passive House criteria for the specific energy use, as stated by FEBY.
- The low-E coated glazing in combination with a double clear initial window will reduce the period with inner layer temperatures lower than 18 °C below 10% of the occupied time. However, the U-value of such a case (1.34 $W/m^2K$) results in minimum inner pane temperatures of 15.7 °C which are rather low. A triple clear window with a U-value around 0.7 $W/m^2K$ achieve inner pane temperatures of minimum 18°C.
- Triple glazed units with U-values lower than 0.90 $W/m^2K$ combined with shadings of about 75% reflectance in interstitial position, achieved the passive criteria in all orientations. For such windows the percentage of time with inner pane temperatures over 27°C exceeded 10% of the occupied time only at south orientation. As this was not the case for ventilated facades, it becomes reasonable that a ventilated façade is more useful at south orientation.
- Small (<30%) WWR have warmer cavities and the trapped solar gains can be utilized more efficiently with Low-E coatings on the external skin facing the cavity. The absorbing properties of the inner wall are significant for the temperature rise of the air in the cavity.
- Shadings with a solar transmittance of about 6% and absorptance of 25%, 57% and 85% positioned in ventilated cavities resulted in significantly lower (>40%) cooling demand than the base case of this study. The latter was equipped with the most reflective shading of the above cases in internal position. The cross comparison between the ventilated cases showed that shadings with low absorptance and high reflectance were optimum, despite of the effects of ventilation on the shading performance.
- When using very absorptive shadings south orientation should be avoided. In a ventilated façade, these shadings can be used in combination with direct sun and low outdoor temperatures. Thus east orientation may be considered a good option.
- In the case where a high absorptance shading is preferred for aesthetic reasons, it should be combined with wider cavities and large openings, which would provide higher airflow rates and together with the strong buoyancy higher performance could be attained. An additional external (fixed) shading could be also necessary.
- The increase of the cavity depth and opening has a positive influence on both energy use and thermal comfort independently of the WWR. When the cavity is closed the impact of the cavity depth on the heating demand is negligible. A deeper cavity allows for larger airflow if combined with similarly large openings. The airflow reduces the secondary part of the g-value of the ventilated façade system.
- Cavities which have equal opening size and cavity depth typically result in larger airflow rates than wider cavities with the same opening.

- When considering the design of a ventilated double skin façade proper consideration should be given on the vertical temperature profile through the cavity in order not to neglect extremely high temperatures, occurring at greater heights.
- The g-value is a reasonable metric for assessing the cooling performance of different shading options and window systems. In terms of comfort, however, and more specifically inner layer radiant temperatures, the g-value is not enough. Proper consideration should be given on the secondary transmittance of the system, the emittance of the inner layer, the thermal transmittance of the system and in general, the solar properties of the panes of a window.
- Compared to a case without PVs, the integration of PVs with 73% PVR on the outer skin resulted in 28% reduction of the cooling energy use when combined with a highly absorptive shading (a > 80%) at a 0.1m cavity. The respective reduction for a 0.4m cavity was 20%. For these cases the percentage of time with inner layer temperatures higher than 27 °C decreased from 15% to 9% of the occupied time. Despite these results the overall energy use was increased with the addition of PVs and therefore, the system is not recommended. The required performance in terms of cooling and thermal comfort can be achieved just by using a more reflective shading.
- Thermally driven natural ventilation yielded a maximum improvement of the electricity conversion efficiency of the integrated PVs of about 7%. The increase of the annual electricity output however was at 2% for the best case examined. This result can be hardly considered an improvement.

# References


[1] ”International Energy Agency,” [Online]. Available: http://www.iea.org/.

[2] S. Schimschar, J. Grözinger, H. Korte, T. Boermans, V. Lilova and R. Bhar, "Panorama of the European non-residential construction sector," ECOFYS, 2011.

[3] Å. Blomsterberg, ”Energy use in Swedish office buildings,” 2004.

[4] ”Boverket,” [Online]. Available: http://www.boverket.se/sv/.

[5] ”Sveriges Centrum för Nollergihus,” [Online]. Available: http://www.nollhus.se/.

[6] ”Boverkets Författningssmling, BFS 2015:3, BBR 22,” Boverket, 2015.

[7] ”Kravspecifikation för nollenergihus, passivhus och minienergihus - Lokaler - FEBY 12,” Sveriges centrum för Nollenergihus, 2012.

[8] H. Poirazis, ”Double Skin Facades for Office Buildings - Literature review - Report EBD-R--04/3,” Division of Energy and Building Design, Department of construction and architecture, Lund University of Technology, Lund, 2004.

[9] H. Poirazis, ”Single and Double Skin Glazed Office Buildings,” Division of Energy and Building Design, Department of Architecture and Built Environment, Lund University, Faculty of Engineering, LTH, Report EBD-T--08/8, Lund, 2008.

[10] E. Giancola, C. Sanjuan, E. Blanco and M. R. Heras, "Experimental assessment and modelling of the performance of an open joint ventilated façade during actual operating conditions in Mediterranean climate," *Energy and Buildings,* vol. 54, pp. 363-375, 2012.

[11] C. Aparicio-Fernandez, J. Vivancos, P. Ferrer-Gisbert and R. Royo-Pastor, "Energy performance of a ventilated facade by simulation with experimental validation," *Applied Thermal Engineering,* vol. 66, pp. 563-570, 2014.

[12] A. S. Andelkovic, B. Gvozdenac-Urosevic, M. Kljajic and M. G. Ignjatovic, "Experimental research of the thermal characteristics of a multi-storey naturally ventilated double skin facade," *Energy and Buildings,* vol. 86, pp. 766-781, 2015.

[13] M. Shameri, M. Alghoul, K. Sopian, M. Zain, M. Fauzi and O. Elayeb, "Perspectives of double skin facade systems in buildings and energy saving," *Renewable and Sustainable Energy Reviews,* vol. 15, pp. 1468-1475, 2011.

[14] S. Barbosa and K. Ip, "Perspectives of double skin facades for naturally ventilated buildings: Areview," *Renewable and Sustainable Energy Reviews,* vol. 40, pp. 1019 - 1029, 2014.

[15] *ISO standard 15099, Thermal performance of windows, doors and sahding devices - Detailed calculations,* Geneva: International Organization for Standardization, 2003.

[16] P. Eiffert and G. J. Kiss, Building - Integrated Photovoltaic Designs for Commercial and Institutional Structures - A Sourcebook for Architects, NREL / BK - 520 - 25272, 2000.

[17] K. Farkas, I. Andersen and A. G. Hestnes, "Architectural integration of photovoltaic cells, overview of materials and products from an architectural point of view," in *3d International conference on smart and sustainable built environments (SASBE 2009)*, Delft, 2012.

[18] E. Foulaki, P. Paraskeva and V. Vakouli, "Experiments in environmental physics: The photovoltaic cell," Solar lab, 2014.

[19] B. P. Jelle and C. Breivik, "State of the art building integrated photovoltaics," *Energy Procedia,* 2012.

[20] Y. T. Chae, J. Kim, H. Park and B. Shin, "Building energy performance evaluation of building integrated photovoltaic (BIPV) window with semi-transparent solar cells," *Applied Energy,* vol. 129, pp. 217-227, 2014.

[21] L. Olivieri, E. Caamano-Martin, F. J. Moralejo-Vazquez, N. Martin-Chivelet, F. Olivieri and F. J. Neila-Gonzalez, "Energy saving potential of semi-transparent photovoltaic elements for building integration," *Energy,* vol. 76, pp. 572-583, 2014.

[22] Y. T. Chae, J. Kim, H. Park and B. Shin, "Building energy performance evaluation of building integrated photovoltaic (BIPV) window with semi-transparent solar cells," *Applied Energy,* vol. 129, pp. 217-227, 2014.

[23] E. L. Didoné and A. Wagner, "Semi-transparent PV windows: A study for office buildings in Brazil," *Energy and Buildings,* vol. 67, pp. 136-142, 2013.

[24] P. W. Wong, Y. Shimoda, M. Nonaka , M. Inoue and M. Mizuno, "Semi-transparent PV: Thermal performance, power generation, daylight modelling and energy saving potential in a residential application," *Renewable Energy,* vol. 33, pp. 1024-1036, 2007.

[25] S. Xu, W. Liao and J. Kang, "Optimal PV cell coverage ratio for semi-transparent photovoltaics on office building facades in central China," *Energy and Buildings,* vol. 77, pp. 130-138, 2014.

[26] F. Chen, S. K. Wittkopf, P. K. Ng and H. Du, "Solar heat gain coefficient measurement of semi-transparent photovoltaic modules with indoor calorimetric hot box and solar simulator," *Energy and Buildings,* vol. 53, pp. 74-84, 2012.

[27] M. S. Elden, K. Sopian, F. O. Alghoul and A. Abouhnik, "Solar Chimney Model Parameters to Enhance Cooling PV Panel Performance," *Modern Applied Science,* vol. 7, p. 24, 2013.

[28] G. Gan, "Effect of air gap on the performance of building-integrated photovoltaics," *Energy,* 2009.

[29] P. Mirzaei, E. Paterna and J. Carmeliet, "Investigation of the role of cavity airflow on the performance of building-integrated photovoltaic panels," *Solar Energy,* vol. 107, pp. 510-522, 2014.

[30] ASHRAE, *Thermal environmental conditions for human occupancy - ANSI/ASHRAE Standard 55,* 1992.

[31] ”ASHRAE,” [Online]. Available: https://www.ashrae.org/resources--publications/free-resources/ashrae-terminology.

[32] ”WinDat,” [Online]. Available: www.windat.org.

[33] D. van Dijk and H. Oversloot, "WIS, The International tool to calculate solar and thermal properties of windows and window components," in *Eighth International IBPSA Conference*, Eindhoven, 2003.

[34] ”Equa,” [Online]. Available: http://www.equa.se/en/ida-ice.

[35] ”NREL System Advisor Model,” National Renewable Energy Laboratory, [Online]. Available: https://sam.nrel.gov/.

[36] ”NREL System Advisor Model,” [Online]. Available: https://sam.nrel.gov/sites/sam.nrel.gov/files/content/documents/pdf/sam-help.pdf.

[37] ”Weather files generated from ASHRAE IWEC 1.1 Weather Files,” [Online]. Available: http://www.equaonline.com/iceuser/ASHRAE_IWEC.html.

[38] K. Carlsson, ”Stomkonstruktioner i moderna kontorhus,” Institutionen for Bygnadsteknik - Kungliga Tekniska Hogskolan, Stockholm, 1965.

[39] Svensk Bygg Norm 67, Statens planverk , 1967.

[40] ”Laboratório de Eficiência Energética em Edificações,” [Online]. Available: http://www.labeee.ufsc.br/antigo/arquivos/publicacoes/Thermal_Booklet.pdf.

[41] ”SVEBY - Branschstandard för energi i byggnader,” [Online]. Available: http://www.sveby.org/wp-content/uploads/2013/06/Brukarindata-kontor-version-1.1.pdf.

[42] K. Flodberg, ”Very Low Energy Office Buildings in Sweden - Simulations with low internal heat gains,” Division of Energy and Building Design, Department of Architecture and Built Environment, Lund University, Faculty of Engineering, LTH, Report EBD-T--12/14, Lund, 2012.

[43] ”Coefficient of Discharge - Theory of Discharge from an Orifice,” [Online]. Available: http://mysite.du.edu/~jcalvert/tech/fluids/orifice.htm.

[44] ”Live@Lund,” [Online]. Available: https://liveatlund.lu.se/departments/ebd/AEBN15/AEBN15_2014VT_100_1_NML__1283/CourseDocuments/Thermal_Properties_of_Building_Materials.pdf.

[45] ”Degree Days: theory and application,” CIBSE Publications, London, 2006.

[46] H. Poirazis and Å. Blomsterberg, "Energy simulations for glazed office buildings in Swedenn," *Energy and BUildings,* vol. 40, pp. 1161 - 1170, 2008.

[47] S. S. e. al, ”Panorama of the European non-residential construction sector,” ECOFYS, 2011.

[48] S. Schimschar, ”Panorama of the European non-residential construction sector,” ECOFYS, 2011.

[49] S. a. I. K. Barbosa, "Perspectives of double skin fa{\c{c}}ades for naturally ventilated buildings: A review," *Renewable and Sustainable Energy Reviews,* 2014.

# Appendix A. Glazing and Shading properties

The following tables summarize the optical and thermal properties of the glazings and shadings examined in this study.

*Table A. 1: Optical and thermal properties of the glazings examined.*

| | | Solar | | | | | Visible | | | Thermal | |
|---|---|---|---|---|---|---|---|---|---|---|---|
| Name | Type | $\tau$ | $r_f$ | $\alpha_f$ | $r_b$ | $\alpha_b$ | $\tau$ | $r_f$ | $r_b$ | $\varepsilon_f$ | $\varepsilon_b$ |
| clear | 6mm clear glass | 0.777 | 0.071 | 0.152 | 0.071 | 0.152 | 0.884 | 0.08 | 0.08 | 0.84 | 0.84 |
| Optiwhite | 6mm low Iron glass | 0.884 | 0.079 | 0.037 | 0.079 | 0.037 | 0.906 | 0.082 | 0.082 | 0.84 | 0.84 |
| K – glass | 6 mm low -E hard coated | 0.677 | 0.108 | 0.215 | 0.09 | 0.233 | 0.822 | 0.109 | 0.098 | 0.84 | 0.16 |
| Ipasol Neutral 68/34 | 6 mm selective low -E | 0.383 | 0.309 | 0.308 | 0.414 | 0.203 | 0.748 | 0.05 | 0.039 | 0.84 | 0.025 |
| Low-E soft coated | 6 mm low -E soft coated | 0.666 | 0.208 | 0.126 | 0.179 | 0.155 | 0.865 | 0.059 | 0.064 | 0.092 | 0.84 |

*Table A. 2: Optical and thermal properties of the shading devices examined.*

| | | Solar | | | | | Visible | | | Thermal | |
|---|---|---|---|---|---|---|---|---|---|---|---|
| Name | Type | $\tau$ | $r_f$ | $\alpha_f$ | $r_b$ | $\alpha_b$ | $\tau$ | $r_f$ | $r_b$ | $\varepsilon_f$ | $\varepsilon_b$ |
| Verosol Silver White | Reflective Shading | 0.058 | 0.739 | 0.20 | 0.683 | 0.694 | 0.059 | 0.728 | 0.774 | 0.16 | 0.83 |
| Vertisol White Grey | Medium Absorptive shading | 0.039 | 0.395 | 0.566 | 0.395 | 0.566 | 0.028 | 0.355 | 0.355 | 0.85 | 0.85 |
| Luxaflex Star 2692 | Absorptive shading | 0.056 | 0.086 | 0.858 | 0.25 | 0.694 | 0.056 | 0.096 | 0.281 | 0.87 | 0.87 |

# Appendix B. Build-ups and properties of glazing units

The following tables summarize the examined glazing units' setups along with their solar and thermal properties.

*Table B. 1: Solar and thermal properties of double clear window and its combinations with Low-Iron and Low-E coated external skins and different shading devices.*

| | Without shading | | | | With Shading | | | |
|---|---|---|---|---|---|---|---|---|
| | g | Tsol | Tvis | $Ug_{eff}$ / ($W/(m^2K)$) | $g_{eff}$ | $Tsol_{eff}$ | Tvis $_{eff}$ | $Ug_{eff}$ / ($W/(m^2K)$) |
| Double clear | 0.708 | 0.604 | 0.781 | 2.81 | 0.249 | 0.038 | 0.052 | 1.238 |
| Double clear + low-Iron (reflective shading) | 0.687 | 0.542 | 0.718 | 1.82 | 0.139 | 0.036 | 0.05 | 0.994 |
| Double clear + low-Iron (absorptive shading) | 0.687 | 0.542 | 0.718 | 1.82 | 0.21 | 0.031 | 0.041 | 1.347 |
| Double clear + low-Iron (medium absorptive shading) | 0.687 | 0.542 | 0.718 | 1.82 | 0.17 | 0.023 | 0.022 | 1.335 |
| Double clear + low-E (reflective shading) | 0.539 | 0.405 | 0.651 | 1.347 | 0.121 | 0.027 | 0.046 | 0.928 |
| Double clear + low-E (absorptive shading) | 0.539 | 0.405 | 0.651 | 1.347 | 0.218 | 0.023 | 0.037 | 1.012 |
| Double clear + low-E (medium absorptive shading) | 0.539 | 0.405 | 0.651 | 1.347 | 0.179 | 0.017 | 0.02 | 1 |

*Table B. 2: Solar and thermal properties of double clear window and its combinations with Low-Iron and Low-E coated external skins and reflective shading.*

| | Without Shading | | | | With Shading | | | |
|---|---|---|---|---|---|---|---|---|
| | g | Tsol | Tvis | $Ug_{eff}$ / ($W/(m^2K)$) | $g_{eff}$ | $Tsol_{eff}$ | Tvis $_{eff}$ | $Ug_{eff}$ / ($W/(m^2K)$) |
| triple clear | 0.608 | 0.472 | 0.696 | 1.867 | 0.237 | 0.03 | 0.048 | 0.996 |
| Triple clear + low-Iron (reflective shading) | 0.587 | 0.424 | 0.643 | 1.375 | 0.1 | 0.029 | 0.046 | 0.843 |
| Triple clear + low-E (reflective shading) | 0.459 | 0.317 | 0.583 | 1.08 | 0.086 | 0.022 | 0.042 | 0.794 |

*Table B. 3:Build-up of the highly insulated triple glazed units chosen for each examined WWR.*

| WWR | Outer pane | Gap | Middle pane | Gap | Inner pane |
|---|---|---|---|---|---|
| 30% | Optiwhite 6mm low-Iron glass | air / argon 10/90 32mm | clear 6mm | air / argon 10/90 - 16mm | Low-E soft coated |
| 70% | Ipasol Neutral 68/34 | air / argon 10/90 32mm | clear 6mm | air / argon 10/90 - 16mm | Low-E soft coated |

*Table B. 4: Solar and thermal properties of the highly insulated triple glazed units chosen for each examined WWR.*

| | Without Shading | | | | With Shading | | | |
|---|---|---|---|---|---|---|---|---|
| | g | Tsol | Tvis | $Ug_{eff}$ / ($W/(m^2K)$) | $g_{eff}$ | $Tsol_{eff}$ | Tvis $_{eff}$ | $Ug_{eff}$ / ($W/(m^2K)$) |
| Highly insulated TGU 30% WWR (reflective shading) | 0.602 | 0.472 | 0.703 | 0.993 | 0.1 | 0.033 | 0.048 | 0.657 |
| Highly insulated TGU 70% WWR (reflective shading) | 0.285 | 0.212 | 0.577 | 0.662 | 0.064 | 0.017 | 0.039 | 0.559 |

# Appendix C. Operative temperatures

The following tables summarize the operative temperatures analysis for the base cases and the ventilated options with double and triple clear initial windows as well as for the highly insulated triple glazed units chosen for each WWR and different orientations.

*Table C. 1: Peak Operative temperatures and percentage of occupied time that these exceeded 25°C or 26 °C for the base cases and the ventilated options with double clear and triple clear initial windows as well as for the for the highly insulated triple glazed units for 30% and 70% WWR, for south orientation.*

| | Double clear initial window | | | Triple clear initial window | | | |
|---|---|---|---|---|---|---|---|
| **South 70% WWR** | **Base Case** | **Low Iron** | **Low-E** | **Base Case** | **Low Iron** | **Low-E** | **Highly Insulated TGU** |
| max Op.Temp / °C | 26.5 | 25.9 | 25.7 | 26.5 | 25.8 | 25.7 | 26 |
| Top >25°C / (%) | 51.8% | 30.6% | 27.4% | 61.9% | 37.0% | 33.0% | 56.0% |
| Top >26°C / (%) | 2% | 0% | 0% | 3% | 0% | 0% | 1% |
| **South 30% WWR** | | | | | | | |
| max Op.Temp / °C | 25.8 | 25.7 | 25.6 | 25.8 | 25.7 | 25.6 | 25.8 |
| Top >25°C / (%) | 40.4% | 31.8% | 30.6% | 54.9% | 36.8% | 38.4% | 54.9% |
| Top >26°C / (%) | 0% | 0% | 0% | 0% | 0% | 0% | 0% |

*Table C. 2: Peak Operative temperatures and percentage of occupied time that these exceeded 25°C or 26 °C for the base cases and the ventilated options with double clear and triple clear initial windows as well as for the for the highly insulated triple glazed units for 30% and 70% WWR, for north orientation.*

| | Double clear initial window | | | Triple clear initial window | | | |
|---|---|---|---|---|---|---|---|
| **North 70%WWR** | **Base case** | **Low Iron** | **Low-E** | **Base case** | **Low Iron** | **Low-E** | **Highly Insulated TGU** |
| max Op.Temp / °C | 25.6 | 25.5 | 25.5 | 25.7 | 25.5 | 25.5 | 25.6 |
| Top >25°C / (%) | 21.5% | 16.3% | 19.7% | 32.5% | 24.6% | 26.1% | 30.5% |
| Top >26°C / (%) | 0% | 0% | 0% | 0% | 0% | 0% | 0% |
| **North 30%WWR** | | | | | | | |
| max Op.Temp / °C | 25.5 | 25.5 | 25.5 | 27.5 | 25.5 | 25.5 | 25.5 |
| Top >25°C / (%) | 19.0% | 19.0% | 21.9% | 25.8% | 22.3% | 25.6% | 24.8% |
| Top >26°C / (%) | 0% | 0% | 0% | 8% | 0% | 0% | 0% |

*Table C. 3: Peak Operative temperatures and percentage of occupied time that these exceeded 25°C or 26 °C for the base cases and the ventilated options with double clear and triple clear initial windows as well as for the for the highly insulated triple glazed units for 30% and 70% WWR, for east orientation.*

| | Double clear initial window | | | Triple clear initial window | | | |
|---|---|---|---|---|---|---|---|
| **East 70% WWR** | **Base Case** | **Low Iron** | **Low-E** | **Base Case** | **Low Iron** | **Low-E** | **Highly Insulated TGU** |
| max Op.Temp / °C | 26.3 | 25.7 | 25.6 | 26.3 | 25.6 | 29.3 | 25.8 |
| Top >25°C / (%) | 47.6% | 33.5% | 31.2% | 58.6% | 40.5% | 39.4% | 53.9% |
| Top >26°C / (%) | 0% | 0% | 0% | 1% | 0% | 0% | 0% |
| **East 30% WWR** | | | | | | | |
| max Op.Temp / °C | 25.6 | 25.6 | 25.5 | 25.7 | 25.5 | 25.5 | 25.6 |
| Top >25°C / (%) | 41.7% | 33.5% | 32.6% | 43.4% | 38.7% | 39.4% | 48.2% |
| Top >26°C / (%) | 0% | 0% | 0% | 0% | 0% | 0% | 0% |

*Table C. 4: Peak Operative temperatures and percentage of occupied time that these exceeded 25°C or 26 °C for the base cases and the ventilated options with double clear and triple clear initial windows as well as for the for the highly insulated triple glazed units for 30% and 70% WWR, for west orientation.*

| | Double clear initial window | | | Triple clear initial window | | | |
|---|---|---|---|---|---|---|---|
| **West 70% WWR** | **Base case** | **Low Iron** | **Low-E** | **Base case** | **Low Iron** | **Low-E** | **Highly Insulated TGU** |
| max Op.Temp / °C | 26.6 | 26 | 25.7 | 26.6 | 25.8 | 25.7 | 26 |
| Top >25°C / (%) | 42.4% | 27.3% | 23.9% | 42.4% | 32.6% | 30.5% | 52.5% |
| Top >26°C / (%) | 1% | 0% | 0% | 1% | 0% | 0% | 0% |
| **West 30% WWR** | | | | | | | |
| max Op.Temp / °C | 25.8 | 25.6 | 25.5 | 25.9 | 25.9 | 25.7 | 25.8 |
| Top >25°C / (%) | 36.6% | 28.0% | 27.0% | 41.8% | 31.8% | 32.1% | 45.8% |
| Top >26°C / (%) | 0% | 0% | 0% | 8% | 0% | 0% | 0% |

# Appendix D. Equations for naturally ventilated cavities

The main equations for calculating the thermal performance of ventilated glazed cavities are hereby presented. The equations are partly based on [33] and on [15] and are implemented in the software WIS, which was used in the component level analysis. The equations included in the above papers describe the airflow between two connected spaces which can be either other window air gaps either the indoor or the outdoor environment. These equations were rearranged adequately in order to only represent the ventilation case where air is inserted in the cavity from the outdoor and leaves the cavity towards the outdoor, which was the only case examined in this thesis. To get the general form of these equations a reference to the above papers is recommended.

The equations are divided in three parts:

- The first gives the equations used for the calculation of the vertical air temperature profile in the cavity. The convective heat transfer coefficient for closed cavities, the temperature of the surfaces bounding the cavity and the mean air velocity were taken by WIS.
- The second part describes how the mean velocity of the air in the cavity is calculated.
- The third part describes the heat transfer due to ventilation in the cavity.

### 1. Temperature profile inside the cavity

The temperature of the air inside the cavity is not uniform but varies at different heights as warmer air rises due to density differences forming a temperature profile, which is illustrated in Figure D.0.1. The temperature at the highest point is equal to that of the air leaving the cavity while the temperature at the lowest point is equal to that of the incoming air.

The calculation involves the main assumption that the temperature at different heights can be found if the mean air velocity of air is known.

The temperature profile inside the cavity at distance $x$ from the inlet is defined as:

$$T_{cav}\ (x) = T_{av} - \left(T_{av} - T_{cav,in}\right) \cdot e^{-x/H_0} \qquad \textit{( Equation D. 1 )}$$

Where: $T_{cav,in}$ is the temperature of the air at the inlet and is equal to the outdoor air temperature. $T_{av}$ is the average temperature of the surfaces bounding glazing cavity and is calculated as:

$$T_{av} = \frac{T_f + T_b}{2} \qquad \textit{( Equation D. 2 )}$$

Where: $T_f$ is the front temperature of the inner glazing and $T_b$ is the back temperature of the outer glazing.

$H_0$ is the characteristic height of the temperature profile of the cavity (temperature penetration length) and describes the height at which the temperature profile is curved and decreases more steeply (see also Figure D.0.1). It is defined as:

$$H_0 = \frac{\rho \cdot c_p \cdot d \cdot v}{2 \cdot h_{cv}} \qquad \textit{( Equation D. 3 )}$$

Where: $\rho$ is the air density at the temperature $T_{cav,m}$ given by ( Equation D. 7 ), $c_p$ is the specific heat capacity of air, $d$ is the cavity depth, $v$ is the mean air velocity and $h_{cv}$ is the heat convection coefficient for ventilated cavities, calculated as:

$$h_{cv} = 2h_c + 4v$$ *( Equation D. 4 )*

Where: 4 is an empirical coefficient and $h_c$ is the heat convective coefficient for non-ventilated air gaps that depends on the cavity dimensions, the inclination of the cavity and the mean temperature of the bounding surfaces.

At the outlet of a cavity with height $H$, ( Equation D. 1 )becomes:

$$T_{cav}\ (H) = T_{cav\,,out}\ = T_{av} - \left(T_{av} - T_{cav,in}\right) \cdot e^{-H/H_0}$$ *( Equation D. 5 )*

Where: $T_{cav\,,out}$ is the temperature of the outlet.

The above equations show that the temperature of the air leaving the cavity is a function of the inlet air temperature, the convective heat transfer coefficient for ventilated cavities $h_{cv}$, the geometrical characteristics of the cavity, the temperatures of the bounding surfaces $T_f$ and $T_b$ as well as the mean air velocity $v$ of the air in the cavity which remains unknown.

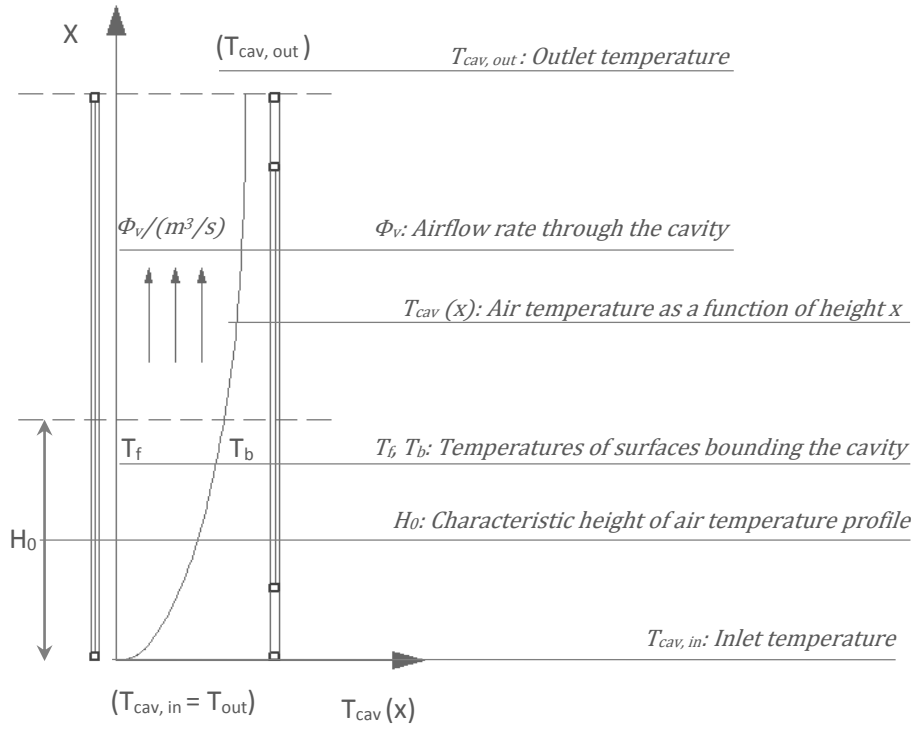


*Figure D.0.1: Vertical Temperature profile in the cavity*

## 2. Air velocity for thermally driven flow in cavities

It is assumed that the difference between the average air temperature in the cavity and the exterior environment produces the pressure difference responsible for driving the airflow through the cavity. The driving pressure difference can be approximated as:

$$\Delta P = \rho_0 \cdot T_0 \cdot g \cdot H \cdot cos\theta \cdot \frac{T_{cav,m} - T_{out}}{T_{cav,m} \cdot T_{out}}$$ *(Equation D. 6 )*

Where $\rho_0$ is the air density at the reference temperature $T_0 = 283K$, $\theta$ is the inclination of the glazing system from the vertical axis, $g$ is the gravity constant equal to 9.81 $m/s^2$ , $H$ is the cavity height, $T_{out}$ is the outdoor air temperature and $T_{cav,m}$ is the thermal equivalent temperature of the air in the cavity (average cavity air temperature) which can be found as:

$$T_{cav,m} = T_{av} - \frac{H_0}{H} \cdot \left(T_{cav,out} - T_{cav,in}\right)$$ *( Equation D. 7 )*

Where: $T_{av}$ is given by ( Equation D. 2 ), $H_0$ by ( Equation D. 3 ), $T_{cav,out}$ by ( Equation D. 5 ), $T_{cav,in}$ is the inlet air temperature equal to the outdoor air temperature and $H$ is the cavity height.

The driving pressure difference (Equation D. 6 ) shall be equal to the sum of pressure losses occurring in the cavity as well as at the inlet and outlet. The flow in the cavity is assumed as a pipe flow. Therefore the following pressure losses are considered:

Bernoulli pressure losses

$$\Delta P_B = 0.5 \cdot \rho \cdot v^2$$ *( Equation D. 8 )*

Hagen Poiseuille pressure losses

$$\Delta P_{HP} = 12 \cdot \mu \cdot \frac{H}{d^2} \cdot v$$ *( Equation D. 9 )*

Pressure loss at the openings

$$\Delta P_Z = 0.5 \cdot \rho \cdot v^2 \left(Z_{in} + Z_{out}\right)$$ *( Equation D. 10 )*

Where $\rho$ is the air density at $T_{cav,m}$ (average air temperature in the cavity), $v$ is the mean air velocity, $\mu$ is the dynamic viscosity of air at $T_{cav,m}$ and $H$ and $d$ are the height and depth of the cavity.

The parameters $Z_{in}$ and $Z_{out}$ are the pressure loss factors at the outlet and inlet openings and depend on their area. They are calculated as:

$$Z_{out} = \left(\frac{A_s}{0.6 \cdot A_{eq,out}} - 1\right)^2$$ *( Equation D. 11 )*

$$Z_{in} = \left(\frac{A_s}{0.6 \cdot A_{eq,in}} - 1\right)^2$$ *( Equation D. 12 )*

Where: $A_s$ is the cavity area, $A_{eq,in}$ and $A_{eq,out}$ are the opening areas at the inlet and outlet respectively.

The cavity area is equal to:

$$A_s = d \cdot L$$ *( Equation D. 13)*

Where: $d$ and $L$ are the cavity depth and width respectively.

By equating equation (Equation D. 6 )with equations ( Equation D. 8 ), ( Equation D. 9 )and ( Equation D. 10 ), and solving for v , the mean air velocity can be found as:

$$v = \frac{\sqrt{{A_1}^2 + (4 \cdot A \cdot A_1)} - A_2}{2A_1} \quad \textit{( Equation D. 14)}$$

Where the terms $A$, $A_1$ and $A_2$ correspond to the above stated pressure losses.

The term $A$ is the driving pressure difference given by (Equation D. 6 )

The term $A_1$ refers to the Bernoulli pressure losses as well as the pressure losses at the inlet and outlet of the cavity and equals:

$$A_1 = 0.5 \cdot \rho + 0.5 \cdot \rho \cdot (z_{out} + z_{in}) = 0.5 \cdot \rho \cdot (1 + z_{out} + z_{in}) \quad \textit{( Equation D.15 )}$$

The term $A_2$ corresponds to the Hagen Poiseuille pressure losses and equals:

$$A_2 = 12 \left( \mu \cdot \frac{H}{d^2} \right) \quad \textit{( Equation D. 16 )}$$

### 3. Heat extraction in cavities by natural ventilation

The heat transfer due to ventilation in ventilated cavities is given by:

$$q_v = \frac{\rho \cdot c_p \cdot \varphi_v \cdot (T_{cav,in} - T_{cav,out})}{H \cdot L} \quad \textit{( Equation D. 17 )}$$

Where $q_v$ is the heat transfer to the gap due to ventilation, $\rho$ is the air density at the mean air temperature (thermal equivalent) of the cavity $T_{cav,m}$ given by ( Equation D. 7 ), $c_p$ is the specific heat capacity of air, $\varphi_v$ is the air flow rate, $H$ is the height of the cavity, $L$ is the length of the cavity, and $T_{cav,in}$ and $T_{cav,out}$ are the inlet and outlet air temperatures respectively.

The airflow rate through the cavity is given by:

$$\varphi_v = v \cdot d \cdot L \quad \textit{( Equation D. 18 )}$$

Where $v$ is the mean air velocity and $d$, $L$ are the depth and length of the cavity respectively.

Consequently, if:

$T_{cav,in} > T_{cav,out}$ then $q_v > 0$ and heat is supplied to the cavity

$T_{cav,in} < T_{cav,out}$ then $q_v < 0$ , heat is extracted from the cavity.

By replacing equation D. 3 – D. 5 and D. 18 to equation D. 17, the latter becomes:

$$q_v = \frac{\rho \cdot c_p \cdot d \cdot v \cdot [T_{cav,in} - T_{av} + (T_{av} - T_{cav,in}) \cdot e^{-(4h_C + 8v) \cdot H / \rho \cdot c_p \cdot d \cdot v}]}{H} \quad \textit{( Equation D. 19 )}$$

The equation shows that the heat extraction from the cavity is a function of the mean air velocity$v$, the cavity height $H$, the cavity depth $d$ , the convective heat transfer coefficient for closed cavities $h_c$, the mean temperature of the surfaces bounding the cavity $T_{av}$ and the inlet temperature $T_{cav,in}$. As seen through Equations D.6 – D.16 , the mean air velocity $v$ is a function of the cavity's geometry ($d$, $L$, $H$ ) as well as the areas of the openings $A_{eq,in}$ and

$A_{eq,out}$ . As the convective heat transfer coefficient for closed cavities $h_c$ depends also on the geometry of the cavity and the temperatures of the bounding surfaces it can be concluded that:

For specific temperature and climatic boundary conditions the heat extraction from the cavity is a function of the latter's geometry characteristics.

# Appendix E. Calculation of overall thermal transmittances

The exposed area, the glazed and frame area and the wall area are given below for each examined window to wall ratio:

$$Exposed\ Facade\ Area\ = 3.3m\ \cdot 2.3m = 7.6\ m^2$$

$$Glazing\ Area\ 30\%\ WWR\ = (1.3m \cdot 2m) - 0.32m \cdot\ (1.3m \cdot 2m) =\ 1.77\ m^2$$

$$Frame\ Area\ 30\%\ WWR\ = 0.32m \cdot\ (1.3m \cdot 2m) = 0.832\ m^2$$

$$Wall\ Area\ 30\%\ WWR\ = 7.6\ m^2 -\ (1.3m \cdot 2m) = 5\ m^2$$

$$Glazing\ Area\ 70\%\ WWR\ = (2.2\ m \cdot 2.4\ m) - 0.24m \cdot\ (2.2\ m \cdot 2.4\ m) = 4.01\ m^2$$

$$Frame\ Area\ 70\%\ WWR\ = 0.24m \cdot\ (2.2\ m \cdot 2.4\ m) = 1.27\ m^2$$

$$Frame\ Area\ 70\%\ WWR\ = 7.6\ m^2 -\ (2.2\ m \cdot 2.4\ m) = 2.32\ m^2$$

The following table summarizes the calculation for the overall U-value of the base case at 70% and 30% WWR.

*Table E. 1: Calculation of the overall thermal transmittance of the base case for 30% and 70% WWR.*

| **70% WWR** | **Area/m²** | **U / (W/(m²K))** | **U · Area / (W/K)** |
|---|---|---|---|
| Exposed Area | 7.60 | - | - |
| Glazing | 4.01 | 2.81 | 11.27 |
| Frame | 1.27 | 3.00 | 3.80 |
| Wall | 2.32 | 0.60 | 1.39 |
| Summation / (W/K) | - | - | 16.47 |
| **Overall U-value/ (W/(m²K))** | = Summation / Exposed Area | | **2.17** |
| | | | |
| **30% WWR** | **Area/m²** | **U / (W/(m²K))** | **U · Area / (W/K)** |
| Exposed Area | 7.60 | - | - |
| Glazing | 1.77 | 2.81 | 4.97 |
| Frame | 0.83 | 3.00 | 2.50 |
| Wall | 5.00 | 0.60 | 3.00 |
| Summation / (W/K) | - | - | 10.46 |
| **Overall U-value/ (W/(m²K))** | = Summation / Exposed Area | | **1.38** |

The following table summarizes the calculation of the overall U-value of the single skin facades equivalent to ventilated options with low-Iron and low-E coated external skins for 70% and 30% WWR. The wall and frame areas are added together.

*Table E. 2: Calculation of the overall thermal transmittance of the single skin facades equivalent to the ventilated options with low-Iron and low-E coated external skins for 30% and 70% WWR.*

| | | Low-Iron Facade | | Low-E Facade | |
|---|---|---|---|---|---|
| **70% WWR** | **Area/m²** | **U / (W/(m²K)** | **U · Area / (W/K)** | **U / (W/(m²K)** | **U · Area / (W/K)** |
| Exposed Area | 7.60 | - | - | - | - |
| Glazing | 4.01 | 1.81 | 7.26 | 1.34 | 5.38 |
| Wall + Frame | 3.59 | 1.20 | 4.30 | 1.05 | 3.77 |
| Summation | - | - | 11.57 | - | 9.14 |
| **Overall U-value/ (W/(m²K))** | = Summation / Exposed Area | | **1.52** | | **1.20** |
| | | | | | |
| **30% WWR** | **Area/m²** | **U / (W/(m²K)** | **U · Area / (W/K)** | **U / (W/(m²K)** | **U · Area / (W/K)** |
| Exposed Area | 7.60 | - | - | - | - |
| Glazing | 1.77 | 1.81 | 3.20 | 1.34 | 2.37 |
| Wall + Frame | 5.83 | 0.86 | 5.02 | 0.77 | 4.49 |
| Summation | - | - | 8.22 | - | 6.86 |
| **Overall U-value/ (W/(m²K))** | = Summation / Exposed Area | | **1.08** | | **0.90** |


LUND UNIVERSITY

Dept of Architecture and Built Environment: Division of Energy and Building Design
Dept of Building and Environmental Technology: Divisions of Building Physics and Building Services